ELSEVIER

Coordination Chemistry Reviews
185–186 (1999) 471–534

COORDINATION CHEMISTRY REVIEWS

Magnetic spectroscopic (EPR, ESEEM, Mössbauer, MCD and NMR) studies of low-spin ferriheme centers and their corresponding heme proteins

F. Ann Walker *

Department of Chemistry, University of Arizona, Tucson, AZ 85721, USA

Contents

* Tel.: +1-520-621-8645; fax: +1-520-621-8407.
E-mail address: awalker@u.arizona.edu (F.A. Walker)

0010-8545/99/$ - see front matter © 1999 Elsevier Science S.A. All rights reserved.
PII: S0010-8545(99)00029-6

Abstract

Over the past few years extensive studies of model hemes have been carried out that are aimed at understanding the effect of axial ligands and porphyrin substituents on the electronic ground state and detailed magnetic properties of these systems themselves, as well as how they relate to the properties of heme proteins. Using variously substituted iron(III) tetraphenylporphyrins and chlorins, with pyridines, pyrazoles and imidazoles as axial ligands, we have identified three types of low-spin ferriheme centers: type I, which have $(d_{xy})^2(d_{xz},d_{yz})^3$ electronic ground states with axial ligands aligned in perpendicular planes; type II, which also have $(d_{xy})^2(d_{xz},d_{yz})^3$ electronic ground states, but with axial ligands aligned in parallel planes; and type III, which have $(d_{xz},d_{yz})^4(d_{xy})^1$ electronic ground states with axial ligands in any orientation. A subset of the latter type, with axial ligands aligned in parallel planes or with strong macrocycle asymmetry that creates rhombic electron paramagnetic resonance (EPR) spectra, cannot be created using a symmetrical porphyrinate ligand, but rather require a modified or reduced heme ring such as a quinoxalinoporphyrin or chlorin. type I centers are characterized by 'large g_{max}' EPR spectra with $g > 3.3$ in most cases and with well-resolved, widely spread magnetic Mössbauer spectra having $A_{zz} > 800$ kG, as well as nuclear magnetic resonance (NMR) spectra that show pyrrole-H resonances in the -10 to -20 ppm range, depending on the temperature, pyrrole-alkyl proton resonances in the $+4$ to $+10$ ppm range, *meso*-H resonances in the $+1$–4 ppm range, and high intensity NIR magnetic circular dichroism (MCD) spectra. In comparison, type II centers have well-resolved rhombic EPR spectra and less-resolved Mössbauer spectra that are broader on the high-energy side, having A_{zz} in the range 450–560 kG, with a well resolved proton NMR spectra including pyrrole-H

resonances in the −15– −30 ppm region, depending on temperature, pyrrole-alkyl proton resonances in the +5 to +16 ppm range, *meso*-H resonances in the 0–6 ppm range, and medium intensity NIR-MCD spectra. Type III centers have axial EPR spectra with $g_{\perp} = 2.6$ or smaller and $g_{\parallel} = 0.9$–1.95, but with $g_{\parallel}$ often not resolved, and with less-resolved Mössbauer spectra that are broader on the low-energy side and have A_{zz} in the range of 350–450 kG, with well-resolved NMR spectra including pyrrole-H resonances in the 0–10 ppm region, pyrrole-alkyl resonaces in the 4 ppm range, *meso*-H resonances in the −30– −90 ppm range, depending on temperature, and MCD spectra throughout the UV–vis and NIR range which are extremely weak and difficult to detect. The spectroscopic data from all of these magnetic spectroscopic techniques are self-consistent in defining the orbital of the unpaired electron, and in some cases, the energy separation between the two different electronic ground-states of low-spin ferrihemes. A wide variety of ferriheme proteins also fit this type I–III classification. Electron spin echo envelope modulation (ESEEM) data are useful in defining the orientation of the *g*-tensor of many of these ferriheme centers. Low-spin iron(III) chlorins are anomalous in exhibiting the spectroscopic properties of a $(d_{xz},d_{yz})^4(d_{xy})^1$ ground state at 4.2 K (EPR, Mössbauer, MCD), but those of a $(d_{xy})^2(d_{xz},d_{yz})^3$ ground state at much higher temperatures (−90– +30°C) (NMR). © 1999 Elsevier Science S.A. All rights reserved.

Keywords: Cytochrome; Ferriheme; Heme protein; Iron(III) porphyrin; Low-spin

1. Introduction

Low-spin iron(III) complexes have been of interest to inorganic and bioinorganic chemists for a very long time [1]. Some of these interests have involved the spectroscopic and magnetic properties of low-spin ferriheme centers of the cytochromes that carry out electron transfer reactions in biological systems. In earlier times, magnetic spectroscopic studies of many ferriheme proteins were the only ways of characterizing the spin state, coordination number, and probable axial ligands of these important centers, and these techniques provided amazingly accurate predictions as to the intimate structure of the iron(III) active sites. An example of this is the prediction of the aliphatic amine + histidine imidazole coordination of cytochrome *f* [2–6]. At present, we are in the fortunate situation that a number of cytochromes *a*, *b*, *c*, *d* and *f* have been characterized not only by various magnetic spectroscopies, but also structurally, either by X-ray crystallography or by nuclear magnetic resonance (NMR) spectroscopic methods, thus allowing us to define accurately the structure–magnetic spectroscopic relationships among these proteins. However, quite a number of membrane-bound cytochromes are still poorly (or not at all) characterized structurally, and for this reason spectroscopic data are still of great importance in allowing us to understand and make reliable predictions about the properties of these centers.

Model ferriheme complexes have played an important role in understanding the ferriheme proteins, in that it has been possible to prepare a large number of closely related, yet subtly different in terms of structure and/or electronic ground state,

low-spin iron(III) porphyrinate complexes and to characterize them structurally and by as many different spectroscopic techniques as possible. It has then been possible to compare the spectroscopic properties to those of the ferriheme proteins in order to see similarities and differences that would aid in the understanding of these protein systems. Low-spin iron(III) porphyrinates are ideal for detailed spectroscopic studies because of the presence of the single unpaired electron in one of the t_{2g} orbitals of the idealized octahedral complex, which makes possible detailed NMR, continuous wave and pulsed electron paramagnetic resonance (EPR), magnetic circular dichroism (MCD), and Mössbauer (including low-temperature magnetic Mössbauer) spectroscopic investigations. Each of these detailed investigations has been separately reported or reported in pairs, discussed and compared to the ferriheme protein system that they best model. As yet, there has not been a summary of all of these studies, in a coherent presentation, of the information obtained from each, and how each type of magnetic spectroscopy compliments the other. Hence, this is the purpose of this review. Some of the data included to fill in this picture have not yet appeared in print, although all of the work should be submitted for publication by the time this review appears. What will become evident by the end of this review is that all of the above-mentioned magnetic spectroscopies provide entirely complimentary and self-consistent information, and, because of the different temperature and magnetic field ranges over which the various measurements are made, the complete picture obtained is greater than the sum of its individual parts. NMR spectroscopy is discussed last, because it is the only one for which spectral measurements are not made at 4.2 K. Hence, because of the 'ambient temperature' range over which NMR measurements are made (-90– $+30$°C in most cases), excited states can contribute to the measured data, which is not the case for most of the other spectroscopies.

2. Overview of the possible axial ligand geometries, d-electron configurations and orbitals

Assuming the porphyrin ring itself to be 4-fold symmetric, the highest molecular symmetry that can occur for a six-coordinate ferriheme complex is D_{4h} (if the two axial ligands are identical, such as those of the cylindrical cyanide ion or alkyl or aryl isocyanides). If the two ligands are not identical, yet neither is planar, then the highest possible symmetry is C_{4v}. If one of the axial ligands is planar, such as a pyridine, pyrazole or imidazole, then the highest symmetry becomes C_{2v}. If both axial ligands are planar, then two possible limiting situations arise: either the two ligands can be in parallel planes (D_{2h}) or in perpendicular planes (D_{2d}). While the symmetry actually observed by X-ray crystallography is usually not perfectly one of these, due to distortions induced by crystal packing and other considerations, such idealized symmetries are useful in categorizing the actual structures of the complexes.

The bonding interactions between each axial ligand and the iron are expected to involve both σ and π interactions; the σ interaction is herein considered to be that

of a filled ligand orbital of σ-symmetry interacting with the empty $3d_z^2/4s/4p_z$ σ-symmetry hybrid orbitals of low-spin iron(III). The π interactions can include both π-donors and π-acceptors, depending on the nature of the axial ligand. Filled p_π orbitals on the ligand donor atom can interact with the $3d_{xz}$ and $3d_{yz}$ orbitals of the iron as π-donors if there is at least one hole in the d_π orbital set, while empty p_π orbitals on the ligand donor atom can interact with the $3d_{xz}$ and $3d_{yz}$ orbitals of the metal as π-acceptors, whether or not there is a hole in the d_π orbital set.

As for the porphyrin ring, the frontier orbitals are shown in Fig. 1, where it can be seen that both the 3e(π) filled porphyrin orbitals and the 4e(π*) empty porphyrin orbitals have proper symmetry to interact with the d_{xz} and d_{yz} orbitals of low-spin iron(III). The filled 3e(π) orbitals can interact by Por ⇒ Fe π–donation if there is at least one hole in the d_π orbitals, while the empty 4e(π*) orbitals can interact by Fe ⇒ Por π–back-donation. As will be discussed further in the NMR section, there

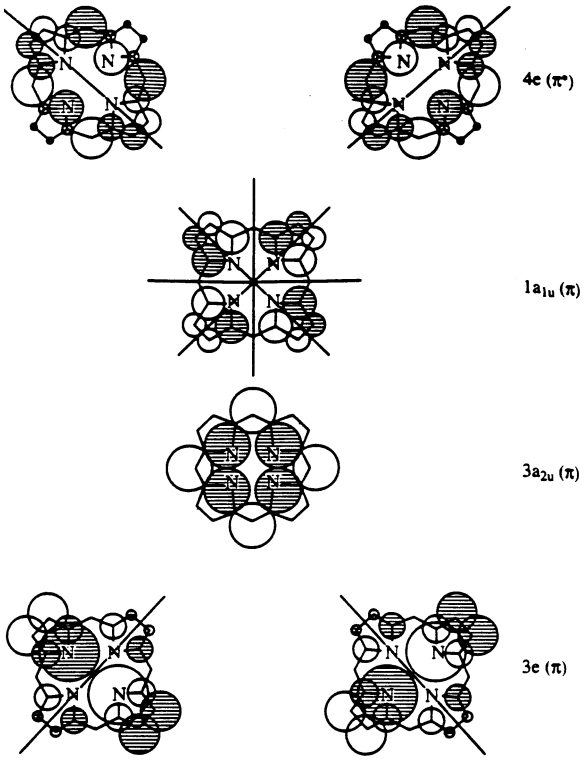

Fig. 1. Nodal properties, relative energies, and electron density distributions in the frontier π orbitals of the porphyrin macrocycle. The 3e(π), $3a_{2u}(\pi)$, and $1a_{1u}(\pi)$ orbitals, and either the $3a_{2u}(\pi)$ or $1a_{1u}(\pi)$ is the HOMO of the porphyrin ring, while the 4e(π*) orbitals are empty, and are thus the lowest unoccupied molecula ornitals (LUMOs) of the porphyrin ring. Note that for a flat porphyrin ring, only the 3e(π) and 4e(π*) orbitals have the proper symmetry (one nodal plane perpendicular to the plane of the porphyrin) for overlap with the metal d_{xz} and d_{yz} (one for each) However, see also Fig. 2, for a ruffled porphyrin ring. Taken from reference [1] with permission from Wiley.

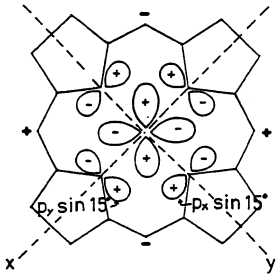

Fig. 2. Possible interaction of the d_{xy} orbital with the porphyrin nitrogens in the case of strong S_4 ruffling [26]. The remaining nitrogen p_z projections have proper symmetry to allow delocalization via the $a_{2u}(\pi)$ porphyrin orbital. Taken from reference [26] with permission from the American Chemical Society.

is ample evidence for interaction between the $3e(\pi)$ orbitals with the $3d_{xz}$ and $3d_{yz}$ orbitals of low-spin Fe(III), but slim to none for the interaction of the $4e(\pi^*)$ orbitals with the low-spin ferriheme metal center.

From a simplistic point of view, we would expect that only the d_π orbitals are capable of interacting with the porphyrin $e(\pi)$ orbitals, and this is strictly true for a planar porphyrin complex. However, if the porphyrin ring is strongly ruffled, so that the p_z orbitals of the porphyrin nitrogens are twisted away from the normal to the mean plane of the porphyrin ring, a component of p_z is present in the *xy* plane, and hence the $3a_{2u}(\pi)$ orbital can interact with the metal $3d_{xy}$ orbital, as shown in Fig. 2. In extreme cases, the amount of unpaired electron delocalization by $Por \Rightarrow Fe$ π-donation to the d_{xy} orbital is so great that the systems have been assumed to be Fe(II) porphyrin cation radicals, as discussed below. Such a continuum of d_{xy} to π cation radical electron configurations of highly ruffled Fe(III) porphyrin and reduced heme macrocycles may provide a more facile electron transfer pathway for reduced heme-containing enzymes such as dissimilatory and assimilatory nitrite and sulfite reductases [7–11], or permit more facile attack of dioxygen on the heme oxidation product known as an oxophlorin, as discussed below in Section 7.6. This d_{xy} interaction with the porphyrin $3a_{2u}(\pi)$ orbital of a ruffled porphyrin ring, however, does not relax the strict orthogonality of the d_{xy} and axial ligand π orbitals, so we expect no π interactions between axial ligands and a filled or half-filled iron d_{xy} orbital.

There are two possible electronic ground states of a low-spin ferriheme system: 1) the more common $(d_{xy})^2(d_{xz},d_{yz})^3$ electron configuration, as observed for most of the electron transfer cytochromes *a*, *b*, *c*, and *f*, and 2) the less common $(d_{xz},d_{yz})^4(d_{xy})^1$ electron configuration, as observed, or believed to be the case, for the low-spin forms of cytochromes *d* (an iron chlorin), d_1 (an iron dioxoisobacteriochlorin) [7–10], and the siroheme (an iron isobacteriochlorin) center of sulfite and assimilatory nitrite reductase [11]. The relationships of these two electron configurations to each other and to the electron configuration of a strictly octahedral complex are shown in Fig. 3 [12]. As is evident in the right side of Fig. 3, the $(d_{xy})^2(d_{xz},d_{yz})^3$ ground state is subject to the Jahn–Teller distortion *whether or not*

the porphyrinate ring is 4-fold symmetric, while the $(d_{xz},d_{yz})^4(d_{xy})^1$ ground state is only subject to a distortion if the macrocycle is highly unsymmetrical, as in the case of chlorin, bacteriochlorin, isobacteriochlorin, dioxoisobacteriochlorin or other such macrocycles, or if the axial ligands are in parallel planes, although that scenerio has not been achieved in a *porphyrin* macrocycle. In terms of synthetic small-molecule models of these systems, a number of investigations of the effect of the relative orientations of planar axial ligands [13–27], and π-donor/acceptor properties of axial ligands [26–29], on the structural and spectroscopic properties of Fe(III) porphyrinates have been reported. We will first review the structural findings and then look at each of the types of spectroscopy used for characterizing these model hemes.

3. Structures of the heme centers of ferriheme models and proteins

Several general porphyrinate ring conformational structures of six-coordinate ferriheme complexes have been observed. Whether the porphyrinate ring is planar or twisted in some way depends to a large extent on the nature of the axial ligands, although porphyrinate substituents also play a role, as will be pointed out below. The deformations of the hemes in proteins may also be brought about by protein

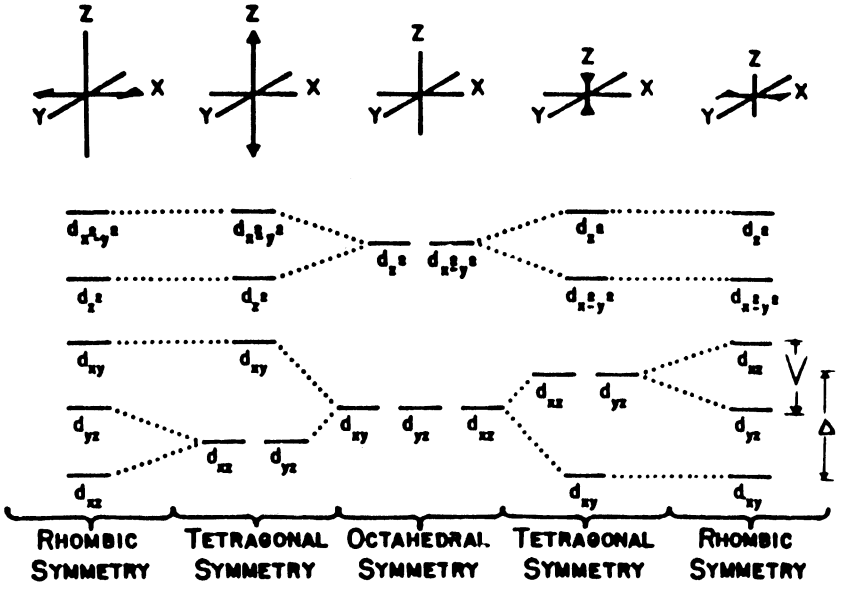

Fig. 3. Splitting of the 3d orbitals of an octahedral ferriheme complex due to tetragonal and rhombic distortion. For low-spin d^5, the unsymmetrical filling of the d_{xz} and d_{yz} orbitals on the right-hand side of the diagram helps to enforce a Jahn–Teller distortion that creates the rhombic symmetry (in the absence of steric constraints that enforce tetragonal symmetry). Taken from reference [113] with permission from Plenum Press.

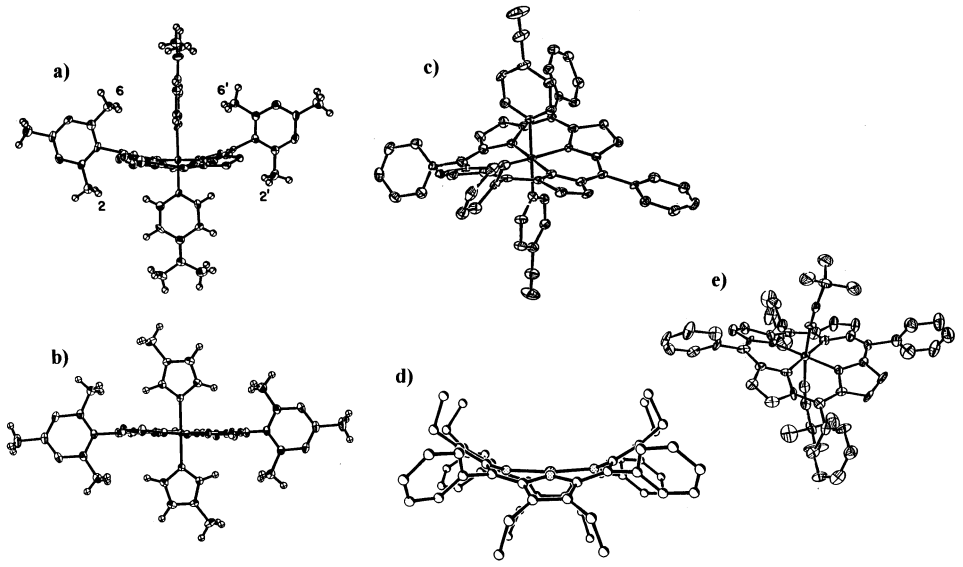

Fig. 4. ORTEP diagrams showing the arrangement of the effectively coplanar mesityl rings and the axial ligands in: (a) $[TMPFe(4\text{-}NMe_2Py)_2]ClO_4$ [17]; (b) molecule 2 of $[TMPFe(N\text{-}MeIm)_2]ClO_4$ [17]. Hydrogen atoms have been drawn artificially small, and two of the mesityl rings (in front and behind the plane of the figure) have been removed to improve clarity. (c) ORTEP diagram of $[TPPFe(4\text{-}CNPy)_2]ClO_4$ showing the strongly ruffled conformation [26]. (d) Side view of CuOETPP looking along the N–Cu–N axis [33]. Note that the saddled conformation creates two pockets for the axial ligands at right angles to each other and lying over the N–M–N bonds. (e) ORTEP diagram for $[TPPFe(t\text{-}BuNC)_2]^+$ showing the strongly ruffled conformation [27]. Taken from the above-listed references with permission from the American Chemical Society.

substituents, and these have recently been analyzed by a normal-coordinate structural decomposition method (NSD) and compared to the same analysis of model hemes [30]. In terms of structures of low-spin model ferrihemes, for complexes having two planar axial ligands in parallel planes, the porphyrinate ring is almost invariably flat [13,17,20], as shown in Fig. 4b. It should be noted that the electronic ground state of most low-spin ferriheme complexes having axial ligands in parallel planes is $(d_{xy})^2(d_{xz},d_{yz})^3$. The orientation of the parallel axial ligands with respect to the N_P–Fe–N_P axis of the porphyrinate ring varies widely among the systems that have been characterized by X-ray crystallography, and only when the planar axial ligands lie close to the N–Fe–N axes does the porphyrinate ring distort to show the consequences of the unsymmetrical low-spin d^5 electron configuration [13], which could be thought of as a structural Jahn–Teller effect of the $(d_{xy})^2(d_{xz},d_{yz})^3$ electronic ground state: if the axial ligand plane lies along the N_1–Fe–N_3 axis, then the N_2–Fe and N_4–Fe bonds are in these cases shorter than the N_1–Fe and N_3–Fe bonds [13], a consequence of the fact that with this orientation of axial ligands, Por $\Rightarrow$ Fe π–donation involves only one of the two d_π orbitals. The orientation of the parallel axial ligands has a small effect on the EPR spectra [15,20], as discussed below.

For complexes having two planar axial ligands in perpendicular planes, the porphyrinate ring is almost invariably distorted from planarity [14,17,18,24]. If the planes of the axial ligands lie over the *meso* positions, then the porphyrinate ring is typically S_4-ruffled [14,17,18,24], with alternate *meso* positions displaced above and below the mean plane of the porphyrin, as shown in Figs. 4a and c. This creates two cavities, one above and one below the porphyrin ring, in which the axial ligands lie, and the rotation of these ligands must be synchronous, with alternate flipping of the *meso* positions and their substituents up and down as the ligands rotate, as discussed further in the NMR section (Section 7.5). Such S_4-ruffled porphyrinate rings are observed for TMPFe(III) complexes of pyridines of a wide range of basicities, as demonstrated in Figs. 4a and c, where the pyridines are 4-NMe_2Py and 4-CNPy, respectively. For complexes with less bulky iron(III) porphyrinates, however, high-basicity pyridines prefer parallel axial ligand orientations and a flat porphyrinate ring, as is true of $[TPPFe(4\text{-}NMe_2Py)_2]^+$ [31], $[\{2,6\text{-}(OCH_3)_2\}_4TPPFe(4\text{-}NMe_2Py)_2]^+$ [25] and $OEPFe(4\text{-}NMe_2Py)_2]^+$ [17]. The siroheme center of sulfite reductase is a very ruffled heme center [11].

For complexes of highly hindered porphyrinates, such as tetraphenyloctachloro, completely halogenated porphyrins [32] or octaalkyltetraphenylporphyrins [33], the extreme crowding of the 12 substituents around the porphyrinate ring creates a strongly saddled conformation, with alternate nitrogens displaced above and below the mean plane of the porphyrin, as shown in Fig. 4d for a copper(II) porphyrinate [33]; similar structures are observed for iron(III) porphyrinates [34]. In this case also, cavities are created for the axial ligands, which then usually bind in perpendicular planes.

If the axial ligands are not planar, as for bis-cyanide or bis-alkyl or aryl isocyanides, then the electron configuration is usually $(d_{xz},d_{yz})^4(d_{xy})^1$ and the conformation of the porphyrinate ring is usually S_4-ruffled [27,28], as shown in Fig. 4e, a result of the $a_{2u}(\pi) \Rightarrow d_{xy}$ donation bonding interaction described by Fig. 2. This is less true of bis-cyanide complexes of iron(III) porphyrinates than of bis-alkyl- or –arylisocyanide complexes, and there is at least one structure of $[TPPFe(CN)_2]^-$ that shows the porphyrinate ring to be fairly planar [35] and the spectroscopic properties consistent with an electron configuration of $(d_{xy})^2(d_{xz},d_{yz})^3$ [23]. However, another structure, admittedly of a 'basket-handle-type' $TPPFe(CN)_2^-$ complex [36], shows a very ruffled porphyrinate ring. NMR and EPR evidence to be discussed below suggests that many *meso*-substituted $[Por\text{-}Fe(CN)_2]^-$ have the $(d_{xz},d_{yz})^4(d_{xy})^1$ electron configuration and are probably highly S_4-ruffled.

We thus arrive at a summary of the porphyrinate ring conformation possibilities of low-spin Fe(III) porphyrinates that: (i) planar, 5-membered ring axial ligands usually stabilize the $(d_{xy})^2(d_{xz},d_{yz})^3$ ground state, parallel orientation of the axial ligands, and a planar porphyrinate ring, while; (ii) planar, 5-membered ring axial ligands with 2-substituents, as well as planar, 6-membered ring axial ligands may stabilize either the $(d_{xy})^2(d_{xz},d_{yz})^3$ or the $(d_{xz},d_{yz})^4(d_{xy})^1$ ground state, depending on their σ-donor, π-donor/acceptor properties. The complexes have perpendicular orientation of the axial ligands and a ruffled porphyrinate ring, except in the special

case of high-basicity pyridines bound to non-hindered iron(III) porphyrinates [17, 31c]. Highly hindered porphyrins such as the octaalkyltetraphenylporphyrins must of necessity have nonplanar porphyrinate rings, and are typically in the saddled conformation, irrespective of the nature of the axial ligands. Planar axial ligands are in perpendicular planes, based on X-ray crystallographic investigations, but in frozen solutions, EPR spectroscopy provides evidence of non-perpendicular orientation [34] (see below, Section 4.4). Cylindrical ligands such as cyanide or alkyl- or arylisocyanides bind to create planar iron(III) porphyrinate rings if the $(d_{xy})^2(d_{xz},d_{yz})^3$ ground state is stabilized, but highly S_4-ruffled porphyrinate rings if the $(d_{xz},d_{yz})^4(d_{xy})^1$ is stabilized. The latter appears to be the case for all organic isocyanides, while which is the case for cyanide complexes appears to depend on the nature of the *meso* substitutents of the iron porphyrinate [37,38] (see also Section 7.7).

4. EPR and ESEEM spectroscopy of low-spin ferriheme models and proteins

Investigations of the molecular structures, electron paramagnetic resonance (EPR) and NMR spectra, and in some cases Mössbauer spectra, of well-defined low-spin ferriheme model compounds with high-basicity pyridines, imidazoles or cyanide ions as the axial ligands have provided conclusive evidence of the existence of two different types of $(d_{xy})^2(d_{xz},d_{yz})^3$ ground state complexes, one of which is characterized by single-feature EPR signals [36] known as 'large g_{max}' signals (Fig. 5a) that are only observed at very low temperatures (4–20 K), while the other of which is characterized by well-resolved rhombic EPR signals (Fig. 5b) that are usually observed at temperatures up to 77 K. EPR signals of this type had been observed for a number of poorly-characterized low-spin ferriheme centers in membrane-bound proteins, particularly those of the *b* hemes of mitochondrial Complex III [40], which are now known to have bis-histidine coordination [41]. Correlated structural and EPR studies have provided proof that the 'large g_{max}' EPR signal is indicative of near-degeneracy of d_{xz} and d_{yz} [15,24,39]. For complexes with planar axial ligands, near-degeneracy correlates with perpendicular alignment of these ligands [15–18]. Hereafter, these complexes will be referred to as type I.

The other type of $(d_{xy})^2(d_{xz},d_{yz})^3$ ground-state complexes, those having well-resolved rhombic EPR signals (Fig. 5b), and including cytochrome b_5 [42,43], mitochondrial cytochrome *a* [44], and methemoglobin-imidazole [45], among many other heme proteins, some of whose EPR parameters are summarized in Table 1, are found to have parallel or near-parallel alignment of the planar axial ligands and marked difference in energy between d_{xz} and d_{yz}. These complexes will hereafter be called type II complexes. Rhombic EPR spectra and the data derived from them were previously analyzed by Blumberg and Peisach using their 'truth diagrams' to predict the axial ligands of each ferriheme protein center that gave rise to such a spectrum [46–49]. However, neither 'large g_{max}' (Fig. 5a) nor the axial-type EPR spectra (Figs. 5c and d) that are indicative of the $(d_{xz},d_{yz})^4(d_{xy})^1$ ground state, hereafter called type III complexes, were considered in those 'truth diagrams.'

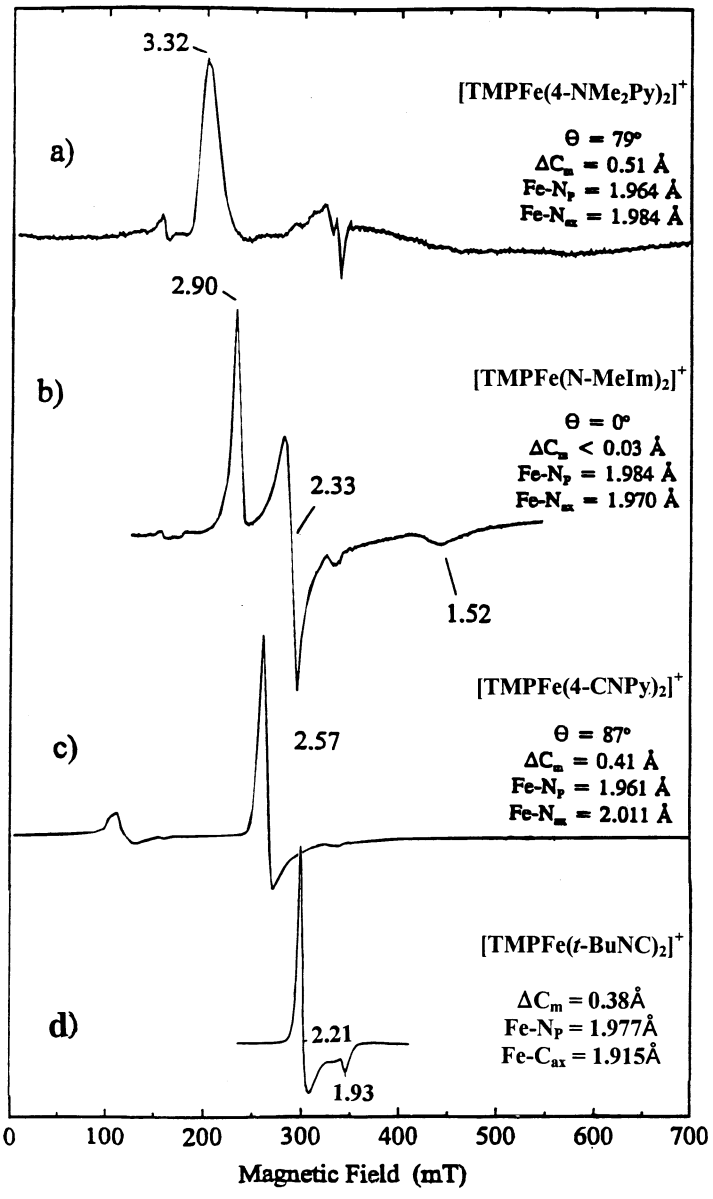

Fig. 5. Typical types of EPR spectra exhibited by low-spin ferriheme complexes [27,29]. (a) 'large g_{max}' type I, as in the case of $[TMPFe(4\text{-}NMe_2Py)_2]^+$. (b) Normal rhombic type II, as in the case of $[TMPFe(N\text{-}MeIm)_2]^+$. (c) Axial type III, with large difference between $g_\perp$ and $g_\parallel$, as in the case of $[TMPFe(4\text{-}CNPy)_2]^+$. (d) Axial type III, with small difference between $g_\perp$ and $g_\parallel$, as in the case of $[TPPFe(t\text{-}BuNC)_2]^+$. Modified from references [27] and [29].

Table 1
EPR g-values, Mössbauer parameters, rhombicities and tetragonalities for low-spin Fe(III) porphyrinates and ferriheme proteins

System	Ligand type	g_{xx}	g_{yy}	g_{zz}	V/λ	Δ/λ	V/Δ	δ (mm s^{-1})	ΔE_Q (mm s^{-1})	A_{xx} (kG)	A_{yy} (kG)	A_{zz} (kG)	Reference
Type I													
Myoglobin-CN	Imidazole, cyanide	0.93	1.89	3.45	0.92	3.31	0.28	0.16	1.46	−320	170	760	[77]
CCP(CN)	Imidazole, cyanide	0.98	2.08	3.17	1.14	2.49	0.46	0.21	1.60	−360	260	680	[77]
Mitochondrial Cytochrome b_{562}	2 Imidazoles			3.44									[40a]
Mitochondrial Cytochrome b_{566}	2 Imidazoles			3.75									[40a]
R. capsulatus Cytochrome b_H	2 Imidazoles			3.46									[40a]
R. capsulatus Cytochrome b_L	2 Imidazoles			3.79									[40a]
$[TPPFe(CN)_2]^-$	2 Cyanides	0.52	1.05	3.70	0.44	6.87	0.06						[23]
$[PPIXFe(CN)_2]^-$	2 Cyanides	1.03	2.42	3.75	1.06	2.33	0.45	0.24	0.35	−430	220	860	[77]
$[PPIXFe(Py)_2]^+$	2 Pyridines	<0.8	1.35	3.53	0.49	3.34	0.15	0.25	1.95	−350	350	860	[77]
$[\{(OMe)_2\}_4TPPFe(2MeImH)_2]^+$	2 Imidazoles[a]	0.48?	1.80?	3.54	0.68	2.43	0.28	0.23	1.99	−346	278	855	[25]
		0.76?	1.70?	3.54	0.76	3.53	0.21	0.23	1.99	−320	178	855	
$[TMPFe(4NMe_2Py)_2]^+$	2 4-NMe_2Pyridines[a]	0.36?	1.91?	3.38	0.70	1.90	0.37		1.75	−362	338	812	[17]
"	"	0.92?	1.80?	3.44	0.89	3.64	0.24		1.75	−331	168	815	
$[TPPFe(2\text{-}MeImH)_2]^+$	2 Imidazoles	0.82	1.87	3.41	0.88	2.96	0.30	0.21	1.71	−247	220	810	[15]
$[TMPFe(2\text{-}MeImH)_2]^+$	2 Imidazoles				3.17								[113]
$[TMPFe(1,2\text{-}Me_2Im)_2]^+$	2 Imidazoles				3.02								[113]
$[OETPPFe(2\text{-}MeImH)_2]^+$	2 Imidazoles				3.27								[34]
$[OETPPFe(N\text{-}MeIm)_2]^+$	2 Iimidazoles				3.18								[34]
$[OETPPFe(CN)_2]^-$	2 Cyanides				3.47								[34]
Type II													
Mitochondrial Cytochrome *c*	Imidazole, thioether	1.25	2.25	3.06	1.48	2.56	0.58						[62]
Cytochrome c_{551}	Imidazole, thioether	1.25	2.05	3.20	1.29	3.59	0.36	0.23	2.03	−320	290	660	[76]
Cytochrome c_2	Imidazole, thioether	1.23	2.11	3.13	1.33	3.08	0.43	0.25	2.26	−350	250	625	[76]
Cytochrome b_5, liver microsomes	2 Imidazoles		1.43	2.23	3.03	1.68	3.23	0.52					[42]
Cytochrome b_5, housefly	2 Imidazoles		1.35	2.22	3.07	1.55	3.08	0.52					[43]
Mitochondrial Cytochrome *a*	2 Imidazoles		1.24	2.24	3.03	1.49	2.52	0.59					[44]
Myoglobin-ImH	2 Imidazoles		1.53	2.26	2.91	1.93	3.31	0.58					[45]
$[OEPFe(4\text{-}NMe_2Py)_2]^+$	2 4-NMe_2 pyridines	1.63	2.28	2.83	2.21	3.56	0.62		2.15	−416	177	446	[17]
$[\{(OMe)_2\}_4TPPFe(NMeIm)_2]^+$	2 Imidazoles	1.49	2.252	2.989	1.79	3.31	0.54	0.23	2.05	−404	176	540	[25]
$[\{(OMe)_2\}_4TPPFe(4NMe_2Py)_2]^+$	2 4-NMe_2 pyridines	1.65	2.32	2.85	2.25	3.44	0.65	0.26	2.28	−420	−50	460	[25]
$[OETPPFe(N\text{-}MeIm)_2]^+$	2 Imidazoles		1.64	2.37	2.73	2.50	2.81	0.89					[34]
$[TPPFe(PzH)_2]^+$	2 Pyrazoles		1.71	2.38	2.62	2.96	2.77	1.07					[67]
$[TPPFe(3\text{-}NH_2PzH)_2]^+$	2 3-NH_2 pyrazoles	1.86	2.28	2.39	4.70	3.74	1.26						[68]
d_1 heme of cytochrome cd_1, *T. pantotropha*	Imidazole, tyrosine	1.84	2.19	2.52	3.61	5.79	0.62						[10]
$P450_{cam}$	Water, thiolate	1.91	2.26	2.45	4.59	5.11	0.90	0.38	2.85	−450	102	191	[79]
$P450_{cam}$(2-PhImH)	2-PhImH, thiolate	1.91	2.25	2.41	4.91	5.04	0.47	0.36	2.85	−440	96	170	[79]
Type III													
$P450_{cam}$?[b]	Water, thiolate	−2.45	2.26	−1.91	−2.81	−6.00	0.47	0.38	2.85	−191	102	450	[79]

Table 1 *(Continued)*

System	Ligand type	g_{xx}	g_{yy}	g_{zz}	V/λ	Δ/λ	V/Δ	δ (mm s^{-1})	ΔE_Q (mm s^{-1})	A_{xx} (kG)	A_{yy} (kG)	A_{zz} (kG)	Reference
$P450_{cam}$(2-PhImH)?[b]	2-PhImH?, thiolate	−2.41	2.25	−1.91	−2.59	−6.20	0.42	0.36	2.85	−170	96	440	[79]
d_1 heme of cytochrome cd_1, *T. denitrificans*	Imidazole,?	−2.50	2.43	−1.70	−0.39	−3.57	0.11	0.20	1.70	−125	−120	320	[7]
d_1 heme of cytochrome cd_1, *T. pantotropha*	Imidazole, tyrosine	−2.52	2.19	−1.84	−3.98	−5.60	0.71						[10]
d_1 heme of cytochrome cd_1, *P. stutzeri*(Zo-Bell)Imidazole,?		−2.42	2.56	−1.58	−2.08	−3.08	0.58						[10]
d_1 heme of cytochrome cd_1, *P. aeruginosa*	Imidazole,?	−2.43	2.51	−1.71	−1.62	−3.61	0.45						[10]
Sirohemin cyanide	2 Cyanides	−2.37	2.37	−1.78	0.00	−4.39	0.00						[136]
$[TPCFe(ImH)_2]^+$	2 Imidazoles	−2.49	2.37	−1.71	−0.73	−3.75	0.19						[72]
$[OEC(ImH)_2]^+$	2 Imidazoles	−2.51	2.37	−1.73	−0.88	−3.84	0.23						[72]
$[((OMe)_2)_4TPPFe(4NMe_2Py)_2]^+$	2 4-CNPyridines	−2.6	2.6	−1.6	0.00	−2.9	0.00						[25]
$[TMPFe(CN)_2]^-$	2 Cyanides	−2.56	2.56	−1.70	0.00	−3.31	0.00						[127]
$[T^iPrPFe(CN)_2]^-$	2 Cyanides	−2.35	2.35	−1.82	0.00	−4.82	0.00						[37]
$[QTPPFe(CN)_2]^-$	2 Cyanides	−2.51	2.25	−1.75	−2.06	−4.36	0.47						[143]
$[OEPFe(t\text{-}BuNC)_2]^+$	2 *t*-butylisocyanides	−2.28	2.28	−1.83	0.00	−5.47	0.00		−1.80	−188	122	363	[27]
$[TPPFe(t\text{-}BuNC)_2]^+$	2 *t*-butylisocyanides	−2.21	2.21	−1.93	0.00	−8.32	0.00		−1.89	−87	230	342	[27]
$[TPPFe(2,6\text{-}xylylNC)_2]^+$	2 2,6-xylylisocyanides	−2.2	2.2	−1.94	0.00	−8.90	0.00	0.08	−1.99	−55	55	400	[28]
$[p\text{-}TTPFe(2,6\text{-}xylylNC)_2]^+$	2 2,6-xylylisocyanides	−2.2	2.2	−1.94	0.00	−8.90	0.00	0.14	−1.81	−55	55	400	[28]
$[m\text{-}TTPFe(2,6\text{-}xylylNC)_2]^+$	2 2,6-xylylisocyanides	−2.14	2.14	−2.14	0.00			0.12	−1.94	−25	25	320	[28]

[a] Two different choices of g_1 and g_2 that bracket the possible range of g_2 were used in simulations. In these cases, g_1 was calculated from Eq. (8).

[b] Electronic ground state re-assigned.Table 2.

Therefore, we will include consideration of their place in the related diagrams presented in this work.

4.1. Theory

On the basis of Griffith's theory [49] and Taylor's formulation [50] the relative energies of the d_{yz}, d_{xz} and d_{xy} orbitals can be calculated from the g-values. The wavefunctions of the Kramers doublet are given by:

$$\begin{aligned} |+> &= a\,|\,d^{+}_{yz}> - ib\,|\,d^{+}_{xz}> - c\,|\,d^{-}_{xy}> \\ |-> &= -a\,|\,d^{-}_{yz}> - ib\,|\,d^{-}_{xz}> - c\,|\,d^{+}_{xy}> \end{aligned} \tag{1}$$

and the normalization condition

$$a^2 + b^2 + c^2 = 1.000 \tag{2}$$

should hold. The three former t_{2g} orbitals are thus mixed by spin-orbit coupling; the three g-values are then given in terms of the mixing coefficients a, b, and c as: [50]

$$\begin{aligned} g_{xx} &= 2[a^2 - (b+c)^2] \\ g_{yy} &= 2[(a+c)^2 - b^2] \\ g_{zz} &= 2[(a+b)^2 - c^2] \end{aligned} \tag{3}$$

Thus, the experimental g-values of low-spin Fe(III) complexes can be used to calculate the orbital mixing coefficients,

$$\begin{aligned} a &= (g_{zz} + g_{yy})/4K \\ b &= (g_{zz} - g_{xx})/4K \\ c &= (g_{yy} - g_{xx})/4K \end{aligned} \tag{4}$$

$$4K = [8(g_{zz} + g_{yy} + g_{xx})]^{1/2} \tag{5}$$

and thereby provide information as to the individual d-orbital character of the orbital of the unpaired electron. In some cases two of the g-values must be measured by single crystal EPR spectroscopy [20–23] or estimated from Mössbauer spectra at 4.2 K in the presence of an applied magnetic field [15,17,25], as will be discussed below in Section 5. Taylor [50] showed that the g-values could also be utilized to calculate the energy separation of the three formerly t_{2g} orbitals:

$$V/\lambda = E_{yz}/\lambda - E_{xz}/\lambda = g_{xx}/(g_{zz} + g_{yy}) + g_{yy}/(g_{zz} - g_{xx}) \tag{6}$$

$$\Delta/\lambda = E_{yz}/\lambda - E_{xy}/\lambda - 2V/\lambda = g_{xx}/(g_{zz} + g_{yy}) + g_{zz}/(g_{yy} - g_{xx}) - 2V/\lambda \tag{7}$$

where V is the energy difference between the d_{xz} and d_{yz} orbitals, Δ is the energy difference between the d_{xy} and the average of the d_{xz} and d_{yz} orbitals, and λ is the spin-orbit coupling constant, whose value is 460 cm^{-1} for the free ferric ion [51] and somewhat smaller for fairly covalent iron(III) complexes such as the ferriheme

centers of interest here [52].[1] The results of such calculations indicate that the parallel orientation is lower in energy, and suggested to us at the time of publication [15] that perpendicular alignment of planar axial ligands could lead to a positive shift in reduction potential of up to 50 mV over that observed for parallel alignment, all other structural and environmental factors being equal. However, as we have shown recently [53], all other structural and environmental factors are *not* equal, and one cannot reliably predict the effect on reduction potentials without considering the effect of axial ligand plane orientation on the partner reduced member of the redox couple, the low-spin Fe(II) energy levels. Structural studies of these systems have shown, perhaps surprisingly, that low-spin Fe(II) porphyrinates show a high preference for parallel alignment of axial ligands, in spite of the symmetrical low-spin d^6 electron configuration. This is probably due in large part to the fact that perpendicular orientation of axial ligands 'encourages' ruffling of the porphyrinate ring, but there is no *electronic* stabilization of a ruffled porphyrinate core for the low-spin d^6 electron configuration [53]. Thus, low-spin Fe(II) porphyrinates appear to abhor the ruffled conformation and hence perpendicular alignment of axial ligands [53]. Only in the case of [TMPFe(1,2-Me_2Im)$_2$] at very low temperatures have we obtained NMR [54] and Mössbauer [55] evidence for a low-spin Fe(II) porphyrinate having axial ligands in perpendicular planes lying over the *meso* positions and an obviously ruffled porphyrinate core.

In fact, reduction potentials are determined by the ratio of axial ligand binding constants for the two oxidation states, $\beta_2^{III}/\beta_2^{II}$ [53], and these binding constants are in turn determined by the balance of σ and π binding preferences of the metal in each oxidation state for the particular ligand used. Hence, the type of EPR spectrum observed can *not* be used to predict the relative reduction potentials of ferriheme complexes or proteins.

One complication in using Eqs. (6) and (7) to determine the energy separations of d_{xy}, d_{xz}, and d_{yz} is that EPR measurements allow calculation of the magnitude, but not the sign, of the g-values of the paramagnetic center. Common use of the expressions derived by Taylor [50] usually assumes that the product of the three g-values, $g_{xx}g_{yy}g_{zz}$ is positive, as has been shown for several heme proteins by Münck, Huynh and coworkers [56]. Furthermore, Taylor showed that $g_{zz} + g_{yy} - g_{xx}$ must be positive [50]. These two conditions, along with Eq. (2), limit the possible choices of signs for the measured g-values. Most workers have also assumed that

$$g_{xx}^2 + g_{yy}^2 + g_{zz}^2 = 16 \tag{8}$$

This expression allows the third g-value to be estimated in cases in which g-strain precludes its direct measurement [57], as has been done for many of the type I centers listed in Table 1. However, while this limit appears to hold for systems having fairly pure $(d_{xy})^2(d_{xz},d_{yz})^3$ ground states, it has recently been shown that for systems having fairly pure $(d_{xz},d_{yz})^4(d_{xy})^1$ ground state, the sum of the squares of

[1] Maltempo has used the value 300 cm^{-1} for low-spin ferrihemes, and we have used 400 cm^{-1} as the maximum possible value of λ.

the g-values has been reported to be as small as 13.1–13.5 for bis-(isocyanide) complexes [27,28], and could be as small as 12, in the limit of no spin-orbit mixing of d_{xy} with the other two d_π orbitals [25–28].

4.2. Experimental EPR data for low-spin ferrihemes

In Table 1 are summarized the EPR parameters for a number of low-spin ferriheme models and proteins having type I, II and III types of spectra. Those systems having been studied by both EPR and Mössbauer spectroscopy are included, as well as some other representative systems to be discussed herein. As is evident, high-basicity pyridine and imidazole complexes of iron(III) porphyrinates have been shown to be good models [15,17] of the bis-histidine-coordinated cytochromes *a*, *b* and *c* that are involved in electron transfer in a large number of organisms, including cytochromes b_5 [58], *a* [46a], and c_3 [59], as well as the membrane-bound cytochromes *b* believed [60] and recently shown to have bis-(histidine) coordination, including the two *b* cytochromes of mitochondrial 'Complex III' (also known as ubiquinone-cytochrome *c* oxidoreductase) [41] and, presumably, chloroplast cytochrome b_6, which has not as yet been structurally characterized. As mentioned above, the orientation of the parallel (or nearly parallel) axial ligands with respect to the porphyrin nitrogens has a small but real effect on the EPR parameters of this type of complex [15,20], as demonstrated in Fig. 6, where the more compressed EPR spectrum has the larger rhombicity (V/Δ) [15], and was later shown by single crystal EPR [20] to be due to the molecules having the parallel imidazole ligands lying very close to the porphyrin N_P–Fe–N_P axis and a difference

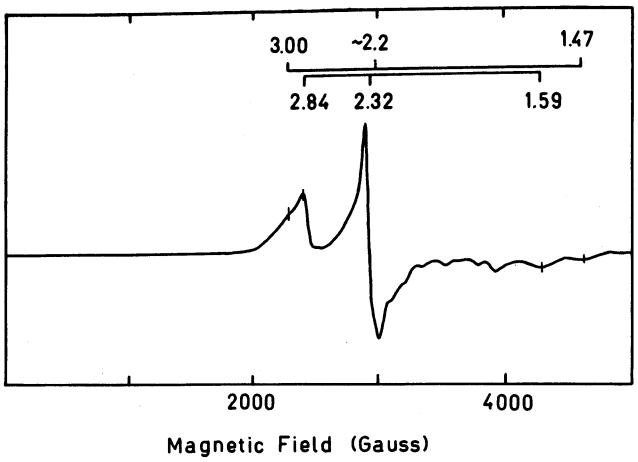

Fig. 6. EPR spectrum of solid [TPPFe(ImH)$_2$]Cl showing two different overlapping rhombic signals [15]. The set with the smaller spread of g-values was later shown to be due to the molecules having axial ligand planes aligned close to the porphyrin nitrogens and that with the larger spread was shown to be due to molecules having axial ligand planes aligned close to the *meso* positions of the porphyrin [20]. Taken from reference [15] with permission from the American Chemical Society.

in bond length for those two N_P–Fe bonds and the two at right angles to the axial ligand planes; the latter Fe–N_P bonds are shorter, due to Por⇒Fe π donation to the half-filled d_π orbital. Unfortunately, the ligand field strength of the particular pyridine or imidazole ligand [17] (and the degree of H-bond donation of the N_δ–H of unhindered imidazoles or the N_ε–H of hindered imidazoles, and hence the degree of imidazolate character [46]) *also* has an effect on the EPR parameters, so it is difficult to separate these two effects in the absence of structural information.

For some years it was common practice to assign the largest *g*-value to the direction of the heme normal, on the basis of results of studies of several proteins, including single crystal EPR data for cytochrome *c* [61], methemoglobin cyanide [45], and several model hemes [20,23]. On the basis of Griffith's theory [49] and Taylor's formulation [50], this assignment was consistent with the major contributor to the orbital of the unpaired electron being d_{yz}, i.e. $a \sim 1$. However, Taylor showed that this sometimes leads to larger calculated energy separations between d_{xz} and d_{yz} (V/λ) than between their average and the lowest-energy d_{xz} orbital (Δ/λ), a situation that he described as an 'improper axis system.' [50] In such cases, he suggested, by permutation of the assignment of *g*-values one could arrive at calculated ligand field energy differences that obeyed the expected relationship $V/\lambda = 2/3$. This permutation typically led to a change in the major contributor to the orbital of the unpaired electron from (d_{xz},d_{yz}) to d_{xy}, i.e. $c \sim 1$, and indicating that d_{xy} was higher in energy than d_{xz} and d_{yz}, thus yielding the 'novel' electron configuration $(d_{xz},d_{yz})^4(d_{xy})^1$. Examples of systems for which this permutation of the assignment of *g*-values was found to be necessary included the bis-(imidazole) complex of octaethyl- and tetraphenylchlorinatoiron(III) [50], as well as the bis-(4-cyanopyridine) [26], bis-(*t*-butylisocyanide) [27] and bis-(2,6-xylylisocyanide) [28] complexes of TPPFe(III). Another type of complex that also appears to have this electronic ground state is that derived from *meso*-hydroxyoctaethylporphyrinatoiron(III) either by formation of the benzoyloxy esters [62] or by simple deprotonation of the hydroxy group to form the macrocycle known as an oxophlorin [63]. Bis-pyridine complexes ranging in basicity from 3,4-dimethylpyridine to 4-acetylpyridine have axial EPR spectra with $g_\perp$ ranging from 2.31 to 2.20 and $g_\parallel$ ranging from 1.73 to 1.90, respectively, and were originally interpreted as being π cation radicals of the Fe(II) macrocycle [62]. However, these *g*-values deviate much too much from 2.0 to represent porphyrin ligand-based unpaired electrons. As discussed in the NMR section below, there is obviously quite a bit of porphyrin $a_{2u}(\pi)$ character to the delocalized unpaired electron density, but based on the *g*-values (and the NMR spectra discussed below) the electron configuration of the six-coordinate oxophlorin complexes is low-spin Fe(III) with a $(d_{xz},d_{yz})^4(d_{xy})^1$ ground state. For the chlorin complexes the EPR spectra are rhombic with close spacing of the two largest *g*-values (g_{xx} and g_{yy}), while in all of the porphyrin complexes of this ground state the EPR spectra are axial (Table 1, type III). There are however, a number of cases for which V/Δ has been shown to be greater than 2/3 in systems that are unequivocally $(d_{xy})^2(d_{xz},d_{yz})^3$ ground states [64–67]. This calls into question the validity of the 'Proper Axis System' rule [50], and raises the question of whether low-spin iron(III) chlorins are indeed type III complexes with

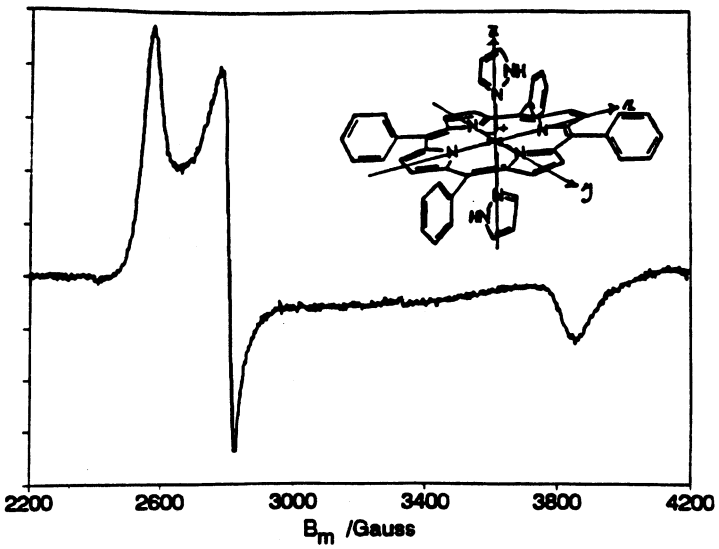

Fig. 7. CW EPR spectrum of 10^{-3} M $[TPPFe(PzH)_2]^+$ in a 1:2 methylene chloride-d_2:toluene-d_8 glass at 4.2 K [67]. The observation of a rhombic EPR spectrum indicates that the axial ligands are coplanar. Although the calculated rhombicity, V/Δ is 1.1 (see text), the ESEEM studies described in Figs. 8 and 9 show that indeed, the z magnetic axis is the normal to the porphyrinate plane [67]. Taken from reference [67] with permission from the American Chemical Society.

$(d_{xz},d_{yz})^4(d_{xy})^1$ ground states. As will be shown below, MCD data are consistent with this ground state for low-spin Fe(III) chlorins, while NMR data are entirely consistent with the opposite, $(d_{xy})^2(d_{xz},d_{yz})^3$, ground state.

4.3. The use of ESEEM spectroscopy to determine the relationship between the molecular frame and the orientation of the g-tensor

Two of the well-characterized complexes that provide the most clear cut violations of Taylor's proper axis system rule that have been discovered recently are the pyrazole (PzH) and 3-aminopyrazole (3-NH_2PzH) complexes of TPPFe(III), where the rhombic EPR parameters yield $V/\Delta = 1.1$ [66] and 1.2 [67], respectively. In each case, ESEEM studies have been utilized to determine the orientation of g_{zz}. What is actually done is to determine the intensity of the distant proton signal (which is mainly due to the β-pyrrole protons), at double the Larmor frequency as a function of magnetic field, as one traverses the EPR spectrum of the complex. Such an EPR spectrum, for the pyrazole complex of TPPFe(III) [66], is shown in Fig. 7. In Fig. 8 are shown the Fourier transforms of the ESEEM time-domain data, at three of the magnetic field positions of Fig. 7. The vertical line marks the position of double the proton Larmor frequency. As is clear from Fig. 8, the intensity of the proton sum frequency peak that are at twice the proton Larmor frequency changes as the field position of the ESEEM spectrum changes [66]. Plots of the calculated intensity

of this peak, that arises mainly from the β-pyrrole protons, for the cases of g_{zz} being the largest and the smallest g-value, together with the experimentally measured peak intensities, are shown in Fig. 9. As is clear, the intensity behavior of the proton sum frequency peak that is not shifted from twice the Larmor frequency clearly defines g_{zz} as the largest g-value, thus confirming that the electron configuration is $(d_{xy})^2(d_{xz},d_{yz})^3$ [66]. The orientation of the in-plane g-values, g_{xx} and g_{yy}, with respect to the axial ligand plane, can be obtained by similar analysis of the near proton (the α-H of the axial ligands) signals that are shifted to slightly higher frequency than double the Larmor frequency [66].

In further ESEEM studies of model ferriheme complexes [68], it became clear that while the orientation of g_{zz} was the same for all complexes studied (pyrazole [66], 3-aminopyrazole [67], 4-dimethylaminopyridine and imidazole complexes [68]), the orientations of g_{xx} and g_{yy} differ in a manner that suggested that as the axial ligands rotate counterclockwise from being eclipsed with the porphyrinate nitrogens, g_{xx} and g_{yy} rotate clockwise, as diagrammed in Fig. 10. We were also able to demonstrate theoretically that this should be the case for most ferriheme systems [69]. Hence, when the (parallel) axial ligands lie over the porphyrin nitrogens, their nodal planes are aligned along g_{xx}, while when they lie over the porphyrin *meso* positions, their nodal planes are aligned along g_{yy}. This finding has considerable importance for NMR studies of ferriheme proteins, where counter-rotation of the g-tensor had previously been assumed in calculating the pseudocontact (dipolar)

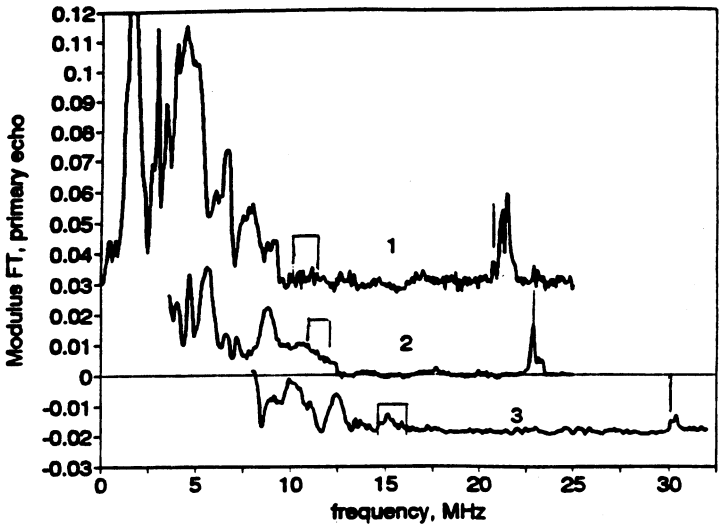

Fig. 8. FT-ESEEM spectra of $[TPPFe(PzH)_2]^+$ obtained at various magnetic fields: (1) 2440, (2) 2680 and (3) 3550 g [67]. The low-frequency part of the second and third spectra has been removed in order to avoid overlap with the first. Thin lines show the position of twice the proton Larmor frequency in each case. The peaks at larger frequency than this were shown to be due to the nearest protons, the α-H of the axial pyrazole ligands. Open squares mark the expected position of fundamental frequencies for distant protons. Taken from reference [67] with permission from the American Chemical Society.

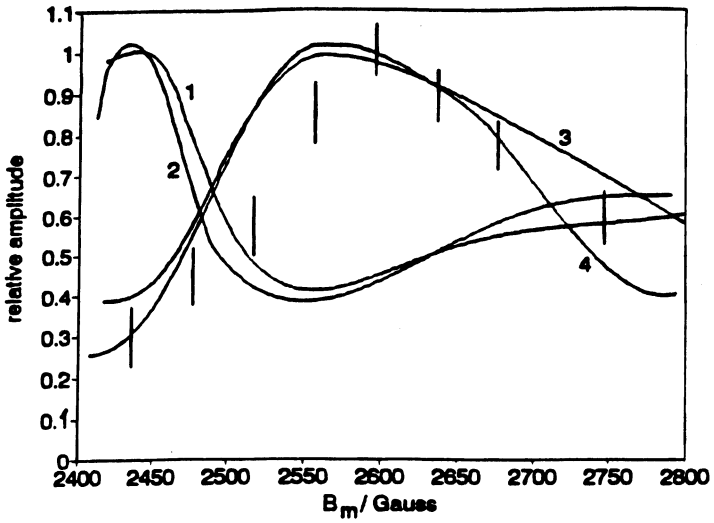

Fig. 9. Experimental (bars) and calculated (solid lines) magnetic field strength dependences of the amplitude of the distant proton v_+ peaks [67]. Parameters used for calculations are (curves 1 and 2) $g_{xx} > g_{yy} > g_{zz}$ and (curves 3 and 4) $g_{zz} > g_{yy} > g_{xx}$. The hyperfine coupling constant, a equals 0 MHz for curves 2 and 4 and -1 MHz for curves 1 and 3. Calculations include eight equatorial β-pyrrole protons of the porphyrinate, eight *ortho*-phenyl protons, and four distant protons of the two pyrazole ligands. The planes of both pyrazole rings are aligned along the x-axis of the coordinate frame shown in Fig. 7. Taken from reference [67] with permission from the American Chemical Society.

contributions to the isotropic shifts of the protons and carbons of the heme [70], and now can be expected in almost all cases [69]. The use of NMR spectroscopy to determine the orientation of the g- or χ-tensor of ferriheme proteins will be discussed in Section 7.10.

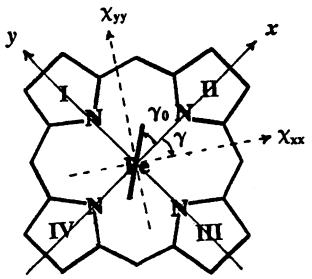

Fig. 10. Heme ring with definition of axes (right-hand coordinate system) and axial ligand rotation angle, γ_0, and position of the magnetic axis χ_{xx} (or g_{xx}) if counter-rotation by an angle γ takes place. If the axial ligand plane is aligned along the x-axis of the heme group, then the expectation is that the minimum magnetic susceptibility tensor component χ_{xx}, will be aligned coincident with the axial ligand plane, along the molecular x-axis. As the ligand rotates counterclockwise, χ_{xx} rotates in a clockwise direction in the majority of cases. Taken from reference [70] with permission from the American Chemical Society.

It is worth mentioning that all of the ESEEM measurements mentioned above were performed at the low edge of X-band frequency, (8.4–8.7 GHz). At this frequency it was not possible to utilize measurements at the very informative canonical high-field extreme of the EPR spectrum because of the loss of resolution between the double-frequency lines of the nearby and distant protons. This problem has now been overcome by developing an ESEEM spectrometer that operates at S-band (3–3.8 GHz) and C-band (1.8–2.4 GHz). Use of these lower frequencies now substantially facilitates data analysis and simulations to the high-field limit of the EPR spectrum, and we have been able to extend our studies over the entire EPR spectral range to heme proteins having g_{xx} values of less than 1.5 [72].

4.4. Strongly saddled ferriporphyrinates versus the power of the Jahn–Teller effect

As mentioned in Section 3, the highly substituted synthetic porphyrins such as octaethyltetraphenylporphyrin have porphyrinate cores that are strongly distorted from planarity in a saddled conformation, with opposite pyrrole rings tipping down and the two adjacent pyrrole rings to those tipping up, as shown in Fig. 4d. The tipping of the pyrrole rings is so extreme that not only non-hindered imidazoles, but also pyridines and even hindered imidazoles (2-MeImH) can bind lying over the N_P–Fe–N_P bonds in perpendicular planes. The EPR spectrum of [OETPPFe(2-MeImH)$_2$]$^+$ is that of a 'large g_{max}' type I center [34]. However, the EPR spectrum of the bis-*N*-methylimidazole analog exhibits two overlapping spectra—that of the 'large g_{max}' type I center, as expected from the X-ray crystal structure, as well as that of a normal rhombic type II center [34]. Because of the difference in relaxation properties of these two signals, it is not possible to quantitate the relative abundance of the types I and II centers in the frozen methylene chloride solution. Molecular modelling experiments suggest that each non-hindered imidazole ligand could potentially rotate from the N_P–Fe–N_P vector by up to 15° [34]. If the two ligands rotated in the same direction by 15° as the solution is frozen, then their relative plane orientations would remain 90°, and the EPR signal would be a 'large g_{max}' (type I) signal, as expected in the absence of this rotation. However, if the two ligands rotated in opposite directions by 15° as the solution is frozen, then their relative plane orientation would be 60°, and this should be sufficient to lift the degeneracy of the d_{xz} and d_{yz} orbitals, hence producing the rhombic (type II) EPR signal. The existence of this rhombic EPR spectrum as one of the two spectral components indicates the power of the Jahn–Teller effect in controlling structure in order to remove the degeneracy of the d_{xz} and d_{yz} orbitals.

4.5. Ambiguities in electronic ground state

Iron chlorin complexes, such as [TPCFe(ImH)$_2$]$^+$ [71], as well as the low-spin Fe(III) forms of cytochromes P450 [78], have been particularly problematic in defining their electronic ground state. The violation of Taylor's 'proper axis system' rule [50] is only moderate for low-spin P450s ($V/\Delta = 0.97$ for P450-2-PhImH, Table 1), and single crystal EPR measurements clearly show the z-axis to be the normal

to the heme plane [64]. In comparison, on the basis of his 'proper axis system' rule Taylor assigned the electronic ground state of $[TPCFe(ImH)_2]^+$ to be $(d_{xz},d_{yz})^4(d_{xy})^1$ [50], with the z-axis thus in the plane of the macrocycle. We have found that ESEEM data are more consistent with the z-axis being in the porphyrinate plane than along its normal (although the data are not completely unequivocal) [72], but NMR data to be discussed below are consistent with the $(d_{xy})^2(d_{xz},d_{yz})^3$ ground state over the temperature range $-90-+30$°C [73]. Interestingly, the magnitudes of the three g-values of the chlorin complex $[OECFe(ImH)_2]^+$ (2.51, 2.37, 1.71) [71] and heme d_1 of cytochrome cd_1 of some of the dissimilatory nitrite reductases (2.50–2.56, 2.42–2.43, 1.70–1.71) [7,10] are very similar to those of $[TPPFe(PzH)_2]^+$ (2.64, 2.36, 1.71) [66], yet the ground state of the former has been assumed [50] to be different from that determined for the latter [66]. Continued study of the chlorin complexes will be required to confirm that this difference in ground state is, in fact, real. In both of these cases, it seems that the low-temperature EPR data (Table 1) *could* be consistent with *either* assignment. Mössbauer data for low-spin P450s, discussed below, do not clarify this question, and the magnetic Mössbauer spectra of $[TPCFe(ImH)_2]^+$ have not been reported. However, those of the d_1 heme of the dissimilatory nitrite reductase of *Thiobacillus denitrificans* have been reported [7] and are consistent with the $(d_{xz},d_{yz})^4(d_{xy})^1$ ground state (see below, Section 5.5). Low temperature MCD spectra, however, are only consistent with the $(d_{xz},d_{yz})^4(d_{xy})^1$ ground state for iron chlorins, but not the $(d_{xy})^2(d_{xz},d_{yz})^3$ ground state for low-spin forms of cytochrome P450 (see below, Sections 6.3 and 6.4).

4.6. Summary of EPR findings

At the present time, then, we know that there are two quite distinct, limiting ground states for low-spin iron(III) porphyrinates that give rise to three different types of EPR spectra: (a) the generally observed $(d_{xy})^2(d_{xz},d_{yz})^3$ state, for which $g_{zz} > g_{yy} > g_{xx}$ and for which the EPR spectra may be either rhombic or 'large g_{max}' in appearance, depending on the relative orientation of planar axial ligands, but in each case with g_{zz} along or near the normal to the heme plane, and; (b) the novel $(d_{xz},d_{yz})^4(d_{xy})^1$ state, for which g_{xx} ca. $g_{yy} > g_{zz}$, where the d_{xz},d_{yz} pair are degenerate, or nearly so, and *below* the d_{xy} orbital in energy. In this case, g_{zz} is aligned in the heme plane, and g_{xx} is presumably aligned along the plane normal (or else g_{xx} and g_{yy} are each aligned at 45° angles to the heme normal). For symmetrical porphyrinate rings, this latter electronic state leads to an *axial* EPR spectrum, with $2.6 \geq g_{\perp} > 2 > g_{\parallel}$ [18,26], and $g_{\parallel}$ may not be resolved due to g-strain.

5. Mössbauer spectroscopy of low-spin ferriheme models and proteins

Mössbauer spectra of ferriheme complexes have been reported for quite some time. Many reports include only the data obtained in the absence of a magnetic field, and usually consist of the isomer shifts, δ, and quadrupole splittings, ΔE_Q,

measured at 77 K or above. The quadrupole splittings are often somewhat temperature-dependent, making their values reported at one or two temperatures not terribly valuable in a quantitative sense for assignment of the electronic ground state. Furthermore, as with the case of g-values, only the absolute value of the quadrupole splitting is obtained from Mössbauer spectroscopy in the absence of a magnetic field. Fewer systems have been carefully characterized at 4.2 K in the presence of a magnetic field of 20–60 kG (2–6 Tesla), where the magnetic hyperfine interaction is well-resolved and theoretical fits of the spectra provide the sign and magnitude of ΔE_Q as well as the hyperfine coupling constants A_{xx}, A_{yy} and A_{zz}.

5.1. Theory

Oosterhuis and Lang derived the expressions for the magnetic hyperfine interaction in magnetic Mössbauer spectra in terms of the orbital coefficients a, b, and c (Eqs. (1)–(5)) and the Fermi contact covalency factor κ [74]. Reformulation of these expressions in terms of the axis system of Taylor [50] yields the following expressions:

$$A_{xx} = P[-4bc - (1+\kappa)(a^2 - b^2 - c^2) + (3/7)(a^2 - 3b^2 - 3c^2) + (6/7)a(b+c)] \quad (9)$$

$$A_{yy} = P[+4ac - (1+\kappa)(a^2 - b^2 + c^2) + (3/7)(3a^2 - b^2 + 3c^2) - (6/7)b(a+c)] \quad (10)$$

$$A_{zz} = P[+4ab - (1+\kappa)(a^2 + b^2 - c^2) + (3/7)(3a^2 + 3b^2 - c^2) - (6/7)c(a+b)] \quad (11)$$

where $P = 620$ kG and $\kappa = 0.35$ [74]. These expressions can then be used to help predict the values of A_{xx}, A_{yy} and A_{zz}, and thus help speed the task of fitting the experimental magnetic Mössbauer spectra. The best fitted values are usually 10% [25] or in some cases as much as 30% [28] smaller than predicted by Eqs. (9)–(11), due to covalency of the Fe–ligand bonds.

Thus, a combination of EPR and magnetic Mössbauer spectra can insure that the orbital coefficients can be calculated and the d-orbital in which the unpaired electron is located can be determined. While orbital coefficients and d-orbital energies calculated from Eqs. (4), (6) and (7) have often been reported and analyzed, until recently there has been little systematic analysis of either the estimated or fitted values of the hyperfine coupling constants for low-spin ferriheme centers. We have recently tried to systematize these data [25], as discussed below.

5.2. Experimental findings

Other than three studies of model hemes having $(d_{xy})^2(d_{xz},d_{yz})^3$ ground states that exhibit 'large g_{max}' EPR spectra having only one resolved feature [15,17,25], the recent studies of the bis-(isocyanide) complexes having $(d_{xz},d_{yz})^4(d_{xy})^1$ electronic ground states [27,28], a number of ferriheme proteins having 'large g_{max}' or 'C Hemichrome' spectra [75–77], several model ferriheme bis-(isocyanide) complexes

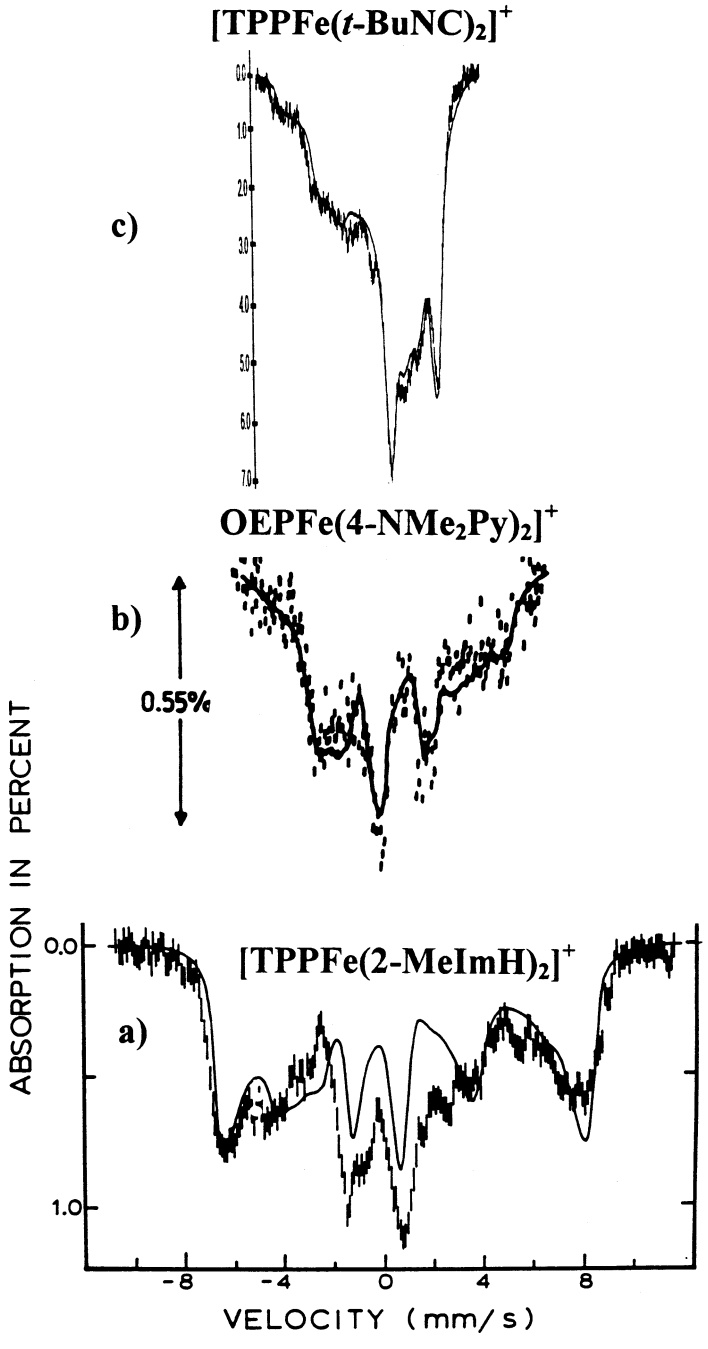
[TPPFe(t-BuNC)2]+
c)
OEPFe(4-NMe2Py)2]+
b)
0.55%
ABSORPTION IN PERCENT
0.0
[TPPFe(2-MeImH)2]+
a)
1.0
-8
-4
0
4
8
VELOCITY (mm/s)

Fig. 11.

having axial EPR spectra [27,28], several low-spin forms of cytochrome P450 [78], and the cytochrome cd_1 hemes of *T. denitrificans* [7], to our knowledge, few other reports of the magnetic Mössbauer spectra of low-spin Fe(III) porphyrinates and ferriheme proteins have appeared. The published data are summarized in Table 1. Debrunner stated some time ago that, on the basis of results obtained up to 1989, no meaningful correlation can be established between the Mössbauer parameters and the axial ligands beyond that incorporated in the 'truth table' of Blumberg and Peisach [46,77]. With the results of our recent study [25], we have been able to find several correlations that should be useful to future workers, although more are still being sought for the $(d_{xz},d_{yz})^4(d_{xy})^1$ systems. The 'large g_{max}', or type I, magnetic Mössbauer spectra are easiest to analyze, because A_{zz} dominates the spectra [15,17,25], as shown in Fig. 11a, and can be estimated from the total spread of the spectrum. The most difficult spectra to analyze are those which give well-resolved rhombic EPR spectra and have $(d_{xy})^2(d_{xz},d_{yz})^3$ electronic ground states, type II in Table 1, Fig. 11b. Type III complexes, those having the $(d_{xz},d_{yz})^4(d_{xy})^1$ ground state, have relatively well-resolved EPR spectra but may have poorly resolved magnetic Mössbauer spectra, as shown in Fig. 11c. Qualitatively, the sign of ΔE_Q can sometimes be correctly predicted by noticing whether the features on the right or left side of the spectrum are broader. If the right-hand (higher energy) side is broader, the sign of ΔE_Q is usually positive and the electron configuration is $(d_{xy})^2(d_{xz},d_{yz})^3$, while if the left-hand (lower energy) side is broader, the sign is usually negative and the electron configuration is $(d_{xz},d_{yz})^4(d_{xy})^1$. The same relative broadness and sharpness usually carry over to the quadrupole doublets measured at higher temperatures in the absence of a magnetic field. It is interesting to note that the quadrupole doublets for five of six TMPFe(III) complexes of substituted pyridines or imidazoles (*N*-MeIm, 2-MeImH, 4-NMe_2Py, 3-EtPy, 3-ClPy, 4-CNPy) [17,18], all but one (*N*-MeIm) of which gave one-feature (large g_{max}) EPR signals, but with decreasing g-value [18], have the right-hand side of the doublet broader than the left (and are known or believed to have $(d_{xy})^2(d_{xz},d_{yz})^3$ ground states [18]), while the fourth pyridine complex (4-CNPy) has the two members of the quadrupole doublet of equal width, the smallest value of $|\Delta E_Q|$ [18], and is known to have the $(d_{xz},d_{yz})^4(d_{xy})^1$ ground state [29]. Interestingly, we have not been able to obtain and analyze the proton sum frequency peaks in the ESEEM spectrum of $[TMPFe(4\text{-}CNPy)_2]^+$ or the TPPFe(III) analog in order to determine the orientation of g_{zz} because of the extremely strong nitrogen modulation observed for this complex, which undoubtedly results from the mixing of $a_{2u}(\pi)$ character, with its

Fig. 11. Mössbauer spectra of (a) type I $[TPPFe(2\text{-}MeImH)_2]^+$ in dimethylformamide recorded at 4.2 K with an external magnetic field of 60 kG applied parallel to the γ-beam. The central two lines are more intense than expected due to a quadrupole doublet resulting from a fast-relaxing low-spin ferric species [15]. (b) type II $[OEPFe(4\text{-}NMe_2Py)_2]^+$ in a wax suspension recorded at 4.2 K in a 60 kG applied magnetic field [17]. (c) type III $[TPPFe(t\text{-}BuNC)_2]^+$ in frozen chlorobenzene solution at 25 K in a 43 kG magnetic field applied parallel to the γ-beam [27]. The solid lines are simulations based on a spin Hamiltonian in the limit of slow spin fluctuations with the parameters listed in Table 1. Modified from the three referenced works.

very large spin densities at the porphyrin nitrogens (Fig. 1), due to ruffling of the porphyrinate ring (Fig. 2). This result is thus consistent with the $(d_{xz},d_{yz})^4(d_{xy})^1$ ground state, although it is not proof of it.

The typical magnetic Mössbauer spectra shown in Fig. 11 can be fit using the values of A_{xx}, A_{yy} and A_{zz} determined from Eqs. (9)–(11), or equivalently, the three g-values, as starting points. Other fitting parameters include the two sets of Euler angles that relate the orientation of the electric field gradient tensor to the quadrupole tensor and the quadrupole tensor to the hyperfine tensor, and the inherent linewidth, Γ. Fits can be obtained most easily for systems that have either fast or slow relaxation of the magnetic states of the ^{57}Fe nucleus, although cases of intermediate rates of nuclear relaxation have been found and treated theoretically recently [28]. Fast relaxation typically occurs for concentrated samples (i.e. powdered natural-abundance samples) at 77 K and above, while slow relaxation typically occurs for dilute samples (i.e. ^{57}Fe-enriched samples in frozen solution) at 4.2 K. By varying the fitting input parameters one can obtain a best fit that yields not only these quantities but also the best value (and sign) of the isomer shift, δ, and the quadrupole splitting, ΔE_Q.

Determinations of the structures of a series of $[(TMP)Fe(L)_2]ClO_4$ complexes in which L is a pyridine (4-NMe_2Py [17], 3-EtPy, 3-ClPy, 4-CNPy and 3-CNPy [18]) or imidazole (*N*-MeIm [17] or 1,2-Me_2Im [24]) confirmed that, as expected from their 'large g_{max}' EPR spectra [17,18], both pyridine and hindered imidazole ligands are aligned in perpendicular planes. However, in a recent study of several complexes of $[\{2,6\text{-}(OCH_3)_2\}_4TPPFeL_2]^+$, where L = 2-MeImH, *N*-MeIm, and 4-NMe_2Py, we showed that the slightly smaller size of the 2,6-$(OCH_3)_2$ substituents as compared to methyls permitted this porphyrinate to have the 4-NMe_2Py ligands in parallel planes, thus producing a type II complex, based upon the EPR and Mössbauer spectra [25]. The unhindered complex $[OEPFe(4\text{-}NMe_2Py)_2]^+$ also has its 4-NMe_2Py ligands in parallel planes and is a type II complex [17], Fig. 11b.

5.3. Summary of Mössbauer data for type I and II centers

Based on the data summarized in Table 1, we arrive at the conclusion that type I centers, in which the axial ligands are in perpendicular planes and only one EPR feature is observed, with g −3.4–3.6, have ΔE_Q values ranging from +1.8 to +1.2 mm s^{-1} and very large A_{zz} (800–1000 kG), while A_{xx} is less than half the magnitude of A_{zz} and of opposite sign, and A_{yy} is the smallest but is not well determined due to insensitivity of the fitting of the spectra to this parameter. For type II centers, in which the axial ligands are in approximately parallel planes (or in the case of cytochrome *c*, where the methionine dominates the ligand effects), the EPR spectra are rhombic and the Mössbauer spectra have larger values (+2.1 to +2.4 mm s^{-1}) of ΔE_Q than for type I complexes and still show A_{zz} to be largest (except for P450 low-spin species), but in these cases its value ranges from 410–660 kG (except for P450 low-spin species). A_{xx} is still of opposite sign, and for the bis-nitrogen donor systems its value is of similar magnitude to that of A_{zz}. A_{yy} is again quite small, tending toward zero. A smooth and continuous correlation is

found between A_{zz} and $|g_{zz}|$ and between A_{zz} and V/Δ for types I and II low-spin ferriheme centers [25], as shown in Fig. 12.

5.4. Ambiguous systems

The low-spin Fe(III) complex of cytochrome P450 and its 2-phenylimidazole complex are the most extreme examples of type II complexes, if they are type II. There have been several reports of the assignment of the largest g-value as g_{zz} [79–81], but on closer inspection, some of these reports are not unequivocal. Some investigators have *assumed* that the largest g-value is g_{zz} [80,81], but Debrunner's

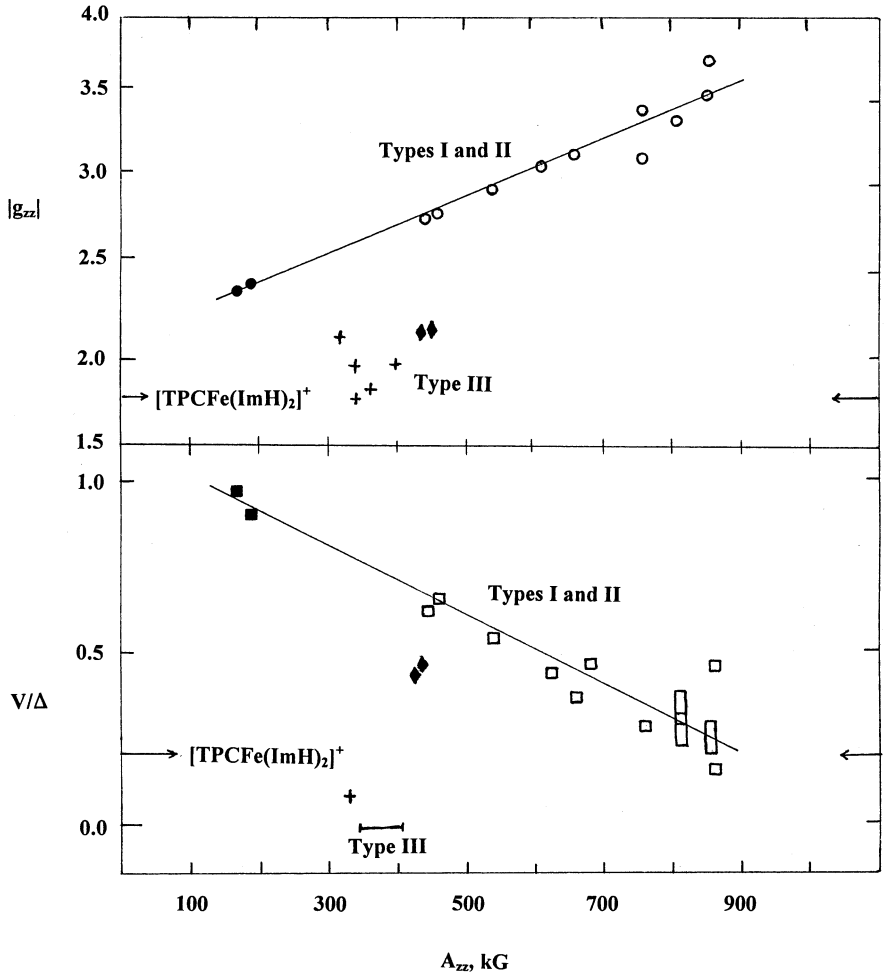

Fig. 12. Correlation of $|g_{zz}|$ and the rhombicity, V/Δ, obtained from EPR g-values, with the largest hyperfine coupling constant, A_{zz}, obtained from fits of magnetic Mössbauer spectra [25]. Open symbols: types I and II centers; solid symbols: cytochrome P450; crosses: type III centers.

former student Devany carried out single crystal EPR measurements that confirm that this is so for the low-spin substrate-free and substrate-bound forms [64]. The Mössbauer spectral type is that of Fig. 11c, broader on the left-hand (lower energy) side, and the quadrupole splitting is quite large in magnitude (2.85 mm s^{-1}), the largest of any type II complex reported thus far. The values of A_{zz} determined for these species are the smallest reported for type II complexes, and they are smaller than A_{xx} by more than a factor of 2. The cytochrome P450 low-spin species and its 2-phenylimidazole complex do fit on the extended correlation lines of Fig. 12 as $(d_{xy})^2(d_{xz},d_{yz})^3$ ground state type II centers. However, as pointed out by Debrunner earlier [78], permutation of the axes (to create a $(d_{xz},d_{yz})^4(d_{xy})^1$ type III ground state) is also consistent with the Mössbauer spectra, and leads to a negative value of ΔE_Q [78], as found for the bis-(*t*-butylisonitrile) complexes of TPPFe(III) (-1.89 mm s^{-1}) and OEPFe(III) (-1.80 mm s^{-1}) [27] and the bis-(2,6-xylylisonitrile) complexes of several TPPFe(III) derivatives (-1.81 to -1.99 mm s^{-1}) [28]. This change in electronic ground state makes A_{zz} the largest hyperfine coupling constant, as shown in the type III portion of Table 1. This assignment also fits the clustered group of points in the correlation between $|g_{zz}|$ and A_{zz} for type III complexes, Fig. 12. An attempt at a correlation between V/Δ and A_{zz} for type III species and the low-spin cytochromes P450 is rather meaningless because of the large number of axial-EPR species for which $V/\Delta = 0$, but is included in Fig. 12. Thus, it could be that cytochromes P450 are poised between these two electronic ground states, and although the species listed in Table 1 appear to be type II species, based upon the single crystal EPR data [64], their Mössbauer spectra are shaped like those of type III species, similar to that of Fig. 11c.

We have shown previously that for other $(d_{xz},d_{yz})^4(d_{xy})^1$ centers, there is significant delocalization of the unpaired electron from the metal d_{xy} orbital to the porphyrinate $a_{2u}(\pi)$ orbital due to Por $\Rightarrow$ Fe π-donation when the porphyrinate core is highly ruffled, and it is possible that such ruffling could account for some of the properties of the compound I state, where the heme center is 2-electrons more oxidized than the Fe(III) resting state. However, existing 3-dimensional structures of cytochromes P450 where the heme is mainly in the high-spin Fe(III) resting state do not show the porphyrinate ring to be nearly as strongly ruffled as some of the simple cytochromes, such as cytochrome *c* [30,82], and both low-temperature MCD [83] and room temperature NMR [84,85] data are indicative of the $(d_{xy})^2(d_{xz},d_{yz})^3$ ground state.

5.5. Unambiguous type III centers

For the 'non-hindered' tetraphenylporphyrinate complex [(TPP)Fe(4-CNPy)$_2$]ClO_4 [26] Fig. 4c, it was shown that for axial ligands that have strong π-acceptor properties there is an *electronic* stabilization of the $(d_{xz},d_{yz})^4(d_{xy})^1$ ground state, resulting in *g*-values of 2.6 and 0.9 [26]. The isocyanide complexes of Fe(III) porphyrinates were then found to have axial EPR spectra with both *g*-values much closer to 2.0, and the magnetic Mössbauer spectra clearly showed that the quadrupole splitting was large and negative [27,28]. The results were

interpreted in terms of a nearly 'pure' $(d_{xz},d_{yz})^4(d_{xy})^1$ electronic ground state with significant (10–34% depending on porphyrin substituents) delocalization of the unpaired electron to the $a_{2u}(\pi)$ orbital by Por⇒Fe π-donation [25,26]. In reference [27] it was pointed out that magnetic Mössbauer spectroscopy is one of the most sensitive tools for defining the d-electronic ground state of low-spin iron(III) porphyrinates.

The dioxoisobacteriochlorin ligand of heme d_1 of cytochrome cd_1 of *T. denitrificans* [7], Table 1, type III, clearly appears to be a type III center. This was not realized at the time of the original publication of the magnetic Mössbauer study, and g_{zz} was assumed to be the largest g-value [7]. Thus, use of Eqs. (9)–(11) yielded $A_{zz} = +190$ kG, $A_{yy} = +170$ kG and $A_{xx} = -290$ kG, which the authors pointed out were inconsistent with the experimental results (Table 1, type III). However, if g_{zz} is assigned to the smallest g-value, with the sign convention being that g_{zz} and g_{xx} are negative [50], then the calculated values of A_{zz}, A_{yy} and A_{xx}, on the basis of Eqs. (9)–(11), are 436, 228 and −265 kG, respectively. The measured A-values are smaller than these (A_{zz}(obs) = 73%A_{zz}(calc)), probably as a result of covalencey of the metal-ligand bonds. A_{yy} is predicted to be positive for either ground state, whereas the measured value is negative (Table 1). However, in our experience, the fitting of the magnetic Mössbauer spectra is rather insensitive to the value of A_{yy}. Added to this is the difficulty of deconvoluting the spectrum of the heme d_1 center in the presence of the heme c center. Unfortunately, to our knowledge, no report of the magnetic Mössbauer spectra of an iron(III) chlorin or isobacteriochlorin has appeared, and thus we cannot generalize from the dioxoisobacteriochlorin of heme d_1 to the chlorin of heme d and the isobacteriochlorin of siroheme. Therefore, further magnetic Mössbauer studies, especially of the last two types of ferriheme centers, should be carried out. In addition, since there appears to be structural diversity among the cytochromes cd_1 from various bacteria [9,10], magnetic Mössbauer studies of additional proteins of this class should be carried out.

For other type III centers, including iron(III) chlorins, axial ligand plane orientation (if there are ligand planes) appears not to be very important; the EPR spectra are axial if the ligands have no planes or if the planar ligands are oriented perpendicular to each other, or else the spectra are rhombic, with the two largest g-values being quite close together, as in the case of the 'green hemes' [50,86–89] and proteins that contain them [89,90]. In these cases, the rhombic splitting may be a result of the asymmetry of the macrocycle, although this has not yet been proven unambiguously. From our limited data (only P450 [78] in the re-arranged axis system, heme d_1 from *T. nitrificans* and $[TPPFe(RNC)_2]^+$ [27,28]) A_{zz} is smaller yet (300–400 kG), A_{xx} varies from smaller to larger than A_{zz}, and we cannot yet make any conclusions about A_{yy}.

5.6. Summary of Mössbauer findings

In terms of the problem posed by Debrunner [77]—that no pattern in EPR/Mössbauer data for low-spin ferrihemes other than the Blumberg–Peisach 'truth diagrams' had yet emerged as of 1989—we have made some simple correlations

between Mössbauer and EPR data[25]. First, there is a direct correlation between the size of $|g_{zz}|$ and A_{zz} for $(d_{xy})^2(d_{xz},d_{yz})^3$ systems, types I and II, as shown in Fig. 12. This correlation is a result of the relationship between Eqs. (1)–(5) and (9)–(11), and should have been evident earlier, except for the scatter in the data reported. Also, for systems in which it is possible to define with certainty the values of g_{xx} and g_{yy} for type I centers, there is a correlation between the rhombicity, V/Δ,and A_{zz}, but for many of the systems reported in the literature it is not clear how the two smallest g-values were determined. 'Large g_{max}' EPR spectra are notorious for exhibiting signals due to extremely minor species, as shown in Fig. 5a, that may appear more intense (in the derivative mode) than that of the g_{max} species, because of the difference in relaxation properties and g-strain for the impurities as compared to the 'large g_{max}' species. Therefore, it is risky to estimate g_{xx} and g_{yy} from the continuous wave EPR spectrum of frozen solution or polycrystalline samples without confirming magnetic Mössbauer spectral data. However, even in this case there is some uncertainty, because the fits for type I complexes are much less sensitive to the values of A_{xx} and A_{yy} (the very components that are usually missing from the EPR spectra) than to A_{zz}. In some cases the value of g_{yy} can be 'bracketed' within a certain range and the corresponding estimate of g_{xx} can be obtained from Eq. (8). In fact, on the basis of unreasonably large value of Δ/λ for some sets of g-values chosen in this way, it is possible to rule out such combinations of g-values. This is because most bis-(imidazole) ferriheme complexes studied to date have values of Δ/λ in the range of 2.9–3.3 [15,17,20,22,25,42–46,91]. Thus, the rhombicities and tetragonalities reported for many type I systems may not be very reliable. In our experience, g_{yy} is always less than 2.0 for 'large g_{max}' species, which calls into question the EPR data for $[PPIXFe(CN)_2]^-$ [76], Table 1. Since the fits of type I centers are not very sensitive to the values of g_{xx} and g_{yy}, the values of A_{xx} and A_{yy} reported are likely fairly insensitive to the choice of these two g-values. However, the rhombic splittings, tetragonalities and rhombicities certainly are sensitive to the values of g_{xx} and g_{yy}, thus making it difficult to detect trends. However, cytochrome $P450_{cam}$ and its 2-phenylimidazole complex are *not* such cases, since all three g-values are well resolved, and it appears that although the correlations shown in Fig. 12 would support either electronic ground state, the single crystal EPR data [64] indicate that the $(d_{xy})^2(d_{xz},d_{yz})^3$ configuration is the electronic ground state of this system, in spite of the V/Δ value being somewhat greater than 2/3 and the Mössbauer spectral shape being that of a type III complex. Furthermore, for the $(d_{xz},d_{yz})^4(d_{xy})^1$ ground state species, where the rhombic splitting is either zero or negative and the Tetragonality is also negative, while the rhombicity is either zero or positive, it is not clear how the EPR and Mössbauer data should be treated in order to be consistent with the $(d_{xy})^2(d_{xz},d_{yz})^3$ ground state species of the Blumberg–Peisach truth diagrams [46]. Nevertheless, the correlations between A_{zz} and either g_{zz} or V/Δ shown in Fig. 12 are remarkably good for the $(d_{xy})^2(d_{xz},d_{yz})^3$ ground state species, and at least appear to produce a reasonable cluster for type III complexes.

6. Low-temperature MCD studies of low-spin ferriheme models and proteins

It has long been known that the ultraviolet and visible region electronic spectra of heme proteins are dominated by the $\pi-\pi^*$ transitions of the porphyrin ring [92,93]. The electronic states of the iron mix with those of the porphyrin π-system making the form of the corresponding magnetic circular dichroism (MCD) spectrum diagnostic of the oxidation and spin-state of the metal ion [94]. Additionally, because it is relatively insensitive to vibrational transitions [95], MCD spectroscopy can be used to observe the electronic transitions of protein-bound hemes in the near-infrared (NIR) region between 1000 and 2500 nm where the absorption spectrum is dominated by vibrational bands. This spectral region has proved especially informative in the case of low-spin ferric hemoproteins because it contains a porphyrin(π) $\Rightarrow$ ferric(d) ($a_{1u} \Rightarrow e_g$) charge transfer (CT) transition, the wavelength of which varies as a function of the energies of the acceptor d-orbitals. The peak wavelength of the transition is consequently diagnostic of the nature of the axial ligands bound to the ferric ion. The correlation can conveniently be expressed as an 'additivity rule' whereby a specific axial ligand is assigned an energy parameter that is independent of the nature of the second ligand. The peak energy of the NIR-CT band is then given simply by the sum of the two appropriate parameters [94,96]. In many cases, the NIR-CT band energy is in itself sufficient to identify the two protein derived heme ligands. Where ambiguity arises, the EPR spectrum is usually sufficient to resolve the assignment. As we will see below, MCD spectra are dominated by the same orbital coefficients $a-c$ that determine the EPR g-values (Eqs. (1)–(5)) and Mössbauer hyperfine couplings (Eqs. (9)–(11)).

The intensities of the NIR-MCD spectra of low-spin ferric hydroporphyrins are significantly lower than those found for analogous iron-porphyrin species. An initial MCD study of the heme cd_1 from a dissimilatory nitrite reductase failed to detect any NIR-CT bands from heme d_1 against the background of intense bands from the c-type heme also present [97], although a more detailed recent study has been able to assign a weak transition to the heme d_1 center of *Pseudomonas stutzeri* (ZoBell) [10]. The low-spin ferric forms of heme d and heme d_1 both give unusual EPR spectra which suggest atypical electronic properties. The intensity of the NIR-CT MCD band of 'normal' low-spin ferric porphyrins is governed by the symmetry at the ferric ion, which is largely determined by the nature and orientation of the axial ligands [98]. It has been suggested that the weak NIR-CT MCD bands of low-spin ferric chlorins result from the loss of the 4-fold symmetry of the macrocyclic π-system which causes a rhombicity *at the ferric ion* greater than is encountered with ferric porphyrins [99,100]. However, such an interpretation does not find support in data reported for other modified porphyrins. A study of three low-spin TMPFe(III) complexes, one each of types I, II and III [29], showed that low NIR-CT MCD intensities can actually result from differences in the electronic character of low-spin ferric ion in porphyrins and chlorins that do not depend on the symmetry of the macrocycle. It was found that the unusual $(d_{xz},d_{yz})^4(d_{xy})^1$ ferric ion electronic ground state can alone lead to reduced NIR-CT band intensities if the 'correct' axial ligands are chosen [29]. Such a ground state is consistent with the

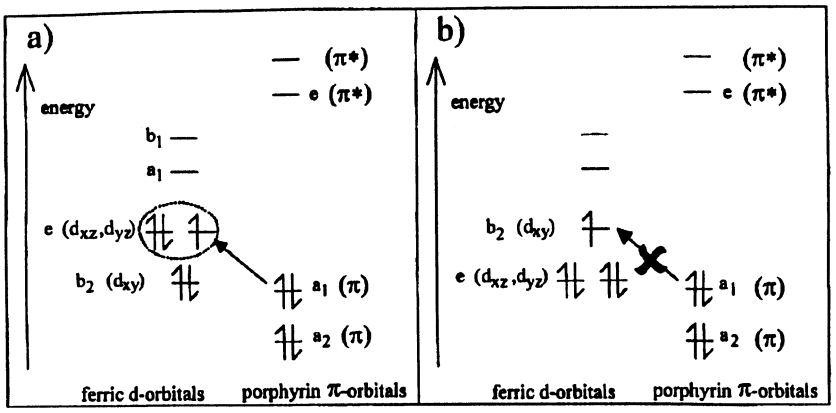

Fig. 13. One-electron energy level scheme for low-spin ferriheme illustrating the porphyrin (π) ⇒ ferric (d) near-infrared charge-transfer (NIR-CT) band. The transition is (a) allowed and *xy* polarized for a pure $(d_{xy})^2(d_{xz},d_{yz})^3$ ground state, but (b) symmetry-forbidden for a pure $(d_{xz},d_{yz})^4(d_{xy})^1$ ground state. The orbitals are labeled according to D_4 symmetry. Taken from reference [29] with permission from the American Chemical Society.

unusual EPR spectra of the type observed for low-spin ferric chlorins [50,86–89] and dioxoisobacteriochlorins [7,10]. These results were obtained not using ferric reduced hemes, but with a 4-fold symmetric ferric *porphyrin* in combination with appropriate axial ligands [29]. Thus, the chlorin or dioxoisobacteriochlorin structures appear to favor a ferric $(d_{xz},d_{yz})^4(d_{xy})^1$ ground state, but are not a prerequisite for its occurrence. These three TMP complexes thus provided the opportunity to compare spectroscopically each type of $(d_{xy})^2(d_{xz},d_{yz})^3$ ground state both with the other and with the $(d_{xz},d_{yz})^4(d_{xy})^1$ ground state [29]. Importantly, this was achieved using a single porphyrin system in which 4-fold symmetry of the π-system is maintained through the use of identical substituents at the four *meso* positions [29].

6.1. Theory of NIR-CT MCD spectra of low-spin ferriheme systems

The low-spin ferric heme NIR transition involves a charge-transfer between orbitals on different centers, namely the porphyrin π-orbitals and the ferric d-orbitals [29]. It can only have non-zero intensity if mixing of orbitals occurs between the two centers. In the case of the heme system considered here, mixing can occur between the 4e(π*) porphyrin orbitals and the metal $e(d_{xz},d_{yz})$ orbitals (Fig. 13). It is assumed that the orbital *x*- and *y*-components mix to an equal extent characterized by a first-order mixing coefficient. Thus the a_1,a_2(porphyrin-π) ⇒ $e(d_{xz},d_{yz})$ charge-transfer transitions borrow intensity from the a_1,a_2(porphyrin-π) ⇒ e(π*) transitions which are responsible for the visible and Soret bands of heme spectra, as shown in Fig. 14. The dipole strength of these π–π* bands is $D_{por} = 1/3|\, m\, |^2$ where *m* is an electric dipole matrix element, $< a_1,a_2|\, m_x\, |e >$, between the ground and excited states. The charge-transfer transition is allowed by symmetry to the d_{xz},d_{yz} set but not to the d_{xy} orbital, Fig. 13. Consequently, *a* and *b*, the Taylor coefficients

for the contribution to the ground state from these two orbitals (Eqs. (1)–(5)), appear in the final expression for the transition dipole moment of the CT transition,

$$D_{ct} = (1/3)\alpha^2(a^2 + b^2)|\, m\, |^2 \tag{12}$$

where α is the first-order mixing coefficient. At liquid helium temperatures, the MCD intensity is dominated by the *C*-term contribution. The magnitude of this *C*-term can be shown to be [99]

$$C_{ct} = (1/3)g_{zz}ab\alpha^2|\, m\, |^2 \tag{13}$$

These expressions already include averaging over all orientations of a randomly distributed frozen solution sample. Thus the ratio of C_{ct} to D_{ct} is a quantity independent of α^2 and $|\, m\, |^2$,

$$C_{ct}/D_{ct} = g_{zz}ab/(a^2 + b^2) \tag{14}$$

When the *C*-term is the only contribution to the MCD, the theoretical parameters C_{ct} and D_{ct} can be directly related to the experimentally observed parameters by

$$\Delta\varepsilon^*/\varepsilon = (C_{ct}/D_{ct})\cdot(\beta_e B/kT) \tag{15}$$

where β_e is the Bohr magneton, B is the magnetic field strength, k is Boltzman's constant, T is the absolute temperature, ε is the absorption intensity and $\Delta\varepsilon^*$ is the MCD intensity in the *linear limit*. To determine these two quantities, we measured the zero moments, $\Delta\varepsilon_0$ and ε_0, of the bands in the respective experimental spectra [29]:

$$\Delta\varepsilon_0 = \int(\Delta\varepsilon/\nu)\mathrm{d}\nu \quad \text{and} \quad \varepsilon_0 = (\varepsilon/\nu)\mathrm{d}\nu \tag{16}$$

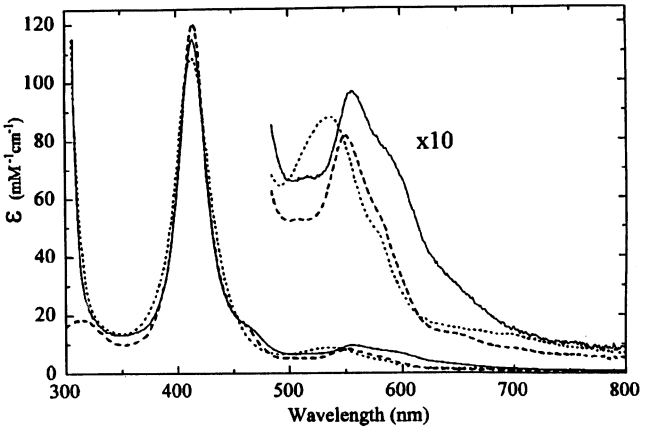

Fig. 14. UV–vis region electronic absorption spectra of ferric TMP complexes in dimethylformamide/acetonitrile at room temperature. (—) 95 μM $[TMPFe(NMe_2Py)_2]^+$, (- - -) 150 μM $[TMPFe(N\text{-}MeIm)_2]^+$, (···) 140 μM $[TMPFe(4\text{-}CNPy)_2]^+$. Taken from reference [29] with permission from the American Chemical Society.

and corrected by extrapolation to the 'linear limit' MCD $\Delta\varepsilon_0^*$, at 4.2 K and 5 T [29,101,102].

6.2. MCD data for low-spin ferriheme systems

Type I species, such as $[TMPFe(4\text{-}NMe_2Py)_2]^+$, show minimal rhombicity and give rise to large g_{max} type EPR spectra in which g_{zz} ca. 3.3 [15,17], Fig. 5a. The other two g-value features are broad and often difficult to detect, as discussed in Section 4. In the theoretical axial limit, where the d_{xz},d_{yz} orbitals are isolated and degenerate, the g-values of the EPR spectrum would approach 4, 0, 0. In this limit, illustrated in Fig. 13a, the NIR-CT transition is xy-polarized and gives rise to maximal MCD intensity, as shown in Figs. 16 and 17, solid line. In reality, however, the presence of spin-orbit coupling precludes the occurrence of the limiting axial system and an effective upper limit of g_z ca. 3.88 is observed. As rhombicity is introduced to such a system, the electron-hole is progressively localized in one of the now non-degenerate d_{xz},d_{yz} orbitals. The NIR-CT transition becomes more x- or y-polarized and the MCD intensity is reduced.

The formal electronic configuration of a typical type II low-spin ferric heme is $(d_{xy})^2(d_{xz}d_{yz})^3$ and the NIR-CT transition occurs from the porphyrin highest occupied molecular orbital (HOMO) to the hole in the (d_{xz},d_{yz}) set. The model of Griffith more accurately describes the unpaired electron as occupying an orbital derived from the three non-σ-bonding d-orbitals (the T_{2g} set in O_h symmetry) [49,50]. In the limit of high tetragonality and zero rhombicity, when the electron hole is distributed equally between the two (Fig. 13a), the NIR-CT band is xy-polarized and the MCD is at its most intense [98], as shown in Fig. 17, solid line. In practice, a pseudo-Jahn–Teller distortion of the porphyrin opposes complete d_{xz},d_{yz} degeneracy. Even for $[TMPFe(4\text{-}NMe_2Py)_2]^+$, where the ligand planes are very nearly perpendicular, the g_{xx} and g_{yy} values are quite different [17]. With increasing rhombicity and loss of degeneracy of the (d_{xz},d_{yz}) pair, the hole becomes progressively localized in one of the two orbitals, leading to rhombic EPR spectra, Fig. 5b. The band then becomes predominantly x- or y-polarized depending on the orbital in which the electron is localized. Since linearly polarized transitions have no net MCD C-term intensity, the NIR-CT MCD band is reduced in intensity, Fig. 17, dashed line. A range of low-spin ferriheme proteins so far examined give rise to NIR-CT MCD bands the peak intensities of which vary at 4.2 K from $\Delta\varepsilon$ ca. 580 [103] to less than 100 M^{-1} cm^{-1} [98]. These values serve to illustrate the range of MCD intensities found for the NIR-CT band, but it is the *intensity ratio* of the MCD to the absorbance which is governed by the symmetry. Implicit in this model is the assumption that the z-axis, defined under Taylor's 'proper axis system' as the direction of tetragonal distortion, is perpendicular to the heme plane and therefore to the plane of the heme π-system [50]. This is indeed the case to within 15° in those hemes for which principal directions of the χ-tensor have been determined relative to molecular axes [21,23,45,61,64,66–68,104].

These spectroscopic properties are common to the NIR-CT MCD band observed for the low-spin ferric state of *a*-, *b*- and *c*-type hemes [94]. They also apply to

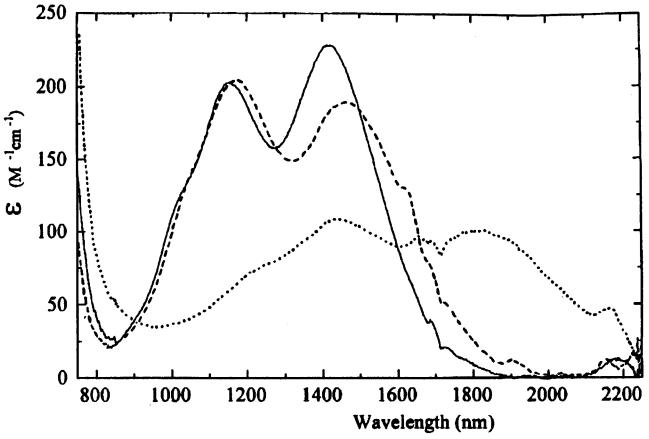

Fig. 15. Near infrared region electronic absorption spectra of 4.76 mM ferric TMP complexes in dimethylformamide/acetonitrile at room temperature. (—) $[TMPFe(NMe_2Py)_2]^+$, (- - -) $[TMPFe(N\text{-}MeIm)_2]^+$, (···) $[TMPFe(4\text{-}CNPy)_2]^+$. Taken from reference [29] with permission from the American Chemical Society.

low-spin ferric octaethyl- and tetraphenylporphyrins (OEP and TPP), although, for the latter, the vibrational structure of the bands is variable. However, proteins containing low-spin ferric heme *d*, such as the cyanide derivative of hydroperoxidase II (HPII) from *Escherichia coli* and octaethylchlorin (OEC) substituted myoglobin with a variety of low-spin ligands, give anomalously weak NIR-CT MCD bands with peak intensities of $\Delta\varepsilon$ ca. 40 $M^{-1}cm^{-1}$ [100]. The ground state electronic parameters calculated, via Taylor's treatment [50], from the EPR spectra of low-spin ferric hemes *d* show *low* rhombicity compared to *b*- and *c*-type hemes. These unusual EPR properties have led to suggestions that low-spin Fe(III) hydroporphyrins have a predominantly $(d_{xz},d_{yz})^4(d_{xy})^1$ ground state [50,87,86,89]. An electronic transition from a porphyrin or chlorin HOMO to a hole in the d_{xy} orbital is symmetry forbidden (Fig. 13b) and therefore would have low intensity in both the absorption and MCD spectrum throughout the visible and NIR region, as demonstrated in Figs. 14–17 for the MCD spectra of the type III complexes as compared to types I and II.

For both $[TMPFe(4\text{-}NMe_2Py)_2]^+$, which gives rise to a large g_{max} EPR signal (type I complex), and $[TMPFe(N\text{-}MeIm)_2]^+$, which gives rise to a rhombic type EPR spectrum (type II complex), the observed quantity $\Delta\varepsilon^*/\varepsilon$ [29] is in excellent agreement with the value calculated from the EPR *g*-values using the method of Thomson and Gadsby [98]. This illustrates clearly how the MCD intensity is derived from the absorption intensity but modulated according to the magnetic properties of the complex. This result, obtained using a particular ferric porphyrinate coordinated by similar ligands [98], also underlines the central role of axial ligand orientation in determining EPR *g*-values and NIR-MCD intensities. These measurements are frequently used to obtain information concerning the nature and orientation of ligands to hemes in proteins for which no three-dimensional structure

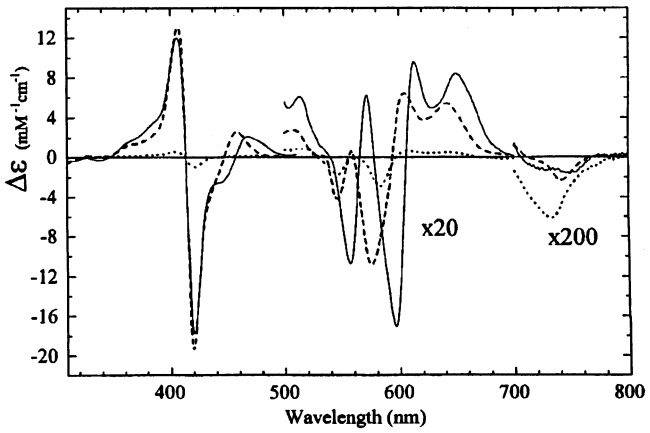

Fig. 16. UV–vis region MCD spectra of low-spin ferric complexes: (—) $[TMPFe(NMe_2Py)_2]^+$, (- - -) $[TMPFe(N\text{-MeIm})_2]^+$, (···) $[TMPFe(4\text{-CNPy})_2]^+$ [29]. Concentrations are approximately ten times greater for the 500–800 nm portion of the spectrum (see original paper for exact values). Spectra were recorded at 4.2 K with a magnetic field of 50 kG. Taken from reference [29] with permission from the American Chemical Society.

is known [3]. The results for the TMPFe(III) complexes of 4-NMe_2Py (type I) and *N*-MeIm (type II) [29], Figs. 16 and 17, constitute an important addition to the MCD data measured for low-spin ferric hemes of confirmed structure. These are necessary to endorse assignments of axial ligand orientation in hemoproteins made using this methodology.

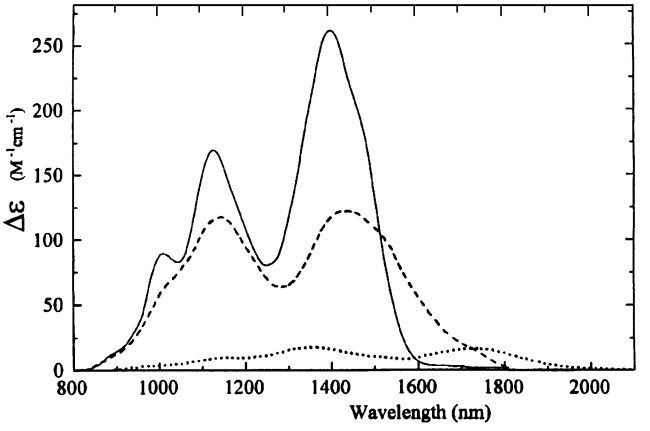

Fig. 17. Near infrared region MCD spectra of low-spin ferric TMP complexes: (—) $[TMPFe(NMe_2Py)_2]^+$, (- - -) $[TMPFe(N\text{-MeIm})_2]^+$, (···) $[TMPFe(4\text{-CNPy})_2]^+$ [29]. Concentrations are given in the original paper. Spectra were recorded at 4.2 K with a magnetic field of 50 kG. Taken from reference [29] with permission from the American Chemical Society.

6.3. Analysis of the data for type III systems

The same analysis does not fully describe the properties of the type III complex, $[TMPFe(4\text{-}CNPy)_2]^+$, where the ligands are also known to be approximately perpendicular [18], a situation which confers effective 4-fold symmetry on the ferric ion, if the ruffling of the porphyrinate ring is ignored. Despite this 4-fold symmetry, the properties of the 4-CNPy complex are distinct from those of the 4-NMe_2Py complex: The NIR-MCD is extremely weak (Fig. 17) and the EPR spectrum is axial with g-values [18] which have been interpreted as indicating a $(d_{xz},d_{yz})^4(d_{xy})^1$ ground state. Since a charge-transfer process from either of the two highest occupied porphyrin π-orbitals to the hole in the ferric d_{xy}-orbital is symmetry forbidden (Fig. 13), substantially reduced intensity would be anticipated for the NIR-CT band in both the electronic absorption and the MCD spectra of the 4-CNPy complex (type III). This is indeed true for the UV–vis MCD bands (Fig. 16), which is approximately 11% of the intensity of the same MCD band for the 4-NMe_2Py complex (type I). However, the NIR-CT absorption intensity for the type III 4-CNPy complex (Fig. 15) is as high as ca. 67% of the intensities for the types I 4-NMe_2Py and II *N*-MeIm complexes. This high absorption may result from the fact that the porphyrin ring of the type III 4-CNPy complex is significantly deformed from planarity. The strong porphyrin ⇒ Fe(III) π-bonding in this and other related complexes leads to a shortening of the ferric ion to pyrrole nitrogen bonds. This is accommodated by ruffling of the macrocycle [18,26]. An important aspect of such ruffling is the tilting of the individual pyrrole rings such that the ferric d_{xy} orbital can form an effective overlap with the pyrrole-nitrogen p_z orbitals (Fig. 2). This allows delocalization of the unpaired spin onto the porphyrin via the $a_{2u}(\pi)$ orbital [26].

For the type III complex $[TMPFe(4\text{-}CNPy)_2]^+$ and other complexes with the 'unusual' $(d_{xz},d_{yz})^4(d_{xy})^1$ ground state, mixing of porphyrin a_{2u} with ferric d_{xy} introduces $a_{1u} \Rightarrow a_{2u}$ character into the NIR-CT band which, in the lower symmetry of the ruffled system, represents *linearly z-polarized* electric dipole intensity [29]. This will invariably contribute to the absorption, but could also in principle add to the MCD intensity because the transition already has *xy* character [29]. The MCD intensity at 4.2 K is dominated by the temperature dependent C-term intensity and this is proportional to the expression [105]:

$$g_{xx}\langle a|m_y|j\rangle\langle j|m_z|a\rangle + g_{yy}\langle a|m_z|j\rangle\langle j|m_x|a\rangle + g_{zz}\langle a|m_x|j\rangle\langle j|m_y|a\rangle \quad (17)$$

where a and j are the ground and excited state wavefunctions. The residual $(d_{xy})^2(d_{xz},d_{yz})^3$ character of the ground state that results from spin-orbit coupling [49,50] is already contributing to the MCD via the third term of this expression. Because the g_{xx} and g_{yy} values are equal in magnitude but of opposite sign, the first and second terms cancel and no net increase in MCD intensity results. This is an important result, which accounts for the low intensity of the NIR-CT MCD bands (Figs. 16 and 17) while allowing the same bands in the *absorption* spectra to have

reasonable intensity (Figs. 14 and 15). Even if the values of g_{xx} and g_{yy} are not of *equal* magnitude, as in the rhombic spectra of the ferric hydroporphyrins reported to date [7,10,50,71,86–91,103,106], they are in each case of *similar* magnitude and hence, with opposite sign, the first and second terms will *nearly* cancel in these cases.

An important conclusion from the work described in reference [29] is that the novel $(d_{xz},d_{yz})^4d_{xy})^1$ ground state indicated by the unusual axial EPR g-values of the type III complex $[TMPFe(4\text{-}CNPy)_2]^+$ is in itself sufficient to result in anomalously low NIR-CT MCD intensities, Fig. 17. This has important implications for the interpretation of the magneto-optical spectra from proteins containing ferric hydroporphyrins. A 'Taylor analysis' of the EPR g-values reported for low-spin ferric hydroporphyrins [7,10,50,71,86–91,103,106], both in proteins and in model compounds, points to all these species having a predominantly d_{xy} ground state. The few examples investigated by MCD spectroscopy to date give low UV–vis [107] and NIR-CT [99,100] intensities which have been interpreted as resulting from unusually high rhombicity at the ferric ion arising from the chlorin and formyl-substituted porphyrin macrocycles [99,100,108,109]. On the basis of the arguments presented in the previous paragraph and elsewhere [29], this appears to be a misinterpretation; the d_{xy} ground state *of itself* leads to low NIR-CT MCD intensities.

The d_{xz},d_{yz} orbitals are stabilized in $[TMPFe(4\text{-}CNPy)_2]^+$ by use of strong π-acceptor axial ligands, resulting in the $(d_{xz},d_{yz})^4(d_{xy})^1$ ground state. In the absence of suitable axial ligands, the chlorin macrocycle itself may serve to provide this stabilization by more favorable π^*–(d_{xz},d_{yz}) interactions. Ruffling, which is believed to be easier for chlorins than for porphyrins [110,111], would help this process. This ruffling would tend to lead to shorter $Fe–N_P$ bonds, thus facilitating the $Fe(\pi) \Rightarrow$ chlorin(π^*) back-bonding that would help to stabilize the d_{xz},d_{yz} orbitals. Furthermore, ruffling would cause rotation of the p_z orbitals of the chlorin, isobacteriochlorin or dioxoisobacteriochlorin nitrogens, just as it does for the porphyrins [26] (Fig. 2), which can facilitate their overlap with the d_{xy} orbital (Fig. 2), thus mixing in the chlorin equivalent of porphyrin a_{2u} character. Interestingly, the siroheme macrocycle of sulfite reductase is very ruffled [11]. Where rhombicity is observed in the EPR spectra of low-spin ferric chlorins, especially those bound in proteins, it may result from *either* axial ligand orientation *or* unsymmetrical reduced macrocycle, *or both*. Our recent report [29] has examined the effect on the MCD of one of the several unusual properties of a ferric chlorin (the $(d_{xz},d_{yz})^4(d_{xy})^1$ ground state) and has shown that this one property is sufficient to reduce NIR-CT intensity to the level observed for actual low-spin ferric chlorins. It is not yet clear what additional influence is exerted by ligand orientation and by the chlorin ring itself. The EPR spectra of low-spin ferric chlorin model complexes with known perpendicular and parallel ligands would be of great value in clarifying this point, and such investigations are underway. Preliminary EPR investigations of bis-ligand complexes of Fe(III) pyropheophorbide *a* methyl ester show that for L = *N*-MeIm, 4-NMe_2Py, 4-CNPy, and 2-MeImH, the EPR spectra of all complexes are rhombic and are all consistent with $(d_{xz},d_{yz})^4(d_{xy})^1$ ground states, yet the individual g-values

are unique for each complex [112], suggesting secondary effects due to axial ligand orientation and basicity for these low-spin Fe(III) chlorin complexes. These and related complexes are thus interesting systems for detailed investigation by electronic absorption and MCD spectroscopy.

6.4. MCD studies of low-spin ferriheme forms of cytochrome P450

The MCD spectra of low-spin Fe(III) forms of cytochrome P450 BM-3 [83], a bacterial P450, shows the type of intense UV–vis and NIR-CT MCD spectra exhibited by the types I and II model hemes shown in Figs. 16 and 17, rather than the very low-intensity type III complex. This is strong evidence that the electron-configuration of these low-spin Fe(III) P450 species is $(d_{xy})^2(d_{xz},d_{yz})^3$, in agreement with the single crystal EPR results. Thus the 'borderline' nature of the EPR and Mössbauer parameters for low-spin forms of Fe(III) cytochrome P450 (Table 1, Fig. 12) appears to be fortuitous.

7. NMR studies of low-spin ferriheme models and proteins

Unlike the spectroscopies discussed above, which focus almost entirely upon the electron configuration and orbital occupation of the metal, ^{1}H-NMR spectroscopy focuses on the unpaired electron density at various ligand positions [113,114], and derives the orbital occupation of the metal by first noting the pattern of chemical shifts of porphyrin substituents observed and then, based on this pattern, the orbital occupation of the macrocycle, and from there, following symmetry considerations, the metal orbital occupation. The orbitals involved, for low-spin Fe(III) porphyrinates, are the $e(\pi)$ and $a_{2u}(\pi)$ frontier orbitals of the porphyrin ring (Fig. 1), depending on whether the electron configuration of the metal is $(d_{xy})^2(d_{xz}d_{yz})^3$ or $(d_{xz},d_{yz})^4(d_{xy})^1$, respectively. And because the temperatures at which NMR spectra are measured are much higher than those used for EPR, ESEEM, Mössbauer and MCD spectroscopies, it is possible that thermally-accessible excited states will be populated, thus modifying the interpretation of the ^{1}H isotropic shift results, especially if one does not realize that an excited state is contributing to the spectra!

7.1. Temperature dependence of NMR spectra in the presence of a thermally-accessible excited state

The temperature dependence of the isotropic shifts of paramagnetic complexes in general and low-spin ferrihemes in particular has long been explained as following the Curie law [113–115]. This is approximately true. However, as described previously elsewhere [116], in most cases there are excited states that are within $(1–3)kT$ of the ground state, and hence paramagnetic complexes with such a thermally-accessible excited state do not follow the simple Curie law, but rather an expanded Curie law that takes into account the excited state: [117,118]

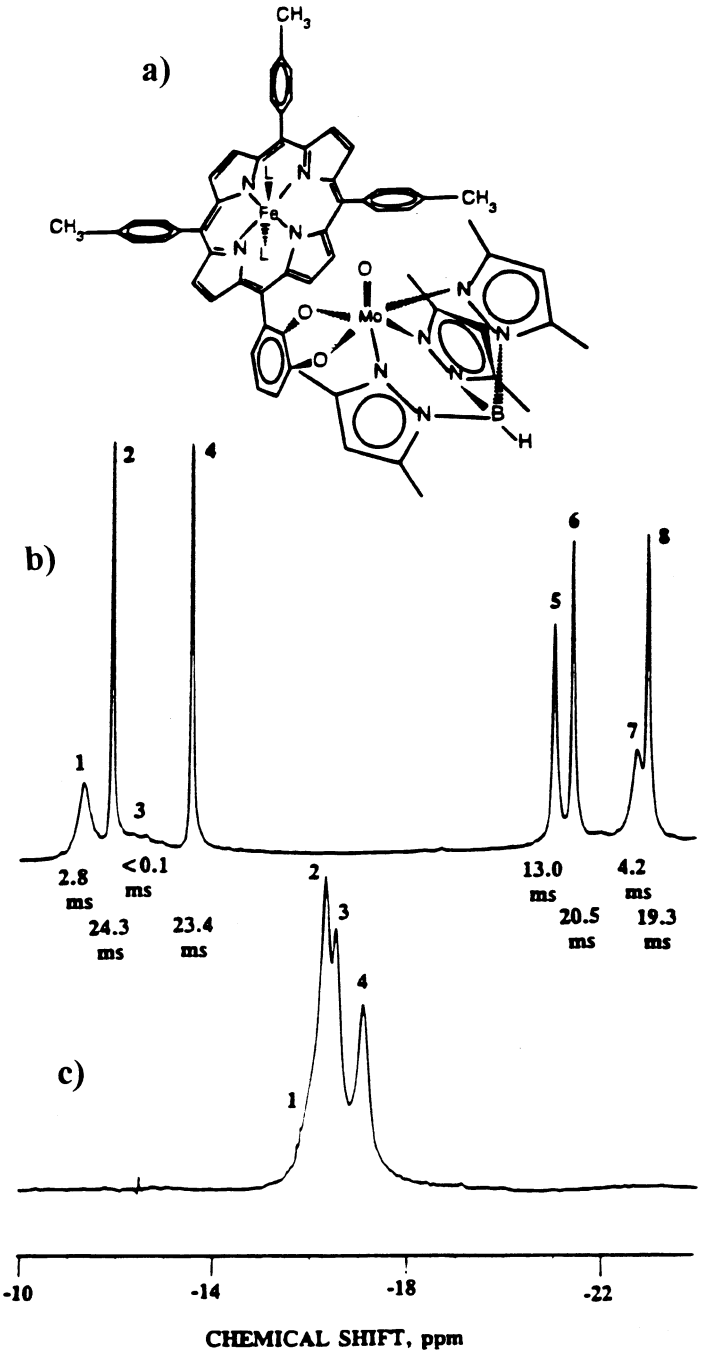

Fig. 18. (a) Structure of the {tri-p-tolyl[2,3-[((hydrotris(3,5-dimethylpyrazolyl)borato)-oxomolybdenum)dioxy]phenyl]porphyrinato}-bis-(L)iron(III) complex, [Fe(2,3-Mo–TTP)(*N*-MeIm)$_2$]Cl, where L = *N*-methylimidazole. (b) 500 MHz spectra of the pyrrole protons at 296 K in CD_2Cl_2 showing the effect of the hindered axial ligand rotation for [Fe(2,3-Mo–TTP)(*N*-MeIm)$_2$]$^+$ and (c) lack thereof for [Fe(3,4-Mo–TTP)(*N*-MeIm)$_2$]$^+$. Peak numbering is given in increasing order from downfield to upfield, the order of increasing contact shifts of the pyrrole protons. Modified from reference [117].

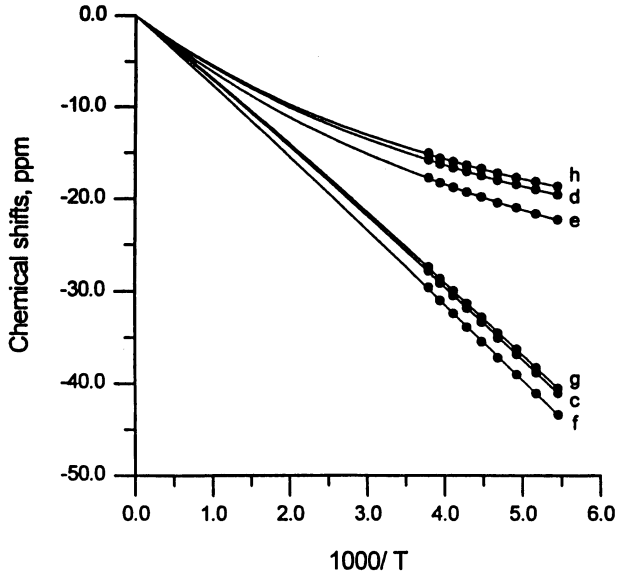

Fig. 19. Plot of the calculated Curie behavior for [Fe(2,3-Mo–TTP)(*N*-MeIm)$_2$]Cl for an energy separation $\Delta E = 160$ cm^{-1} [116,117]. Taken from reference [116] with permission from the American Chemical Society.

$$\delta_n^{\text{con}} = (F/T)\{W_1 C_{n1}^2 + W_2 C_{n2}^2 \mathrm{e}^{-\Delta E/kT}\}/\{W_1 + W_2 \mathrm{e}^{-\Delta E/kT}\} \quad (18)$$

where δ_n^{con} is the contact shift of each proton or carbon of interest, F is the Curie factor that relates the contact shift to the orbital coefficients, T is the absolute temperature, W_1 and W_2 are the weighting factors for the ground and excited state orbital (equal if the spin multiplicities of ground and excited states are the same), C_{n1} and C_{n2} are the orbital coefficients for position n in the ground and excited states, respectively, ΔE is the energy separation between ground and excited states, k is the Boltzmann constant. Several model ferrihemes and ferriheme proteins [116], including a Mo(V)-appended [TPPFe(*N*-MeIm)$_2$]$^+$ complex [117], for which one axial ligand is prevent from rotating by the bulky 2,3-Mo(V) complex, have been analyzed in this manner (Figs. 18 and 19). The values of ΔE range from very small for non-hindered unsymmetrically-substituted TPPFe(III) derivatives [116] to 160 cm^{-1} for the Mo(V)-appended [TPPFe(*N*-MeIm)$_2$]$^+$ complex [116,117], 400–700 cm^{-1} for cytochrome b_5 [116,118], and 498 cm^{-1} for *Aplysia* cyanometmyoglobin [116,119]. These ΔE values represent the difference in energy between the two 3e(π) orbitals (Fig. 1) of the heme (see below for further details), and hence also the ΔE between the d_{xz} and d_{yz} orbitals of Fig. 3. The values of V (Eq. (6)) calculated from the EPR g-values of each of the latter proteins, where the axial ligands are fixed in orientation, are 540–800 and 313–368 cm^{-1}, respectively [116], depending on the value of the spin-orbit coupling constant, λ, utilized [52][2]. For delocalization to

[2] See footnote 1.

occur from the porphyrin to the low-spin Fe(III) by Por⇒Fe π-donation, we should expect that $\Delta E = V$ [116], and this appears to be true to within the experimental error of the NMR-derived ΔE values for the heme proteins mentioned above. Hence, together with EPR, but unlike Mössbauer and MCD spectroscopies, from NMR spectra we not only learn about the electronic ground state, but also, frequently, the first excited electronic state of the complex.

7.2. Contributions to the observed shift and the use of the contact shift to determine the orbital used in spin delocalization

The ^{1}H and ^{13}C observed shifts of the porphyrin ring are given by

$$\delta_{obs} = \delta_{dia} + \delta_{para} \tag{19}$$

The paramagnetic contribution to the observed shift, δ_{para}, can be further subdivided into the contact and dipolar contributions:

$$\delta_{para} = \delta_{con} + \delta_{dip} \tag{20}$$

The dipolar shift is also called the pseudocontact shift. Of the two contributions to δ_{para}, the contact shift carries the information about the shape of the π-orbital of the low-spin ferriheme complex. Hence, it is often necessary to determine the size and sign of the dipolar (pseudocontact) shift, in order to subtract it from δ_{para} to obtain δ_{con} [114]. In so doing we must recall the concept of counter-rotation of the g-tensor with rotation of planar axial ligands away from the porphyrin nitrogens [69].

The simplest expression for the contact contribution to the isotropic shift is

$$\delta_{con} = A < g > \beta_e S'(S'+1)/3\gamma_N \hbar k T \tag{21}$$

where A is the hyperfine coupling constant, $< g >$ is the average g-value, β_e is the Bohr magneton, S' is the effective spin of the metal, γ_N is the magnetogyric ratio of the nucleus being observed, $\hbar$ is Planck's constant divided by 2π, k is the Boltzmann constant and T is the absolute temperature. This equation is valid if g-values are directly proportional to magnetic susceptibilities, χ_{ii}, which is only approximately true [114], and the presence of a thermally-accessible excited state will require combination with Eq. (18). The hyperfine coupling constants thus obtained are related to the spin density at each position of the macrocycle according to the McConnell equation [120]:

$$A = Q\rho_C/2S' \tag{22}$$

Where $Q_H = -63$ MHz for protons bound to a carbon that is a member of a π-system, $Q_H = +70$–75 MHz for methyl groups attached to a π-system, and $Q_C = -39(\gamma_H/\gamma_C) = -155$ MHz for a carbon that is a member of a π-system [114]. Because Q_H is negative for protons attached to carbons that are part of a π-system, such protons have negative contact shifts and may appear very far upfield [113–115]. The values of ρ_C determined from Eq. (22) can then be compared to the orbital coefficients for each carbon, calculated from simple Hückel [121] or more

sophisticated methods. Such calculations of contact shifts (as well as the dipolar shift contributions) to the observed shifts of a symmetrical octamethylferriheme as a function of the orientation of the planar axial ligands have recently been reported, and have been used to predict the heme methyl and *meso*-H shifts of a wide variety of heme proteins [122], as summarized in Fig. 20.

The dipolar shifts, which were included in the calculations that gave rise to Fig. 20, are given by

$$\delta_{dip} = (N/12)\{[\chi_{zz} - (1/2)(\chi_{xx} + \chi_{yy})](\cos^2\theta - 1)/r^3\} + (1/2)\{[\chi_{xx} - \chi_{yy}](3\sin^2\theta\cos 2\Omega)/r^3\} \quad (23)$$

where N is Avogadro's number, χ_{ii} are the principal components of the magnetic susceptibility tensor in SI units[3]. θ is the angle between the proton-metal vector and the z molecular axis, r is the length of this vector, and Ω is the angle between the projection of this vector on the xy plane and the x axis [113,115]. The terms $(3\cos^2\theta - 1)/r^3$ and $(\sin^2\theta\cos 2\Omega)/r^3$ are typically known as the axial and rhombic geometric factors, respectively, and the terms in Eq. (23) to which they belong are often called the axial and rhombic contributions to the dipolar shift, respectively. Axial geometric factors for protons at the β-pyrrole and *meso* positions of the commonly utilized model hemes, tetraphenylporphinatoiron, TPPFe, and octaethylporphinatoiron, OEPFe, have been calculated from x-ray crystallographic data for the low-spin Fe(III) complexes [113,115].

If the complex of interest has only one thermally populated spin multiplet with effective spin S, then

$$\chi_{ii} = \{\mu_0\beta^2 S(S+1)/3kT\}/g_{ii}^2 \quad (24)$$

where μ_0 is the permitivity of free space and β is the Bohr magneton, and Eq. (23) can be simplified to

$$\delta_{\mathrm{dip}} = [\mu_0\beta^2 S(S+1)/72\pi kT] \times \{[2g_{zz}^2 - (g_{xx}^2 + g_{yy}^2)](3\cos^2\theta - 1)/r^3 + 3(g_{xx}^2 - g_{yy}^2)(\sin^2\theta\cos 2\Omega)/r^3\} \quad (25)$$

The axial g anisotropy, Δg_{ax}^2, is positive for $(d_{xy})^2(d_{xz},d_{yz})^3$ ground states and negative for $(d_{xz},d_{yz})^4(d_{xy})^1$ ground states. This information is useful to keep in mind when reading papers on the determination of the magnetic anisotropies of paramagnetic heme proteins, discussed below in Section 7.10. In all cases for which the magnetic axes and anisotropies have been reported, Δg_{ax}^2 is positive.

7.3. Ligand exchange and its effect on chemical shifts

An important consideration in studying the NMR spectra of low-spin ferriheme model complexes is that axial ligand binding constants vary markedly with temperature, and at higher temperatures ligand exchange is very fast. Since the mechanism for ligand exchange is dissociative [123] and the intermediate in the ligand exchange

[3] χ (SI) = $(4\pi \times 10^{-6})$ χ (cgs emu)

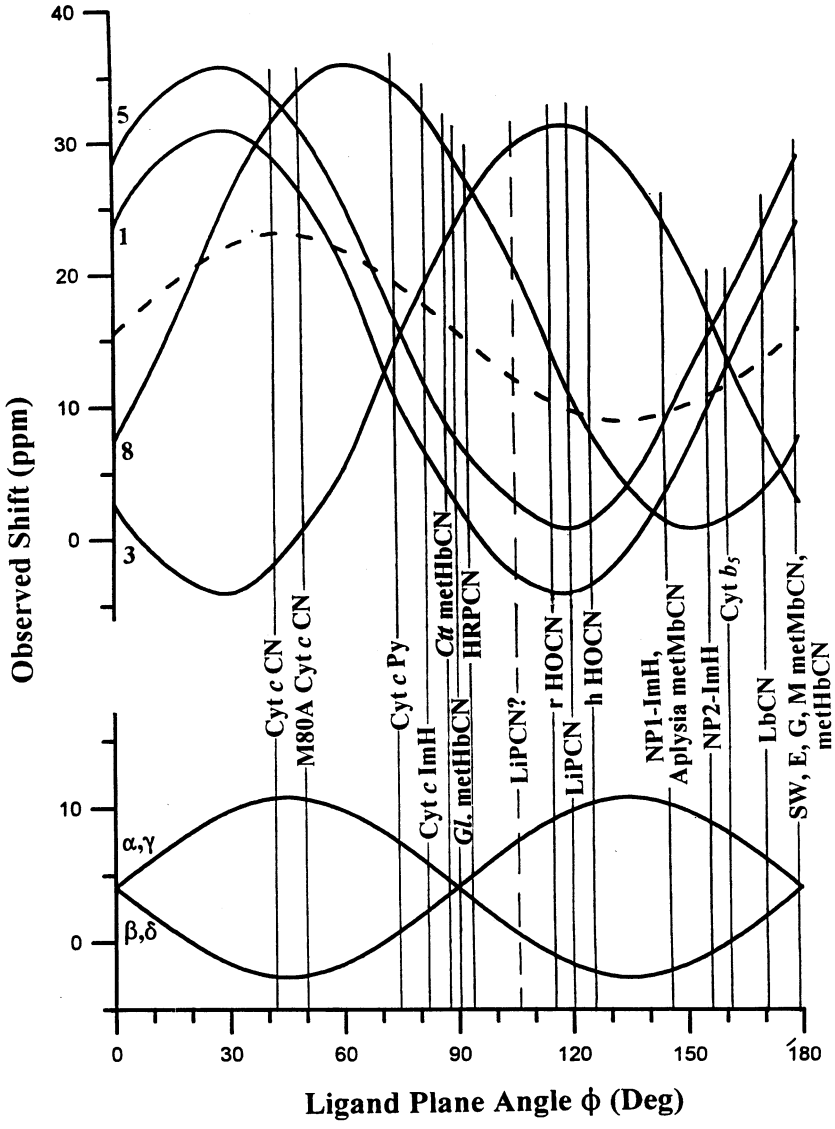

Fig. 20. Plot of the dependence of the observed shift on the orientation of a planar axial ligand (or two parallel axial ligands) [122]. The plot is specific for protohemin-containing proteins. Only the four heme methyls and *meso*-H of protohemin are included, and a ± 2.4 ppm adjustment to the contact shifts of the heme methyls has been made, to account for the effect of the 2,4-vinyl substituents of protohemin. The energy separation of the heme orbitals, ΔE, was taken as 560 cm^{-1}. The dashed line represents the dependence of the average heme methyl shift on the orientation of the axial ligand(s). Taken from reference [122] with permission from Elsevier.

processes of low-spin, bis-ligated ferrihemes is the five-coordinate mono-L intermediate, which is high-spin, the presence of a small amount of this intermediate can shift the NMR resonances of the ferriheme complex in the direction of those of the high-spin intermediate, and thus cause deviations from the expected temperature dependences of Eq. (18), as well as erroneous calculated contact shifts. To avoid this, unless one wishes to work with a very large amount of excess ligand present, it is usually necessary to make sensitive temperature-dependent measurements of chemical shifts and linewidths well below room temperature, and, in order to avoid the effects of chemical exchange on both the isotropic shifts and the NOESY/EXSY spectra, it is often necessary to work well below -35°C. This has become very clear to us in our studies of $[TMPFe(2\text{-}MeImH)_2]^+$ discussed below, as well as studies of $[OETPPFe(2\text{-}MeImH)_2]^+$, where chemical exchange could nearly be stopped on the NOESY/EXSY time scale only at -90°C at 300 MHz [34].

7.4. Characteristics of the NMR shifts of the two ground states of low-spin ferriheme complexes

The two different electronic ground states for low-spin ferriheme systems that have been discussed in previous sections give rise to very different patterns of proton (and carbon) isotropic shifts. For the $(d_{xy})^2(d_{xz}d_{yz})^3$ ground state species, spin density is delocalized to the porphyrin ring by Por$\Rightarrow$Fe π-donation from the 3e(π) orbitals to the hole in d_{xz} and/or d_{yz}. This places most of the spin density at the β-pyrrole positions of the porphyrin ring (Figs. 1 and 21) and gives rise to rather negative chemical shifts for the pyrrole-H of $[TPPFe(N\text{-}MeIm)_2]^+$ derivatives (Fig. 18), and nearly zero chemical shifts at the *meso*-positions, if no mixing of the 4e(π^*) orbitals is assumed. However, there is some evidence that there is a small amount of π spin density, in addition to a larger σ spin density, at the *meso*-positions of $(d_{xy})^2(d_{xz}d_{yz})^3$ ground state systems [122]. It is the removal of degeneracy of the two 3e(π) orbitals due to the presence of planar axial ligands in parallel alignment [122] or the creation of extreme difference in the electronic effects at *meso*-positions of the heme (as for the cyanoferriheme complex of heme-heme oxygenase [124]) that creates differences in the contact shifts of ferriheme complexes such as those demonstrated for axial ligand plane orientation in Fig. 20.

In general, the type II TPPFe(III) complexes having axial ligands in parallel planes in the solid state have somewhat larger observed pyrrole-H shifts than their corresponding type I counterparts, although the axial ligands of the type II complexes are rotating extremely fast at all temperatures studied, and the barrier to both synchronous and asynchronous rotation is very low (see also Section 7.5). This is clearly demonstrated by the *N*-MeIm and 2-MeImH complexes of the Mo(V)-appended TPPFe(III) derivative, where the average pyrrole-H shifts at -60°C are -20 and -27 ppm, respectively [125]. This is likely a result of the mixing of a small amount of $a_{2u}(\pi)$ character into the ruffled 2-MeImH complex. Likewise, for type I TMPFe(III) complexes with pyridines of decreasing basicity, the pyrrole-H resonance position at -80°C shifts from -30.9 ppm (4-NMe_2Py) to $+2.1$ ppm (4-CNPy) [18]. The latter is clearly not a type I, but rather a type III complex, as

discussed below. Because the shift is a smooth function of the pK_a of the conjugate acid of the pyridine ligand, it is difficult to say where the $(d_{xy})^2(d_{xz},d_{yz})^3$ electron configuration ends and the $(d_{xz},d_{yz})^4(d_{xy})^1$ begins, partly because the energy separation between the two electronic ground states decreases as one moves from the right to the left extreme of the orbital diagram of Fig. 3 [124] and so both states are populated thermally as a function of the particular ligand and the temperature. Curie plots of the whole series of pyridine ligands create a family of lines of decreasing negative slope to increasing positive slope as one goes from [TMPFe(4-$NMe_2Py)_2]^+$ to [TMPFe(4-$CNPy)_2]^+$ [126].

7.5. The effect of unsymmetrical ligands on the NMR spectra of type I complexes, and measurement of the rates of ligand rotation

For type I complexes having unsymmetrical planar ligands, such as [TMPFe(2-$MeImH)_2]^+$, the asymmetry of the perpendicularly-oriented 2-MeImH ligands in perpendicular planes lying over the *meso* positions creates four different pyrrole-H

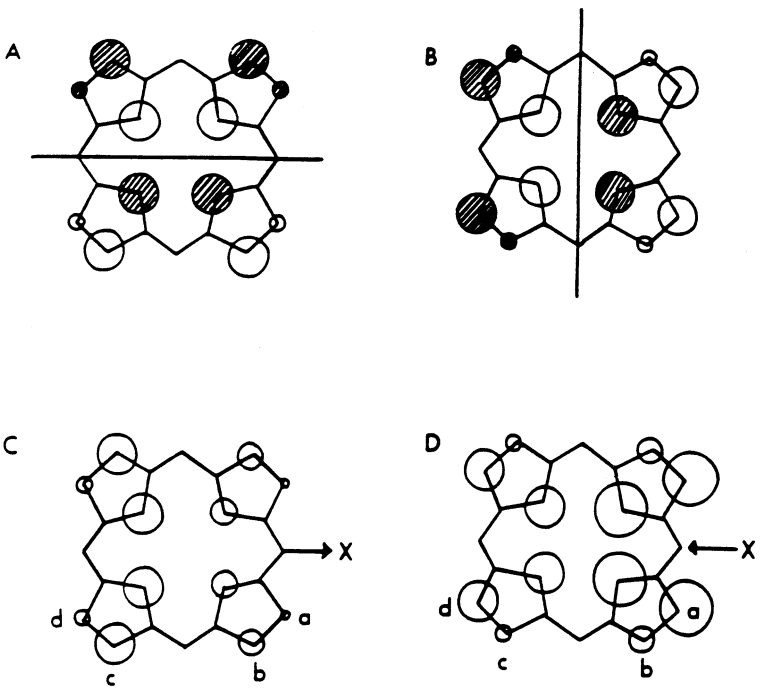

Fig. 21. Electron density distribution and symmetry properties of (A,B) the pair of degenerate 3e(π) orbitals of symmetrical tetraphenylporphyrins or any porphyrin having axial ligand planes aligned along the *meso* positions; (C,D) modification of A and B due to the presence of one relatively electron-withdrawing or -donating *meso*-substituent, respectively. Note that in either C or D, four β-pyrrole environments are expected due to unpaired electron delocalization via these modified orbitals. Taken from reference [12] with permission from New Journal of Chemistry.

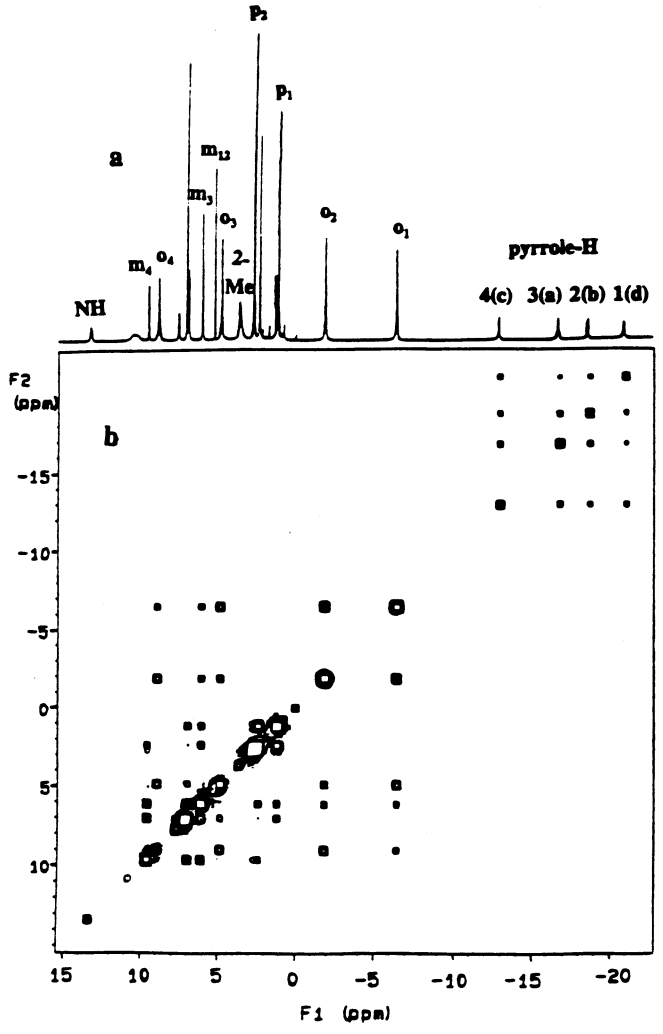

Fig. 22. (a) 1D ^{1}H-NMR spectrum of $[TMPFe(2\text{-}MeImH)_2]^+$ at -55 C in CD_2Cl_2. (b) Magnitude NOESY/EXSY spectrum at the same temperature [128]. the 4×4 matrices of chemical exchange cross-peaks for pyrrole-H, *ortho*-CH_3, and *meta*-H resonances. Taken from reference [128] with permission from the American Chemical Society.

resonances, as well as four *ortho*-CH_3, four *meta*-H and two *para*-CH_3 resonances [127,128], as shown in Fig. 22. The average chemical shift of the four pyrrole-H resonances is in accord with the expectations for type I complexes mentioned above, that the shifts are not as negative as for the *N*-MeIm type II complex. Using EXSY cross peak intensities [128], saturation transfer techniques [129], and T_2 measurements [130], we have measured the rates of axial ligand rotation as a function of temperature. We find that the activation enthalpy is about 50 kJ mol^{-1}

and the entropy of activation is about zero, within experimental error [128–130]. It should be noted that molecular mechanics calculations indicate that the lowest activation barriers are achieved if the perpendicular ligands rotate synchronously [129]. Even in this lowest energy barrier situation, large-amplitude movements of the substituents of the ruffled porphyrin ring are required in order for the ligands to rotate by 90°. At room temperature, the 2-MeImH ligands rotate about 10^4 s^{-1}, and 1,2-Me_2Im ligands rotate about five times faster [52], despite (or perhaps because of) their slightly bulkier structures [24]. Comparative studies of the type I complex [TMPFe(4-NMe_2Py)$_2$]$^+$ show that the barrier to ligand rotation is so much lower in this case that the rate cannot be measured by any NMR technique. The corresponding Co(III) complex, for which the rates of rotation of other ligands are at least 10^4 times slower, has its 4-NMe_2Py ligands rotating at least a million times per second at 298 K [53], suggesting that for [TMPFe(4-NMe_2Py)$_2$]$^+$ the rates of ligand rotation could be limited by the rate of bond vibrations, or specifically, porphyrin ring deformations. This gives quite a different view of these ferriheme complexes than that obtained from the structures of Fig. 4, and confirm that they are incredibly fluxional. An additional 2D-NMR study of [TMPFe(2-MeImH)$_2$]$^+$ provided the complete assignment of the spectrum of the complex using ROESY techniques [131].

The bis-(*N*-methylimidazole) and bis-(2-methylimidazole) complexes of OETPPFe(III) have also been studied by NMR spectroscopy [34]. The spectra are consistent with the axial ligands being in perpendicular planes lying over the N_P–Fe–N_P bonds. Despite their congested and seemingly rigid structures (Fig. 4d), these complexes are highly fluxional, and there is still some residual EXSY cross peak intensity for the [OETPPFe(2-MeImH)$_2$]$^+$ complex at -90°C. Chemical exchange phenomena include axial ligand rotation as well as simultaneous ethyl group rotation [34].

7.6. NMR spectra of type III ferriheme complexes

Of the 'pure' $(d_{xz},d_{yz})^4(d_{xy})^1$ systems having EPR *g*-values very near 2.0, magnetic Mössbauer spectra that are broader on the low-energy side, and low-intensity low-temperature MCD spectra that have been studied by NMR spectroscopy thus far, the first report was for that of [TPPFe(*t*-BuNC)$_2$]$^+$ [132]. The ^{1}H-NMR resonances, with pyrrole-H resonance at $+10$ ppm at 298 K was shown to follow the Curie law. The magnetic susceptibility of the complex was measured, which also clearly showed that this was a $S = 1/2$ paramagnetic complex [132]. Strong alternation in the direction of the *meso*-phenyl-H shifts suggested large π spin density at the *meso* positions [132]. A later NMR, EPR and magnetic Mössbauer study showed that for [OEPFe(*t*-BuNC)$_2$]$^+$, there is very small π delocalization to the β-pyrrole positions, as evidenced by only a 0.5 ppm downfield shift of the α-CH_2 resonances (but there is some σ spin delocalization to those positions, for the TPP analog has observed pyrrole-H shifts of about 10 ppm, amounting to about a 1 ppm *downfield* shift), while there is very large π spin delocalization to the *meso*-H positions of [OEPFe(*t*-BuNC)$_2$]$^+$ [27], as shown in Fig. 23, where the *meso*-H

resonance is at −37 ppm at 30°C, −63 ppm at −78°C, and −80 ppm at −98°C (Fig. 24). The Curie plot for this complex is shown in Fig. 24, where it can be seen that there is a thermally-accessible excited state in this case also. In this case the ΔE is the energy difference between the $(d_{xz},d_{yz})^4(d_{xy})^1$ ground state and the $(d_{xz},d_{yz})^3(d_{xy})^2$ excited state. For $[OEPFe(t\text{-}BuNC)_2]^+$, this$\Delta E$ is 296 cm^{-1} [27]. For the related substituted TPPFe(2,6-xylylisocyanide)$_2]^+$ complexes, the ΔE is considerably smaller, probably near 70 cm^{-1}, although it is difficult to estimate such a small ΔE [28], and in general, it appears that TPPFe(III) complexes with isocyanides have smaller energy gaps between the two electronic ground states than do β-alkylporphyrin analogs.

One might wonder if the large π spin delocalization to the *meso* positions of type III complexes could be indicative of delocalization to the 4e(π*) orbitals (Fig. 1) by

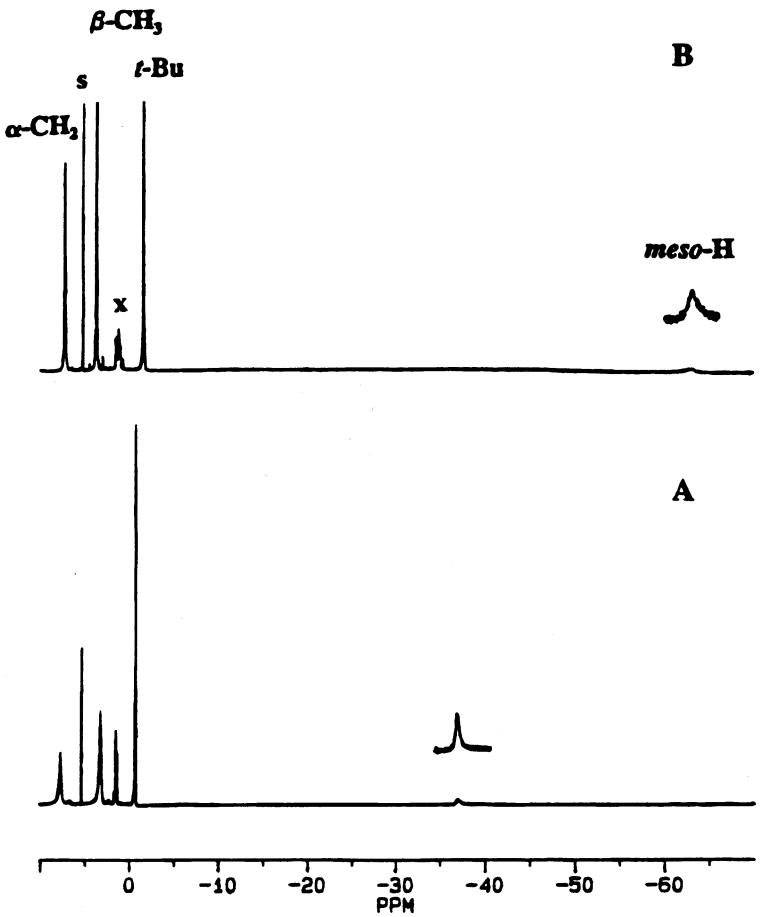

Fig. 23. The ^{1}H-NMR spectra of $[OEPFe(t\text{-}BuNC)_2]^+$ in CD_2Cl_2 recorded at (A) 303 K and (B) 195 K [27]. Assignments of the resonances are given in (B). Taken from reference [27] with permission from the American Chemical Society.

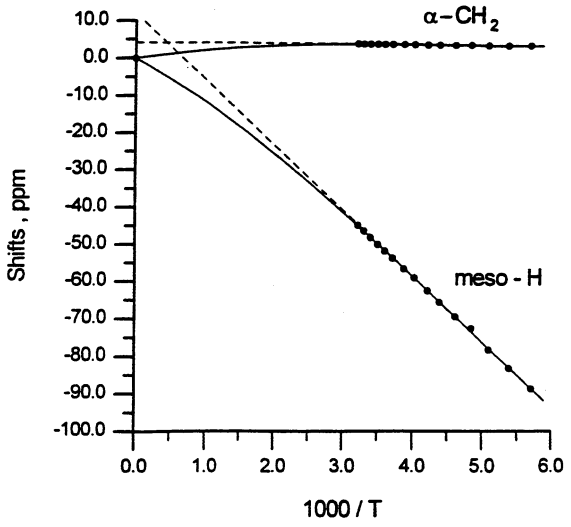

Fig. 24. Curie plot of the *meso*-H and α-CH_2 resonances of $[OEPFe(t\text{-}BuNC)_2]^+$ [27]. The dashed lines show the linear dependence, while the solid lines show the temperature dependence expected on the basis of a thermally-accessible excited state with $\Delta E = 296\ cm^{-1}$. Taken from reference [27] with permission from the American Chemical Society.

Fe ⇒ Por π* back-donation involving the d_{xz} and/or d_{yz} orbitals, rather than delocalization involving Por ⇒ Fe π-donation from the $3a_{2u}(\pi)$ orbital of the ruffled porphyrinate ring, as suggested in Sections 2 and 3 above. However, in addition to the fact that the metal orbitals are much too low in energy to interact very much with the 4e(π*) orbitals, the near-zero shifts of the pyrrole-H of $[TPPFe(t\text{-}BuNC)_2]^+$ and the correspondingly small shift of the α-CH_2 resonance of $[OEPFe(t\text{-}BuNC)_2]^+$ exclude this possibility: While the *meso*-C orbital coefficient of the Hückel orbitals [121] (unperturbed by the metal d_π orbitals) is 2.4 times larger than the pyrrole-C coefficient for the 4e(π*) orbitals, the latter coefficient is more than 5.3 times larger than it is for the 3e(π) orbital. Thus, if the 4e(π*) orbitals were involved in spin delocalization, the β-pyrrole substituents would exhibit much larger contact shifts than do those of types I and II $(d_{xy})^2(d_{xz},d_{yz})^3$ ground state complexes. Certainly, inclusion of the metal d_π orbitals increases the orbital coefficients for the new set of metal-3e(π) combination orbitals (because the metal d_π orbitals induce some mixing of the 3e(π) and 4e(π*) orbitals), the higher-energy of which is the singly occupied molecular orbital (SOMO) [121], but it is unlikely to increase them to a larger size than calculated for the 4e(π*) orbitals in the absence of the metal. In contrast, the $3a_{2u}(\pi)$ orbital has orbital coefficients for the *meso*-C that are 1.4 times larger than those for the 4e(π*) orbitals, while the average pyrrole-C coefficient is only about half the size of that for the 3e(π) orbitals, and again, the orbital coefficient for the 3e(π) orbitals changes upon inclusion of the metal d_π orbitals in the calculation. The bottom line is that despite the crudeness of the simple Hückel calculations, we can exclude the participation of the 4e(π*) orbitals on the basis of both electron density and energy considerations.

TPPFe(III) complexes with phosphonite ligands such as $P(OMe)_2Ph$ are also type III complexes with $(d_{xz},d_{yz})^4(d_{xy})^1$ ground states, but with a much smaller ΔE between it and the $(d_{xz},d_{yz})^3(d_{xy})^2$ excited state than for the isocyanide complexes [133]. The pyrrole-H resonance occurs at +2.6 ppm at 20°C for this complex. In comparison, the corresponding bis-(phosphine) complexes, such as the PMe_3 complex, are type I complexes with 'large g_{max}' EPR spectra [113] and pyrrole-H resonance at −20.4 ppm at 30°C [134].

The iron(III) isobacteriochlorin known as sirohemin is found in sulfite and assimilatory nitrite reductases [11]. The dicyanoiron(III) complex of the extracted macrocycle has been studied by NMR spectroscopy [135], where it was shown that 13 and 17 α-CH_2 protons of the propionates of the two fully aromatic pyrrole rings have resonances in the 13.7–10.3 ppm region, while the 12 and 18 α-CH_2 resonances of the acetate groups of the same two pyrrole rings lie in the 7.0–5.2 ppm region at 15°C in D_2O, pH 6.0. The 2 and 7 methyls of the saturated pyrrole rings are found in the diamagnetic region at 3.2 and 0.6 ppm, and the four *meso*-H resonances occur at −5.1, −26.3, −30.4 and −58.1 ppm [135]. The basis for assignment of these *meso*-H resonances to the 5, 10, 15 and 20 positions [135] is not clear, for it does not follow the symmetry of the molecule; apparently only COSY spectra were obtained, and no NOESY spectra. The large negative *meso*-H shifts are indicative of a_{2u}-type L⇒Fe spin delocalization of the unpaired electron for the ground state, consistent with a $(d_{xz},d_{yz})^4(d_{xy})^1$ electronic ground state. Consistent with this, an axial EPR signal is observed at low temperatures (15–20 K) with *g*-values of 2.37 and 1.78 [135]. The upfield relative shifts of the *meso*-H resonances compared to the spin densities calculated from our simple Hückel program, MPORPH [121], suggest an assignment $15 < 5 < 10,20$, but this should be confirmed on the basis of NOESY spectra. The 17 and 13 α-CH_2 resonances exhibit anti-Curie behavior, suggesting that the $(d_{xz},d_{yz})^3(d_{xy})^2$ excited state is thermally accessible. Considerably more information, including assignments of the *meso*-H resonances, could be obtained on this system if a complete NOESY spectral study were carried out over a range of temperatures. Nevertheless, enough information is available to conclude that the system clearly has a $(d_{xz},d_{yz})^4(d_{xy})^1$ electronic ground state with significant delocalization to the isobacteriochlorin equivalent of the $3a_{2u}(\pi)$ for a porphyrin, Fig. 1, the latter as concluded by the authors [135]. The symmetry designation of that orbital for the isobacteriochlorin ring system is $a_1(\pi)$. Based on the anti-Curie behavior of the 13,17 α-CH_2 resonances but the 'Curie' behavior of the *meso*-H, the excited state orbital is probably the former $e(\pi)$ orbital having a node through the 5,15-*meso*-positions. The sirohemin cyanide complex of the sulfite reductase protein has very similar NMR spectra, and the sulfite and nitrite complexes of the sirohemin-containing protein are fairly similar as well [135].

The esters of *meso*-hydroxyoctaethylporphyrinatoiron(III), as the bis-pyridine complexes (pyridines of a range of basicities), the bis-*N*-methylimidazole complex, as well as the bis-pyridine or cyanide, pyridine complexes of the deprotonated *meso*-hydroxyoctaethylporphyrinatoiron(III), also known as the oxophlorin, all show two *meso*-H resonances (ratios 2:1) at very negative chemical shifts [62,63]. The oxophlorin derived from protoheme is an intermediate in the oxidation of

heme to verdoheme by the enzyme heme oxygenase [136]. The chemical shifts decrease as the basicity of the axial ligand increases and range from −141.9, −195.8 ppm (4-OAcPy) to −81.8, 99.6 ppm (3,4-Me_2Py) to −40.3, −39.8 ppm (*N*-MeIm) for the esters [62], and −118, −152 ppm (bis-pyridine) and −70, −90 ppm (Py, CN−) for the iron(III) oxophlorins [63]. This is another interesting case of the degree of $a_{2u}(\pi)$ character decreasing as the basicity of the axial ligand increases, as observed previously also for the pyridine complexes of TMPFe(III) [18,126]; clearly the oxophlorin ring system has a much greater tendency to have the $(d_{xz},d_{yz})^4(d_{xy})^1$ ground state than does the porphyrin ring, with a given axial ligand, yet the trend is still the same as for the porphyrin system with pyridines of increasing basicity [18,126]. These oxophlorin-based systems were originally assigned to be $[Fe(II)DEPD]^{+\bullet}$ π cation radical electronic structures [62]. However, neither the EPR *g*-values (which deviate too much from 2.0 to represent porphyrin-based unpaired electrons) nor the sharpness of the *meso*-H-NMR signals (which do, however, become broader with lower-basicity pyridine ligands) [62], because organic radicals in the absence of any other source of unpaired electrons such as the $Fe(II)NO(P^{+\bullet})$ complexes reported by Morishima and coworkers [137]) have *extremely* broad to undetectable NMR signals, are consistent with that formulation. Nevertheless, the large, negative *meso*-H shifts for the 4-acetylpyridine complex of the ester of *meso*-hydroxyoctaethylporphyrinatoiron(III) [65] represent up to 72% occupation of the $a_{2u}(\pi)$ orbital by the unpaired electron, while the *meso*-H shift of the $[OEPFe(t\text{-}BuNC)_2]^+$ complex represents only about 27% occupation of that orbital, if simple Hückel calculations [121] are at all meaningful. The biological relevance of the $(d_{xz},d_{yz})^4(d_{xy})^1$ ground states of these partially oxidized heme macrocycles is not entirely clear, although some radical character of the partially oxidized macrocycle may make it more susceptible to attack by the diradical O_2, or its $Fe(III)–O_2^{-\bullet}$ superoxide analog.

7.7. The schizophrenia of bis-cyanide complexes of low-spin ferrihemes

The NMR spectra of the bis-cyanide complexes of several naturally-derived ferriheme complexes [115,138] have been reported. These NMR studies showed that the spread of the heme methyl resonances is strongly dependent on the nature of the 2,4-substituents of the heme, in a manner that may now be interpreted as being a function of both the electron density distribution in each of the 3e(π) orbitals as modified by the electronic effects of the substituents [121], and the energy separation between the two [116]. There was, even in 1979, some indication that the *meso*-H of these bis-cyanide complexes were exposed to more spin density than were those of the corresponding bis-imidazole complexes [115]. Nevertheless, the 'large g_{max}' EPR spectrum of $[PPIXFe(CN)_2]^-$ [45] indicated that this was a $(d_{xy})^2(d_{xz},d_{yz})^3$ ground state system. Simple $[TPPFe(CN)_2]^-$ complexes have also been studied [139], but with no evidence of 'anomalous' contact shifts for the resonances, aside from a small alternation in the direction of the phenyl-H shifts. However, more recently it has been shown that the bis-cyanide complexes of *meso*-substituted Fe(III) porphyrinates having alkyl substituents of increasing size

($H < CH_3 < C_2H_5 < i$-Pr) [37], *meso*-tetrachiroporphyrinatoiron(III) derived from (1*R*)-*cis*-caronaldehyde acid methyl ester and pyrrole [140], *meso*-tetracyclohexylporphyrinatoiron(III) [141], quinoxalinotetraphenyl-porphyrinatoiron(III) [142], tetramesitylporphyrinatoiron(III) [112], and even *mono-ortho*-substituted derivatives of TPPFe(III) [38] show varying degrees of shift of the pyrrole-H resonances toward the limiting +10.82 ppm value (in CD_2Cl_2) indicative of the purest $(d_{xz},d_{yz})^4(d_{xy})^1$ ground state reported thus far [141]. These recent results demonstrate the extremely low energy barrier to ruffling of the porphyrinate ring, as well as the interconnection (and perhaps continuum) between types I and III ferriheme complexes. The bis-(2-methylimidazole) complex of *tetrakis-meso*-isopropylporphyrinatoiron(III) and the bis-(1,2-dimethylimidazole) complex of *tetrakis-meso*-cyclohexylporphyrinatoiron(III) are other cases where type III NMR spectra are observed, with four pyrrole-H resonances at 3.2, 4.3, 7.4 and 7.8 ppm at −35°C [143] and 11.1, 10.6, 7.6 and 6.2 ppm at −20°C [141], respectively. Presumably, the bulky *meso*-isopropyl and −cyclohexyl groups encourage the porphyrin to ruffle even more than does a *meso*-phenyl or –mesityl group, hence stabilizing the $(d_{xz},d_{yz})^4(d_{xy})^1$ ground state.

A look at the degree of ruffling of the low-spin iron(III) porphyrinates whose structures have been reported (Table 2) reveals that for TPP and TMP complexes, if the average deviation of the *meso*-carbons, ΔC_m, is 0.55 Å or greater, the electronic ground state is $(d_{xz},d_{yz})^4(d_{xy})^1$, while if it is smaller than 0.51 Å the electronic ground state is $(d_{xy})^2(d_{xz},d_{yz})^3$. The single ambiguity in this correlation is the bis-(1,2-Me_2Im) complex of TMPFe(III), which has the largest value of ΔC_m,

Table 2
Porphyrinate core distortion, ΔC_m, Fe–N_P bond length, and EPR spectral type for a series of ferriheme centers

Porphyrinate	Axial ligands	Average ΔC_m (10^2 Å)	Av Fe–N_P (Å)	EPR spectral type	Reference
TPP	CN^-	4	2.000	Large g_{max}	[35]
TPP	Py	25	1.982	Large g_{max}	[23]
TMP	5-MeImH	32	1.981	Large g_{max}	[a]
OEP	*t*-BuNC	38	1.977	Axial	[27]
OETPP	2-MeImH	9	1.974	Large g_{max}	[34]
TPP	2-MeImH	39	1.970	Large g_{max}	[13]
TMP	3-CNPy	36	1.968	Axial	[18]
TMP	4-NMe_2Py	51	1.965	Large g_{max}	[17]
TMP	3-EtPy	43	1.964	Large g_{max}	[18]
TMP	4-CNPy	41	1.961	Axial	[18]
p-TTP	2,6-XylylNC	56	1.961	Axial	[28]
TPP	4-CNPy	55	1.952	Axial	[26]
TPP	*t*-BuNC	64	1.951	Axial	[27]
TPP(handle)	CN^-	64	1.949	?	[36]
TMP	1,2-Me_2Im	72	1.937	In between	[24,113]

[a] O.Q. Munro, J.A. Serth-Guzzo, I. Turowska-Tyrk, K. Mohanrao, F.A. Walker, P.G. Debrunner, W.R. Scheidt, in preparation.

0.72 Å, but whose EPR spectral type is intermediate between that of a large g_{max} and that of an axial system. The g_{max} value of 3.02 is much smaller than those of most other bis-(hindered imidazole) complexes (3.3 and greater, although it is clear that the TMPFe(III) complex with 2-MeImH is also somewhat lower than this, Table 1) but larger than any of the axial type III species (2.6 and smaller, Table 1). In fact, the EPR signal for this complex is very broad, as was also observed earlier for the TMPFe(III) complex with 3-chloropyridine [18], which was also considered to be very close to the crossover point of the two electronic ground states. Thus, we see the $[TMPFe(1,2\text{-}Me_2Im)_2]^+$ complex as being 'frustrated' by having strong π donor ligands that strongly favor the $(d_{xy})^2(d_{xz},d_{yz})^3$ ground state, but a very ruffled porphyrinate ring that strongly favors the $(d_{xz},d_{yz})^4(d_{xy})^1$ ground state.

For the one octaethylporphyrinatoiron(III) complex having the $(d_{xz},d_{yz})^4(d_{xy})^1$ ground state, the value of ΔC_m, is 0.38 Å, suggesting that this β-pyrrole substituted, tetra-*meso*-H porphyrinate, the most similar to the naturally-occurring ferriheme centers, switches to the $(d_{xz},d_{yz})^4(d_{xy})^1$ ground state at far lower degrees of ruffling than do the tetraphenylporphyrinates. No structures of *meso*-alkyl porphyrinatoiron(III)-bis-ligand complexes having $(d_{xz},d_{yz})^4(d_{xy})^1$ ground states have yet been reported; it would certainly be interesting to compare the structures of the series of bis-(cyanide) complexes reported by Nakamura, et al. [37] and those of Latos-Grazynski, et al. [140–142]. The impression, based on NMR results, however, is that *meso*-substituted porphyrinates ruffle very readily, and are probably much more ruffled than the octaethylporphyrinate and the naturally-occurring porphyrinates.

The fact that bis-(cyanide) and -(2-methylimidazole) complexes may be type I complexes with $(d_{xy})^2(d_{xz},d_{yz})^3$ ground states or type III complexes with $(d_{xz},d_{yz})^4(d_{xy})^1$ ground states, depending on the degree of ruffling of the porphyrinate ring, raises some interesting questions that will need to be answered in the coming years. First of all, what is the energy barrier for ruffling of OEPFe(III) or one of the naturally-occurring ferrihemes to the extent that the electronic ground state would switch from $(d_{xy})^2(d_{xz},d_{yz})^3$ to $(d_{xz},d_{yz})^4(d_{xy})^1$ for a physiologically relevant set of axial ligands? We have seen that 2-MeImH and $1,2\text{-}Me_2Im$ ligands can give rise to a $(d_{xz},d_{yz})^4(d_{xy})^1$ center in low-spin iron(III) porphyrinates that ruffle readily [18]. Secondly, for a type III center, since the degree of delocalization of the single unpaired electron from the d_{xy} orbital to the porphyrinate $a_{2u}(\pi)$ orbital by $Por \Rightarrow Fe$ π-donation appears to be so great as to create confusion as to whether this is a porphyrinate- or an iron-based electron, is the formation of a type III center a prelude to transfer of the highly-delocalized electron to an electron acceptor? Third, does formation of a type III center by distortion of the porphyrinate plane within a protein such as heme-heme oxygenase [124,144] help to make the α-*meso* position susceptible to attack to form the *meso*-hydroxy porphyrin or oxophlorin, and at this stage of heme oxidation is the oxophlorin more susceptible to attack by O_2 or the superoxo form of $Fe(II)–O_2 \Leftrightarrow Fe(III)–O_2^-$? Fourth, does the $(d_{xz},d_{yz})^4(d_{xy})^1$ ground state have a weaker Fe–NO bond and thus help to cause NO to dissociate from the Fe(III)–NO centers of dissimilatory nitrite reductases, as suggested previously [10]? Shelnutt and coworkers have quantified the types of

distortion of the porphyrinate ring for a large number of model complexes and proteins [30], and it would be interesting to analyze the degree of ruffling of these systems in terms of ΔC_m to see what the likely candidates are among ferriheme proteins of known structures for a switch in electronic ground state.

7.8. The anomaly of low-spin ferric chlorins

As we have indicated above, based on EPR, Mössbauer and MCD spectroscopy (all measurements done at 4.2 K), the electronic ground state of low-spin ferric chlorins is $(d_{xz},d_{yz})^4(d_{xy})^1$. ESEEM measurements are also more consistent with this ground state than with the $(d_{xy})^2(d_{xz},d_{yz})^3$ ground state, although the results are not unequivocal [72]. However, the NMR spectra of the cyanide complexes of a naturally-derived ferric chlorin [144] and its complex with apomyoglobin [145], and $[TPCFe(ImH)_2]^+$ [112] are clearly indicative of the $(d_{xy})^2(d_{xz},d_{yz})^3$ ground state, in terms of the observed shifts of the pyrrole-H of the synthetic chlorin [112], as well as the alkyl substituent shifts of the naturally-derived cyanoiron(III) chlorin ring [144,145]. In all of these cases, the shifts of β-pyrrole substituent protons are much too large and of *meso*-H much too small to be consistent with the $(d_{xz},d_{yz})^4(d_{xy})^1$ ground state found for the sirohemin cyanide system [135]. The temperature dependence of the pyrrole-H of $[TPCFe(ImH)_2]^+$ behaves a modified Curie law (Eq. (18)) with ΔE in the range of 200–300 cm^{-1} and orbital coefficients that are consistent with an $a_{2u}(\pi)$-type unpaired electron configuration in the excited state [114]. For the ground state, La Mar and coworkers suggested the involvement of an $a_{1u}(\pi)$-type orbital, which, for the chlorin macrocycle has the proper symmetry to interact with the d_π orbitals, to explain the observed shifts of the protons of the saturated ring of the naturally-derived cyanoiron(III) chlorin [144]. As nearly consistent as these data concerning ground and excited state are with each other, they are inconsistent with EPR, Mössbauer and MCD data presented in previous sections, and also inconsistent with the behavior of the isobacteriochlorin, sirohemin cyanide [135]. In fact, it may be that chlorins are unique and that it is a mistake to lump together all of the reduced hemes. The major difference in the experimental conditions used for the other techniques and NMR spectroscopy is the temperature, and we wonder whether it is possible that when the low-spin ferric chlorin complexes are frozen, they snap into a ruffled ring conformation that favors the $(d_{xz},d_{yz})^4(d_{xy})^1$ at 4.2 K, yet at ambient temperatures the chlorin ring is fairly planar and the ground state is $(d_{xy})^2(d_{xz},d_{yz})^3$. Additional studies will be required to answer this most puzzling question.

7.9. NMR spectra of low-spin ferriheme forms of cytochromes P450

The proton NMR spectra of the cyanide complexes of cytochrome $P450_{cam}$ [84] and $P450_{RR1}$ [85] have been reported. In the former case, there are two signals likely arising from heme methyls at 22.3 and 11.7 ppm [84], while for the latter these peaks are observed at 26 and 21.4 ppm [85]. There are also resonances in the -3 to -6 ppm region [85], suggesting in both cases a typical $(d_{xy})^2(d_{xz},d_{yz})^3$ ground

state for these low-spin Fe(III) cytochromes P450. The reason for this conclusion is that, as discussed above, the paramagnetic shifts of alkyl substituents on a $(d_{xz},d_{yz})^4(d_{xy})^1$ ground-state ferriheme are so small that these resonances would not be shifted out of the diamagnetic spectral envelope of the protein. The conclusion that the ground state is $(d_{xy})^2(d_{xz},d_{yz})^3$ is consistent with the MCD [83] and single crystal EPR results [64].

7.10. The use of NMR spectroscopy to determine the orientation of the g- or χ-tensor of ferriheme proteins

In a molecule large enough that there are many protons that experience only dipolar (pseudocontact) shifts, rather than a combination of dipolar and contact shifts, it is possible to use the dipolar shifts to determine the orientation of the g- or χ-tensor of the paramagnetic center by NMR spectroscopy. Such is the case for ferriheme proteins, and a number of such determinations of the orientation of the g- or χ-tensor have been reported [144–162]. On the other hand, for model low-spin ferriheme centers, all or most of the protons in the molecule are close enough to the paramagnetic center that they may, at least in theory, experience a combination of contact and dipolar shifts, thus precluding the quantitative separation of the two contributions and determination of the orientation of the g- or χ-tensor by NMR spectroscopy.

In order to determine the orientation of the g- or χ-tensor, the resonances of the protein side chain protons must be assigned for both the diamagnetic and paramagnetic oxidation states of the protein, and then the differences in these proton resonance shifts, together with the distances and angles between the paramagnetic center and each proton relative to some reference coordinate system, determined either from the crystal structure or the NMR-determined structure, are used to map the magnetic anisotropy of the paramagnetic protein. For ferriheme proteins for which the orientation of the g- or χ-tensor and magnitude of the axial component of the magnetic anisotropy, $\Delta\chi_{ax}$ (Eq. (23)) or Δg^2_{ax} ($g^2_{zz} - 1/2(g^2_{xx} + g^2_{yy})$, Eq. (25)), have been determined, the reported values of $\Delta\chi_{ax}$ or Δg^2_{ax} are all positive, indicating that g_{zz} and χ_{zz} are larger than the x an y components of these tensors. This indicates, as discussed in Section 4.2, that in all of the reported determinations the electronic ground state is $(d_{xy})^2(d_{xz},d_{yz})^3$. In all of the reported cases as well, the proteins studied have rhombic EPR spectra and are thus type II systems. In these cases, the in-plane g_{xx} and g_{yy} or χ_{xx} and χ_{yy} orientations often, though not always, agree with those predicted on the basis of the orientation of the nodal plane of the filled p_π orbital(s) of the axial ligand(s), together with the concept of counter-rotation of the g-tensor with rotation of the axial ligand(s) away from the N_P–Fe–N_P axis nearest the projection of the nodal plane(s) of the axial ligand(s) [69]. Specific examples for which the orientation of the x and y magnetic axes agrees with the predictions based on the counter-rotation concept [69] include sperm whale metmyoglobin cyanide [146], shark metmyoglobin cyanide [147], *Aplysia* metmyoglobin cyanide [148], horseradish peroxidase cyanide [150], lignin peroxidase cyanide [149] and *Rhodobacter capsulatus* cytochrome c_2 [150]. Those for which the magnetic axes

agree with the predictions based on the counter-rotation concept [69] in which one of two axial ligands is more important in determining the orientation of the g-tensor include bovine liver microsomal cytochrome b_5 [151–154], rat microsomal cytochrome b_5 orientations A and B (if χ_{xx} and χ_{yy} are reversed) [155–157], horse heart cytochrome c [158] and yeast *iso*-1 cytochrome c [159–161]. Those for which the orientation of the magnetic axes does not agree with the predictions based on the counter-rotation concept [69] include Met⇒Ala yeast cytochrome c cyanide [162] and cytochrome c [163]. The reasons for the lack of agreement for these two cases, plus the necessity of switching χ_{xx} and χ_{yy} for the rat microsomal cytochrome b_5 molecules A and B [155,156], may in some cases be due to a mistake in axis transformations, or to other unknown factors. In several cases, including cytochrome c_6 [164], it is not possible to determine what the orientation of the tensor is from the information given in the publication. In any case, it appears that the overwhelming proof of the concept of counter-rotation of the g- or χ-tensor [69] will be quite useful for checking the results of such magnetic axis determinations in the future, in order to avoid mistakes in axis transformations. This concept, plus the assumption that the nodal plane of the e(π) orbital is determined by the same ligand p_π nodal plane, were the bases for construction of the plot of observed shift versus orientation of the nodal plane of the axial ligand shown above in Fig. 20.

Finally, it should be reiterated that in all cases where the orientation of the magnetic axes of the heme in a protein has been determined by NMR spectroscopy, the orientation of these axes have been consistent with the type II $(d_{xy})^2(d_{xz},d_{yz})^3$ ground state (χ_{zz} perpendicular or nearly perpendicular to the plane of the heme, axial ligands in nearly parallel planes, or at least, not in perpendicular planes). To the knowledge of this investigator, there has been no report of a heme protein whose magnetic axes have been determined having those axes indicative of the type III $(d_{xz},d_{yz})^4(d_{xy})^1$ ground state (χ_{zz} in the plane of the heme).

7.11. Summary of the NMR results for low-spin ferriheme complexes

The NMR spectra of low-spin ferriheme model complexes provide confirmation of the same two electronic ground states and the three different types of complexes as discussed in previous sections for EPR, Mössbauer, and MCD spectroscopy. In addition, considerably more information about excited electronic states and fluxionality is also obtained from NMR spectroscopy. However, low-spin ferric chlorins, which have the $(d_{xz},d_{yz})^4(d_{xy})^1$ ground state at low temperatures, based upon EPR, Mössbauer and MCD data, clearly have the $(d_{xy})^2(d_{xz},d_{yz})^3$ at ambient temperatures, based on NMR data.

8. Summary

This work has shown that low-spin ferric TMP and related complexes giving rise to limiting case 'large g_{max}' EPR spectra [15,17,25,29] and widely spread Mössbauer spectra [15,17,25] that are broader on the high-energy side (type I) and those that

give rise to rhombic EPR spectra [15,17,25,29] and much less widely spread Mössbauer spectra [15,17,25] that are broader on the high-energy side (type II). Both types I and II ferriheme centers show strongly upfield-shifted pyrrole-H-NMR resonances [113] and variable NIR-CT MCD intensities [29] which are consistent with the theoretical model described earlier [98]. This theoretical treatment was originally derived for a formal $(d_{xy})^2(d_{xz},d_{yz})^3$ configuration [98], and in its original form fails to describe the system with a predominantly $(d_{xz},d_{yz})^4(d_{xy})^1$ ground state, which has an axial EPR spectrum [26–29], less widely-spaced Mössbauer spectrum [27,28] that is broader on the low-energy side, and pyrrole-H shifts [27,28,132] somewhat more typical of diamagnetic iron porphyrinates (type III). Consideration of the effect of the opposite signs of g_{xx} and g_{yy} [50] on the matrix elements of Eq. (17) largely accounts for the loss of NIR-MCD intensity in $[TMPFe(4\text{-}CNPy)_2]^+$. This loss in MCD intensity is thus evidence for the $(d_{xz},d_{yz})^4(d_{xy})^1$ ground state and thus supports the assignments made from Taylor analysis of the EPR g-values, magnetic Mössbauer and NMR spectra. The MCD results [29] importantly establish that disruption of π-orbital symmetry is not itself a prerequisite for these unusual properties: The d_{xy} ground state can be stabilized in iron porphyrins by using weak σ-donor, strong π-acceptor axial ligands, or by the presence of bulky *meso*-substituents that increase the liklihood of ruffling, while in iron chlorins it appears that the reduced macrocycle itself, with a variety of axial ligands, is sufficient to stabilize this electron configuration at low temperatures. However, the electron configuration at ambient temperatures is $(d_{xy})^2(d_{xz},d_{yz})^3$, based on NMR spectra.

Acknowledgements

The excellent work of the students, postdoctoral associates, visiting scientists, and collaborators listed in the references, and in terms of collaborators, especially the research groups of Professors W.R. Scheidt, B.H. Huynh, G.P. Gupta, P.G. Debrunner, A.X. Trautwein, A.J. Thomson, and G. Simonneaux, in carrying out the work that is described in this chapter is gratefully acknowledged. Financial support from the US National Institutes of Health, grant DK31038 and the Arizona Materials Characterization Program, have been absolutely vital in obtaining the results from this laboratory that are summarized herein.

Appendix A. Glossary of abbreviations and terms used

EPR	electron paramagnetic resonance
ESEEM	electron spin echo envelope modulation
MCD	magnetic circular dichroism
NMR	nuclear magnetic resonance
HOMO	highest occupied molecular orbital
SOMO	singly occupied molecular orbital
LUMO	lowest unoccupied molecular orbital

CCP	cytochrome *c* peroxidase

Porphyrin and related macrocyclic ligands

OEP	dianion of octaethylporphyrin
TPP	dianion of tetraphenylporphyrin
p-TTP	dianion of *tetrakis*-(*meso*-p-tolyl)porphyrin
m-TTP	dianion of *tetrakis*-(*meso*-m-tolyl)porphyrin
$\{2,6\text{-}(OCH_3)_2\}_4$-TPP	dianion of *tetrakis*-(*meso*-2,6-dimethoxyphenyl)porphyrin
TMP	dianion of tetramesitylporphyrin
PPIX	dianion of protoporphyrin IX
TPC	dianion of tetraphenylchlorin
OEC	dianion of octaethylchlorin
OEPO	trianion of octaethyloxophlorin
OETPP	dianion of octamethyltetraphenylporphyrin
T^{i}PrP	dianion of *tetrakis*-*meso*-isopropylporphyrin
QTPP	dianion of quinoxalinotetraphenylporphyrin

Axial ligands

t-BuNC	*t*-butylisonitrile
4-CNPy	4-cyanopyridine
Py	pyridine
4-MePy	4-methylpyridine
3,4-Me_2Py	3,4-dimethylpyridine
4-NMe_2Py	4-dimethylaminopyridine
N-MeIm	*N*-methylimidazole
2-MeImH	2-methylimidazole
1,2-Me_2Im	1,2-dimethylimidazole
2-PhImH	2-phenylimidazole
PzH	pyrazole
3-NH_2PzH	3-aminopyrazole

References

[1] F.A. Walker, U. Simonis, in: R.B. King (Ed.), Encyclopedia of Inorganic Chemistry, vol. 4, Wiley, Chichester, 1994, pp. 1785–1846.
[2] J.N. Seidow, L.E. Vickery, G. Palmer, Arch. Biochem. Biophys. 204 (1980) 101.
[3] P.M.A. Gadsby, J. Peterson, N. Foote, C. Greenwood, A.J. Thomson, Biochem. J. 246 (1987) 43.
[4] E.J. Rigby, G.R. Moore, J.C. Gray, P.M. Gadsby, S.J. George, A.J. Thomson, Biochem. J. 256 (1988) 571.
[5] D. Simpkin, G. Palmer, F.J. Devlin, M.C. McKenna, G.M. Jensen, P.J. Stephens, Biochemistry 28 (1989) 8033.
[6] S.E. Martinez, D. Huang, A. Szczepaniak, W.A. Cramer, J.L. Smith, Structure 2 (1994) 95.
[7] B.H. Huynh, M.C. Lui, J.J.G. Moura, I. Moura, P.O. Ljungdahl, E. Münck, W.J. Payne, H.D. Peck, D.V. DerVartanian, J. LeGall, J. Biol. Chem. 257 (1982) 9576.
[8] C.K. Chang, W. Wu, J. Biol. Chem. 261 (1986) 8593.

[9] (a) V. Fülöp, J.W.B. Moir, S.J. Ferguson, J. Hajdu, J. Mol. Biol. 232 (1993) 1211. (b) V. Fülöp, J.W.B. Moir, S.J. Ferguson, J. Hajdu, Cell 81 (1995) 369. (c) D. Nurizzo, M.-C. Silvestrini, M. Mathieu, F. Cutrozzol, B.D. Bourgeois, V. Fülöp, J. Hajdu, M. Brunori, M. Tegoni, C. Cambillau, Structure 5 (1997) 1157.
[10] M.R. Cheesman, S.J. Ferguson, J.W.B. Moir, D.J. Richardson, W.G. Zumft, A.J. Thomson, Biochemistry 36 (1997) 16267.
[11] B.R. Crane, L.M. Siegel, E.D. Getzoff, Science 270 (1995) 59.
[12] F.A. Walker, U. Simonis, H. Zhang, J.M. Walker, T.M. Ruscitti, C. Kipp, M.A. Amputch, B.V. Castillo, S.H. Cody, D.L. Wilson, R.E. Graul, G.J. Yong, K. Tobin, J.T. West, B.A. Barichievich, New J. Chem. 16 (1992) 609.
[13] W.R. Scheidt, S.R. Osvath, Y.J. Lee, J. Am. Chem. Soc. 109 (1987) 1958.
[14] W.R. Scheidt, J.F. Kirner, J.L. Hoard, C.A. Reed, J. Am. Chem. Soc. 109 (1987) 1963.
[15] F.A. Walker, B.H. Huynh, W.R. Scheidt, S.R. Osvath, J. Am. Chem. Soc. 108 (1986) 5288.
[16] K. Hatano, M.K. Safo, F.A. Walker, W.R. Scheidt, Inorg. Chem. 30 (1991) 1643.
[17] M.K. Safo, G.P. Gupta, F.A. Walker, W.R. Scheidt, J. Am. Chem. Soc. 113 (1991) 5497.
[18] M.K. Safo, G.P. Gupta, C.T. Watson, U. Simonis, F.A. Walker, W.R. Scheidt, J. Am. Chem. Soc. 114 (1992) 7066.
[19] W.R. Scheidt, D.M. Chipman, J. Am. Chem. Soc. 108 (1986) 1163.
[20] R. Quinn, J.S. Valentine, M.P. Byrn, C.E. Strouse, J. Am. Chem. Soc. 109 (1987) 3301.
[21] S.M. Soltis, C.E. Strouse, J. Am. Chem. Soc. 110 (1988) 2824.
[22] M.P. Byrn, B.A. Katz, N.L. Keder, K.R. Levan, C.J. Magurany, K.M. Miller, J.W. Pritt, C.E. Strouse, J. Am. Chem. Soc. 105 (1983) 4916.
[23] D. Inniss, S.M. Soltis, C.E. Strouse, J. Am. Chem. Soc. 110 (1988) 5644.
[24] O.Q. Munro, H.M. Marques, P.G. Debrunner, K. Mohanrao, W.R. Scheidt, J. Am. Chem. Soc. 117 (1995) 935.
[25] H. Flint, V. Schünemann, M. Müther, A.X. Trautwein, J.R. Polam, C.T. Watson, F.A. Walker, in preparation.
[26] M.K. Safo, F.A. Walker, A.M. Raitsimring, W.P. Walters, D.P. Dolata, P.G. Debrunner, W.R. Scheidt, J. Am. Chem. Soc. 116 (1994) 7760.
[27] F.A. Walker, H. Nasri, I. Turowska-Tyrk, K. Mohanrao, C.T. Watson, N.V. Shokhirev, P.G. Debrunner, W.R. Scheidt, J. Am. Chem. Soc. 118 (1996) 12109.
[28] G. Simonneaux, V. Schünemann, C. Morice, L. Carel, L. Toupet, H. Winkler, A.X. Trautwein, F.A. Walker, in preparation.
[29] M.R. Cheesman, F.A. Walker, J. Am. Chem. Soc. 118 (1996) 7373.
[30] (a) W. Jentzen, X.-Z. Song, J.A. Shelnutt, J. Phys. Chem. B 101, (1997) 1684. (b) J.A. Shelnutt, X.-Z. Song, J.-G. Ma, S.-L. Jia, W. Jentzen, C.J. Medforth, Chem. Soc. Rev. 27 (1998) 31.
[31] F.A. Walker, D. Reis, V.L. Balke, J. Am. Chem. Soc. 106 (1984) 6888.
[32] E.R. Birnbaum, J.A. Hodge, M.W. Grinstaff, W.P. Schaefer, L. Henling, J.A. Labinger, J.E. Bercaw, H.B. Gray, Inorg. Chem. 34 (1995) 3625.
[33] L.D. Sparks, C.J. Medforth, M.-S. Park, J.R. Chamberlain, M.R. Ondrias, M.O. Senge, K.M. Smith, J.A. Shelnutt, J. Am. Chem. Soc. 115 (1993) 581.
[34] H. Ogura, C.J. Medforth, K.M. Smith, J. Fajer, F.A. Walker, in preparation.
[35] W.R. Scheidt, K.J. Haller, K. Hatano, J. Am. Chem. Soc. 102 (1980) 3017.
[36] M. Schappacher, J. Fischer, R. Weiss, Inorg. Chem. 28 (1989) 390.
[37] M. Nakamura, T. Ikeue, H. Fujii, T. Yoshimura, J. Am. Chem. Soc. 119 (1997) 6284.
[38] U. Simonis, in preparation.
[39] J.C. Salerno, J.S. Leigh, J. Am. Chem. Soc. 106 (1984) 2156.
[40] (a) J.C. Salerno, J. Biol. Chem. 259 (1984) 2331. (b) M.B. Valkova-Valchanova, A.S. Saribas, B.R. Gibney, P.L. Dutton, F. Daldal, Biochemistry 37 (1998) 16242.

[41] (a) D. Xia, C.-A. Yu, H. Kim, J.-Z. Xia, A.M. Kachurin, L. Zhang, L.Yu, J. Deisenhofer, Science 277 (1997) 60. (b) S. Iwata, J.W. Lee, K. Okada, J.K. Lee, M. Iwata, B. Rasmussen, T.A. Link, S. Ramaswamy, B.K. Jap, Science 281 (1998) 64.
[42] R. Bois-Poltoratsky, A. Ehrenberg, Eur. J. Biochem. 2 (1967) 361.
[43] V.I. Guzov, H.L. Houston, M.B. Murataliev, F.A. Walker, R. Feyereisen, J. Biol. Chem. 271 (1996) 26637.
[44] R. Aasa, S.P.J. Albracht, K.E. Falk, B. Fanne, T. Vanngard, Biochim. Biophys. Acta 476 (1976) 260.
[45] H. Hori, Biochim. Biophys. Acta 251 (1971) 227.
[46] (a) W.E. Blumberg, J. Peisach, in: B. Chance, T. Yonetani, A.S. Mildvan (Eds.), Probes of Structure and Function of Macromolecules and Membranes, vol. 2, Academic Press, New York, 1971, p. 215. (b) J. Peisach, W.E. Blumberg, A. Adler, Ann. N.Y. Acad. Sci. 206 (1973) 310.
[47] D.L. Brautigan, B.A. Feinberg, B.M. Hoffman, E. Margoliash, J. Peisach, W.E. Blumberg, J. Biol. Chem. 252 (1977) 574.
[48] G. Palmer, in: D. Dolphin (Ed.), The Porphyrins, vol. IV, Academic Press, New York/London/Orlando, FL, 1979, p. 313.
[49] (a) J.S. Griffith, Nature 180 (1957) 30. (b) J.S. Griffith, Mol. Phys. 21 (1971) 135.
[50] C.P.S. Taylor, Biochim. Biophys. Acta 491 (1977) 137.
[51] B.N. Figgis, J. Lewis, in: H.B. Jonassen, A. Weissberger (Eds.), Techniques of Inorganic Chemistry, vol. IV, Wiley Interscience, New York, 1965, p. 159.
[52] M.M. Maltempo, J. Phys. Chem. 61 (1974) 2540.
[53] M.K. Safo, M.J.M. Nesset, F.A. Walker, P.G. Debrunner, W.R. Scheidt, J. Am. Chem. Soc. 119 (1997) 9438.
[54] J.R. Polam, T. Kh. Shokhireva, K. Raffii, U. Simonis, F.A. Walker, Inorg. Chim. Acta 265/1–2 (1997) 109.
[55] M. Grodzicki, H. Flint, H. Winkler, F.A. Walker, A.X. Trautwein, J. Phys. Chem. 101 (1997) 4202.
[56] B.H. Huynh, M.H. Emptage, E. Münck, Biochim. Biophys. Acta 534 (1978) 295.
[57] S. De Vries, S.P.J. Albracht, Biochim. Biophys. Acta 546 (1979) 334.
[58] F.S. Mathews, E.W. Czerwinski, P Argos, in: D. Dolphin (Ed.), The Porphyrins, vol. VII, Academic Press, New York, 1979, p. 108.
[59] (a) M. Pierrot, R. Haser, M. Frey, F. Payan, J.-P. Astier, J. Biol. Chem. 257 (1982) 14341. (b) Y. Higuchi, M. Kusunoki, Y. Matsuura, N. Yasuoka, M. Kakudo, J. Mol. Biol. 172 (1984) 109.
[60] (a) W.R. Widger, W.A. Cramer, R.G. Herrmann, A. Trebst, Proc. Natl. Acad. Sci. USA 81 (1984) 674. (b) G.T. Babcock, W.R. Widger, W.A. Cramer, W.A. Oertling, J. Metz, Biochemistry 24 (1985) 3638.
[61] C. Mailer, C.P.S. Taylor, Can. J. Biochem. 50 (1972) 1048.
[62] I. Morishima, H. Fujii, Y. Shiro, S. Sano, Inorg. Chem. 34 (1995) 1528.
[63] A.L. Balch, R. Koerner, L. Latos-Grazynski, J.E. Lewis, T.N. St. Claire, E.P. Zovinka, Inorg. Chem. 36 (1997) 3892.
[64] P.W. Devaney, Ph.D. Dissertation, University of Illinois, 1980.
[65] H. Nasri, Y. Wang, B.H. Huynh, F.A. Walker, W.R. Scheidt, Inorg. Chem. 30 (1991) 1483.
[66] A.M. Raitsimring, P. Borbat, T. Kh. Shokhireva, F.A. Walker, J. Phys. Chem. 100 (1996) 5235.
[67] V. Schünemann, A.M. Raitsimring, F.A. Walker, in preparation.
[68] A.M. Raitsimring, F.A. Walker, J. Am. Chem. Soc. 120 (1998) 991.
[69] N.V. Shokhirev, F.A. Walker, J. Am. Chem. Soc. 120 (1998) 981.
[70] D.L. Turner, Eur. J. Biochem. 227 (1995) 829.
[71] A.M. Stolzenberg, S.H. Strauss, R.H. Holm, J. Am. Chem. Soc. 103 (1981) 4763.
[72] A.V. Astashkin, A.M. Raitsimring, F.A. Walker, submitted for publication.
[73] T.Kh. Shokhireva, F.A. Walker, in preparation.
[74] W.T. Oosterhuis, G. Lang, Phys. Rev. 178 (1969) 439.
[75] A. Dwivedi, W.A. Toscano, P.G. Debrunner, Biochim. Biophys. Acta 576 (1979) 502.
[76] D. Rhynard, G. Lang, K. Spartalian, T. Yonetani, J. Chem. Phys. 71 (1979) 3715.

[77] P.G. Debrunner, in: A.B.P. Lever, H.B. Gray (Eds.), Iron Porphyrins, Part 3, VCH, Weinheim, 1989, pp. 137–227.
[78] M. Sharrock, P.G. Debrunner, C. Schulz, J.D. Lipscomb, V. Marshall, I.C. Gunsalus, Biochim. Biophys. Acta 420 (1976) 8.
[79] R.I. Murray, M.T. Fisher, P.G. Debrunner, S.G. Sligar, in: P.M. Harrison (Ed.), Metalloproteins. Part 1: Metal Proteins with Redox Roles, Verlag Chemie, Weinheim, 1985, pp. 157–206.
[80] Y.-C. Fann, N.C. Gerber, P.A. Osmulski, L.P. Hager, S.G. Sligar, B.M. Hoffman, J. Am. Chem. Soc. 116 (1994) 5989.
[81] H.-L. Lee, A.F. Dexter, Y.-C. Fann, F.J. Lakner, L.P. Hager, B.M. Hoffman, J. Am. Chem. Soc. 119 (1997) 4059.
[82] P.R. Ortiz de Montellano (Ed.), Cytochrome P450, 2nd ed., Plenum Press, New York, 1995.
[83] J. McKnight, M.R. Cheesman, A.J. Thomson, J.S. Miles, A.W. Munro, Eur. J. Biochem. 213 (1993) 683.
[84] R.M. Keller, K.J. W(thrich, P.G. Debrunner, Proc. Natl. Acad. Sci. USA 69 (1972) 2073.
[85] L. Banci, I. Bertini, L.D. Ellis, R. Pierattelli, Biophys. J. 65 (1993) 806.
[86] J.C. Gudat, J. Singh, D.C. Wharton, Biochim. Biophys. Acta 292 (1973) 376.
[87] B.B. Muhoberac, D.C. Wharton, J. Biol. Chem. 258 (1983) 3019.
[88] B.B. Muhoberac, Arch. Biochem. Biophys. 233 (1984) 682.
[89] E.D. Coulter, M. Sono, C.K. Chang, O. Lopez, J.H. Dawson, Inorg. Chim. Acta 240 (1995) 603.
[90] J. Sutherland, C. Greenwood, J. Peterson, A.J. Thomson, Biochem. J. 233 (1986) 893.
[91] D.L. Kessler, K.V. Rajogopalan, J. Biol. Chem. 247 (1972) 6566.
[92] M. Gouterman, in: D. Dolphin (Ed.), The Porphyrins, vol. III, Academic Press, New York, 1978, pp. 1–165.
[93] F. Adar, in: D. Dolphin (Ed.), The Porphyrins, vol. III, Academic Press, New York, 1978, pp. 165–209.
[94] M.R. Cheesman, C. Greenwood, A.J. Thomson, Adv. Inorg. Chem. 36 (1991) 201.
[95] L.A. Nafie, T.A. Keiderling, P.J. Stephens, J. Am. Chem. Soc. 98 (1976) 2715.
[96] P.M.A. Gadsby, A.J. Thomson, J. Am. Chem. Soc. 112 (1990) 5003.
[97] J. Sutherland, C. Greenwood, J. Peterson, A.J. Thomson, Biochem. J. 233 (1986) 893.
[98] A.J. Thomson, P.M.A. Gadsby, J. Chem. Soc. Dalton Trans. (1990) 1921.
[99] Q. Peng, Ph.D. Thesis, University of Alabama, 1994.
[100] Q. Peng, R. Timkovich, P.C. Loewen, J. Peterson, FEBS Lett. 309 (1992) 157.
[101] P.N. Schatz, R.L. Mowery, E.R. Krausz, Mol. Phys. 35 (1978) 1537.
[102] A.J. Thomson, M.K. Johnson, Biochem. J. 191 (1980) 411.
[103] S.E.J. Rigby, G.R. Moore, J.C. Gray, P.M.A. Gadsby, S.J. George, A.J. Thomson, Biochem. J. 256 (1988) 571.
[104] G.A. Helcké, D.J.E. Ingram, E.F. Slade, Proc. R. Soc. London Ser. B 169 (1968) 275.
[105] S.B. Piepho, N. Schatz, Group Theory in Spectroscopy with Applications to Magnetic Circular Dichroism, Wiley, New York, 1983, p. 86.
[106] J.H. Dawson, A.M. Bracete, A.M. Huff, S. Kadkhodayan, C.M. Zeitler, M. Sono, C.K. Chang, P.C. Loewen, FEBS Lett. 295 (1991) 123.
[107] A.M. Bracete, S. Kadkhodayan, M. Sono, A.M. Huff, C. Zhuang, D.K. Cooper, K.M. Smith, C.K. Chang, J.H. Dawson, Inorg. Chem. 33 (1994) 5042.
[108] M. Sono, A.M. Bracete, A.M. Huff, M. Ikeda-Saito, J.H. Dawson, Proc. Natl. Acad. Sci. USA 88 (1991) 11148.
[109] A.M. Huff, C.K. Chang, D.K. Cooper, K.M. Smith, J.H. Dawson, Inorg. Chem. 32 (1993) 1460.
[110] A. Pfaltz, B. Jaun, A. Fässler, A. Eschenmoser, R. Jaenchen, H.H. Gilles, G. Diekert, R.K. Thauer, Helv. Chim. Acta 65 (1982) 828.
[111] K.M. Barkigia, M.A. Thompson, J. Fajer, R.K. Pandey, K.M. Smith, M.G.H. Vincente, New J. Chem. 16 (1992) 599.
[112] T. Kh. Shokhireva, A.M. Raitsimring, F.A. Walker, unpublished results.
[113] F.A. Walker, U. Simonis, in: L.J. Berliner, J. Reuben (Eds.), Biological Magnetic Resonance: NMR of Paramagnetic Molecules, vol. 12, Plenum Press, New York, 1993, pp. 133–274.

[114] F.A. Walker, in: E.I. Solomon, K. Hodgson (Eds.), Spectroscopic Methods in Bioinorganic Chemistry, American Chemical Society, Washington, DC, 1998, pp. 30–61.
[115] G.N. La Mar, F.A. Walker, in: D. Dolphin (Ed.), The Porphyrins, Academic Press, New York, 1979, pp. 61–157.
[116] N.V. Shokhirev, F.A. Walker, J. Phys. Chem. 99 (1995) 17795.
[117] P. Basu, N.V. Shokhirev, J.H. Enemark, F.A. Walker, J. Am. Chem. Soc. 117 (1995) 9042.
[118] R.M. Keller, K. Wüthrich, Biochim. Biophys. Acta 285 (1972) 326.
[119] D.H. Peyton, G.N. La Mar, U. Pande, F. Ascoli, K.M. Smith, R.K. Pandey, D.W. Parish, M. Bolognesi, M. Brunori, Biochemistry 28 (1989) 4880.
[120] H.M. McConnell, J. Chem. Phys. 24 (1956) 764.
[121] H. Tan, U. Simonis, N.V. Shokhirev, F.A. Walker, J. Am. Chem. Soc. 116 (1994) 5784.
[122] N.V. Shokhirev, F.A. Walker, J. Biol. Inorg. Chem. 3 (1998) 581.
[123] G.N. La Mar, F.A. Walker, J. Am. Chem. Soc. 94 (1972) 8607.
[124] G. Hernandez, A. Wilks, R. Paolesse, K.M. Smith, P.R. Ortiz de Montellano, G.N. La Mar, Biochemistry 35 (1994) 6632.
[125] P. Basu, A.M. Raitsimring, J.H. Enemark, F.A. Walker, Inorg. Chem. 36 (1997) 1088.
[126] C.T. Watson, Ph.D. Dissertation, University of Arizona, 1996.
[127] F.A. Walker, U. Simonis, J. Am. Chem. Soc. 113 (1991) 8652.
[128] N.V. Shokhirev, T. Kh. Shokhireva, J.R. Polam, C.T. Watson, K. Raffii, U. Simonis, F.A. Walker, J. Phys. Chem. A 101 (1997) 2778.
[129] K.I. Momot, F.A. Walker, J. Phys. Chem. A 101 (1997) 2787.
[130] K.I. Momot, F.A. Walker, J. Phys. Chem. A 102 (1998) 0000.
[131] T. Kh. Shokhireva, M.J.M. Nesset, F.A. Walker, Inorg. Chim. Acta 272–2 (1998) 204.
[132] G. Simonneaux, F. Hindre, M. Le Plouzennec, Inorg. Chem. 28 (1989) 823.
[133] M. Guillemot, G. Simonneaux, J. Chem. Soc. Chem. Commun. (1995) 2093.
[134] G. Simonneaux, P. Sodano, Inorg. Chem. 27 (1988) 3956.
[135] J. Kaufman, L.M. Siegel, L.D. Spicer, Biochemistry 32 (1993) 8782.
[136] P.R. Ortiz de Montellano, Acc. Chem. Res. 31 (1998) 543.
[137] S. Ozawa, H. Fujii, I. Morishima, J. Am. Chem. Soc. 114 (1992) 1548.
[138] G.N. La Mar, D.B. Viscio, K.M. Smith, W.S. Caughey, M.L. Smith, J. Am. Chem. Soc. 100 (1978) 8085.
[139] G.N. La Mar, J.D. del Gaudio, J.S. Frye, Biochim. Biophys. Acta 498 (1977) 422.
[140] S. Wolowiec, L. Latos-Grazynski, M. Mazzanti, J.-C. Marchon, Inorg. Chem. 36 (1997) 5761.
[141] S. Wolowiec, L. Latos-Grazynski, D. Toronto, J.-C. Marchon, Inorg. Chem. 37 (1998) 724.
[142] J. Wojaczynski, L. Latos-Grazynski, T. Glowiak, Inorg. Chem. 36 (1997) 6299.
[143] M. Nakamura, T. Ikeue, S. Neya, N. Funasaki, N. Nakamura, Inorg. Chem. 35 (1996) 3731.
[144] M.J. Chatfield, G.N. La Mar, W.O. Parker, K.M. Smith, H.-K. Leung, I.K. Morris, J. Am. Chem. Soc. 110 (1988) 6352.
[145] K. Keating, G.N. La Mar, F.-Y. Shiau, K.M. Smith, J. Am. Chem. Soc. 114 (1992) 6513.
[146] S.D. Emerson, G.N. La Mar, Biochemistry 29 (1990) 1556.
[147] Y. Yamamoto, K. Iwafune, N. Nanai, A. Ozawa, R. Chujo, T. Suzuki, Biochem. Jpn. 198 (1991) 299.
[148] J. Qin, G.N. La Mar, F. Ascoli, M. Brunori, J. Mol. Biol. 231 (1993) 1009.
[149] G.N. La Mar, Z. Chen, K. Vyas, A.D. McPherson, J. Am. Chem. Soc. 117 (1995) 411.
[150] D. Zhao, H.M. Hutton, M.A. Cusanovich, N.E. MacKenzie, Protein Sci. 5 (1996) 1816.
[151] R.M. Keller, K. Wüthrich, Biochim. Biophys. Acta 285 (1972) 326.
[152] (a) G. Williams, N.J. Clayden, G.R. Moore, R.J.P. Williams, J. Mol. Biol. 183 (1985) 447. (b) N.G. Veitch, D. Whitford, R.J.P. Williams, FEBS Lett. 269 (1990) 297.
[153] S.J. McLachlan, G.N. La Mar, K.-B. Lee, Biochim. Biophys. Acta 957 (1988) 430.
[154] K.-B. Lee, S.J. McLachlan, G.N. La Mar, Biochim. Biophys. Acta 1208 (1994) 22.
[155] R.D. Guiles, V.J. Basus, S. Sarma, S. Malpure, K.M. Fox, I.D. Kuntz, L. Waskell, Biochemistry 32 (1993) 8329.
[156] S. Sarma, B. Dangi, C.H. Yan, R.J. DiGate, D.L. Barville, R.D. Guiles, Biochemistry 36 (1997) 5645.

[157] S. Sarma, R.J. DiGate, D.B. Goodin, C.J. Miller, R.D. Guiles, Biochemistry 36 (1997) 5658.
[158] P.X. Qi, R.A. Beckman, A.J. Wand, Biochemistry 35 (1996) 12275.
[159] Y. Gao, J. Boyd, G.J. Pielak, R.J.P. Williams, Biochemistry 30 (1991) 1928.
[160] S.F. Sukits, J.E. Erman, J.D. Satterlee, Biochemistry 36 (1997) 5251.
[161] L. Banci, I. Bertini, K.L. Bren, H.B. Gray, P. Sompornpisut, P. Turano, Biochemistry 36 (1997) 8992.
[162] L. Banci, I. Bertini, K.L. Bren, M.A. Cremonini, H.B. Gray, C. Luchinat, P. Turano, J. Biol. Inorg. Chem. 1 (1996) 117.
[163] L. Banci, I. Bertini, H.B. Gray, C. Luchinat, T. Reddig, A. Rosato, P. Turano, Biochemistry 36 (1997) 9867.
[164] L. Banci, I. Bertini, M.A. De la Rosa, D. Koulougliotis, J.A. Navarro, O. Walter, Biochemistry 37 (1998) 4831.